ACS NANO

www.acsnano.org

REVIEW

Structure and Morphology of Lipid Nanoparticles for Nucleic Acid Drug Delivery: A Review

Aniket Udepurkar,[†] Cedric Devos,[†] Peter Sagmeister,[†] Francesco Destro, Pavan Inguva, Soroush Ahmadi, Etienne Boulais, Yufeng Quan, Richard D. Braatz, and Allan S. Myerson*

Cite This: https://doi.org/10.1021/acsnano.4c18274

Read Online

ACCESS | Metrics & More | Article Recommendations

ABSTRACT: **Lipid nanoparticles (LNPs) are a clinically proven platform for protecting and delivering nucleic acid-based therapeutics. These multicomponent particles self-assemble into a core−shell structure with the nucleic acid cargo encapsulated in its core. Despite considerable research efforts to establish structure−efficacy relationships, their morphological and structural characteristics—particularly their internal composition and distribution—remain elusive. This uncertainty arises from several factors, including challenges in characterization, the dynamic nature of LNPs, sample heterogeneity, and poorly understood formulation−structure relationships. This review highlights the current state of research on the structure and morphology of LNPs, characterization techniques, and ongoing efforts to elucidate how formulation parameters affect the structural and morphological LNP properties.**

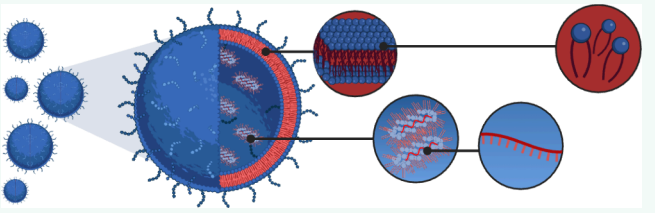

KEYWORDS: *lipid nanoparticles (LNPs), drug delivery, nucleic acid therapeutics, structure and morphology, gene delivery, nanoparticle characterization, nonviral vector, blebs, formulation*

1. INTRODUCTION

Nucleic acid-based therapeutics (NAT) offer a broader therapeutic potential to treat a range of conditions by modulating gene expression in ways not possible using conventional treatments.[1] This potential is achieved by delivering exogenous nucleic acids, including various types of deoxyribonucleic acids (DNAs), ribonucleic acids (RNAs), and related molecules,[2] such as plasmid DNA (pDNA), messenger ribonucleic acid (mRNA), small interfering RNA (siRNA), and antisense oligonucleatides (ASOs). A major challenge for NATs is achieving safe and effective delivery to their target sites of action.[2−4] Nucleic acid moieties are fragile, prone to degradation by serum nucleases in the bloodstream or self-hydrolysis, and can trigger innate immune responses, while their unfavorable physiochemical properties—such as negative charges and large size—make it difficult to cross barriers for cellular uptake and may hinder intracellular transport toward the cytosol or the nucleus.[1−7] Both viral (e.g., retroviruses, adeno-associated viruses, and lentiviruses) and nonviral (e.g., inorganic materials, lipid-based, and polymer-based) delivery vectors have been explored to overcome this challenge.[2−4,8,9] Viral vectors have several limitations, including low loading capacity (particularly for large nucleic acids), safety concerns (such as carcinogenesis and immunogenicity), the challenge of repeated administration, and complex manufacturing processes.[4,9,10] Nonviral vectors have fewer limitations; they are able to deliver large payloads, are safer, and are easier to manufacture.[4] Among the nonviral delivery vehicle, lipid nanoparticles (LNPs; Figure 1) have emerged as the most clinically advanced and versatile platform for delivering NATs although not without challenges that remain to be addressed (see Section 9).

LNPs are synthetic multicomponent delivery vehicles/particles (typically ∼50−120 nm in size) defined by their composition, which typically includes an ionizable cationic lipid along with auxiliary lipids such as phospholipids, cholesterol, and polyethylene glycolated (PEGylated) lipids, all working together to encapsulate a NAT cargo.[12−14] LNPs are often described as a platform technology,[15] as different nucleic acid modalities can be substituted without redesigning the entire

Received: December 17, 2024
Revised: May 15, 2025
Accepted: May 16, 2025

Downloaded via MASSACHUSETTS INST OF TECHNOLOGY on June 12, 2025 at 20:17:54 (UTC).
See https://pubs.acs.org/sharingguidelines for options on how to legitimately share published articles.

© XXXX American Chemical Society

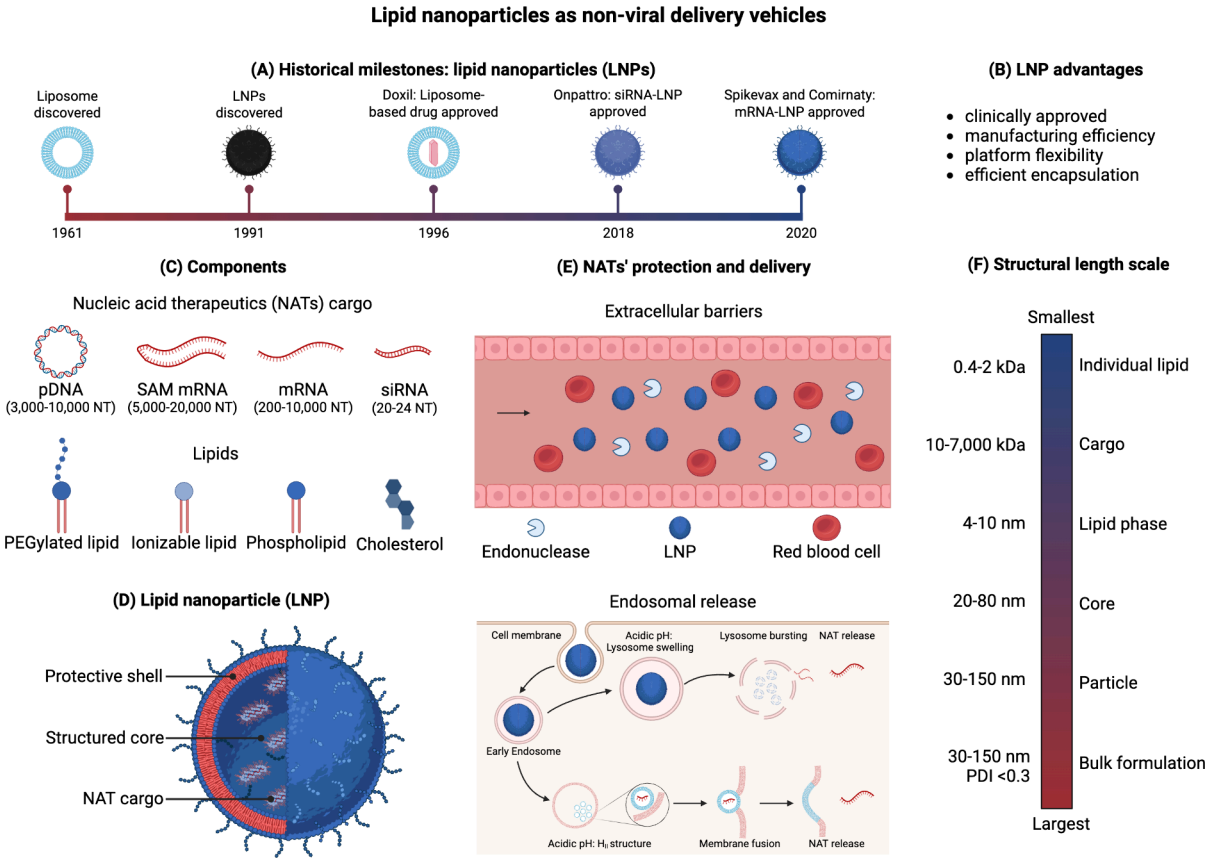

Figure 1. Schematic overview of LNPs as delivery vehicles for nucleic acid-based therapeutics to overcome intra- and extracellular barriers. (A) Key milestones in the development and clinical application of LNPs. (B) Important advantages of using LNPs for NAT delivery over other vectors. (C) Different components that make up a typical LNP. (D) Typical representation of an LNP as a particle with a protective shell to encapsulate a therapeutic cargo within a structured core. (E) (top) Extracellular physiological barriers to the effective delivery of naked NAT: degradation by nucleases and poor cell membrane permeability. (bottom) Endosomal release: the most critical intracellular barrier. Two primary escape mechanisms are illustrated: the proton sponge effect (top) and direct interaction with and disruption of the endosomal membrane (bottom), enabling NAT release into the cytosol. Adapted from ref 11 under the Creative Commons Attribution 4.0 International License. Other intracellular barriers include difficulty in transport to the nucleus and degradation by intracellular enzymes. (F) Overview of the different structural length scales relevant to LNPs. Created with BioRender.com.

delivery system. While this holds some truth, optimized LNPs for one specific nucleic acid cannot be seamlessly applied to another due to variations in the cargo's size, charge density, and intracellular target sites.[8] However, their versatility also enables precise fine-tuning of their distinct physicochemical properties, making them suitable not only for a wide range of therapeutic modalities but also for highly specific targeted delivery.

With the growing interest in NATs,[1,6,16,17] considerable research attention has been devoted to LNPs, to address NAT transfection challenges.[18] Research in the past decade primarily focused on siRNA delivery, with recent efforts increasingly directed toward mRNA, saRNA, and pDNA delivery. This research has led to clinical success, with the Food and Drug Administration (FDA) and European Medicines Agency (EMA) approving an siRNA-based drug delivered via LNPs (Onpattro, developed by Alnylam),[19] followed by the approval of mRNA-loaded LNPs in the coronavirus disease 2019 (COVID-19) vaccines, BNT162b2 (Comirnaty, developed by Pfizer) and mRNA-1273 (Spikevax, developed by Moderna).[18,19] Recently, the EMA approved a new saRNA-based vaccine for COVID-19 called Zapomeran (Kostaive, developed by Arcturus Therapeutics) and the FDA approved a respiratory syncytial virus (RSV) vaccine called mRNA-1345 (mRESVIA, developed my Moderna).[20,21] While current clinically approved LNP formulations have shown considerable success, they are not a one-size-fits-all solution, prompting ongoing efforts to expand their functional capabilities for a broader range of applications. As a result, high-impact LNP research prioritizes screening numerous lipid formulations, particularly ionizable lipids (ILs; see Section 2.1), often leveraging high-throughput screening, combinatorial chemistry, and machine learning[22,23] to identify effective formulations based on functional outcomes such as delivery efficiency, efficacy, and stability—first through *in vitro* screening, followed by *in vivo* evaluation. While this approach enables efficient exploration of the formulation space, it overlooks structural characterization, which requires advanced, nonscalable techniques. Consequently, the internal LNP structure has remained comparatively underexplored.

Understanding LNP structure is essential to establish widely applicable structure−activity relationships, as studies consistently demonstrate a strong correlation between structural and morphological features and LNP transfection efficiency.[24−33] A deeper comprehension of these features is also crucial for identifying critical quality attributes (CQAs) and unraveling the formulation−function relationship, both essential for rational LNP design. LNPs have a more intricate structure than liposomes, which are vesicles with a lipid bilayer and aqueous core with less drug-delivery capabilities[34,35] (Figure 1). Unlike

https://doi.org/10.1021/acsnano.4c18274
ACS Nano XXXX, XXX, XXX−XXX

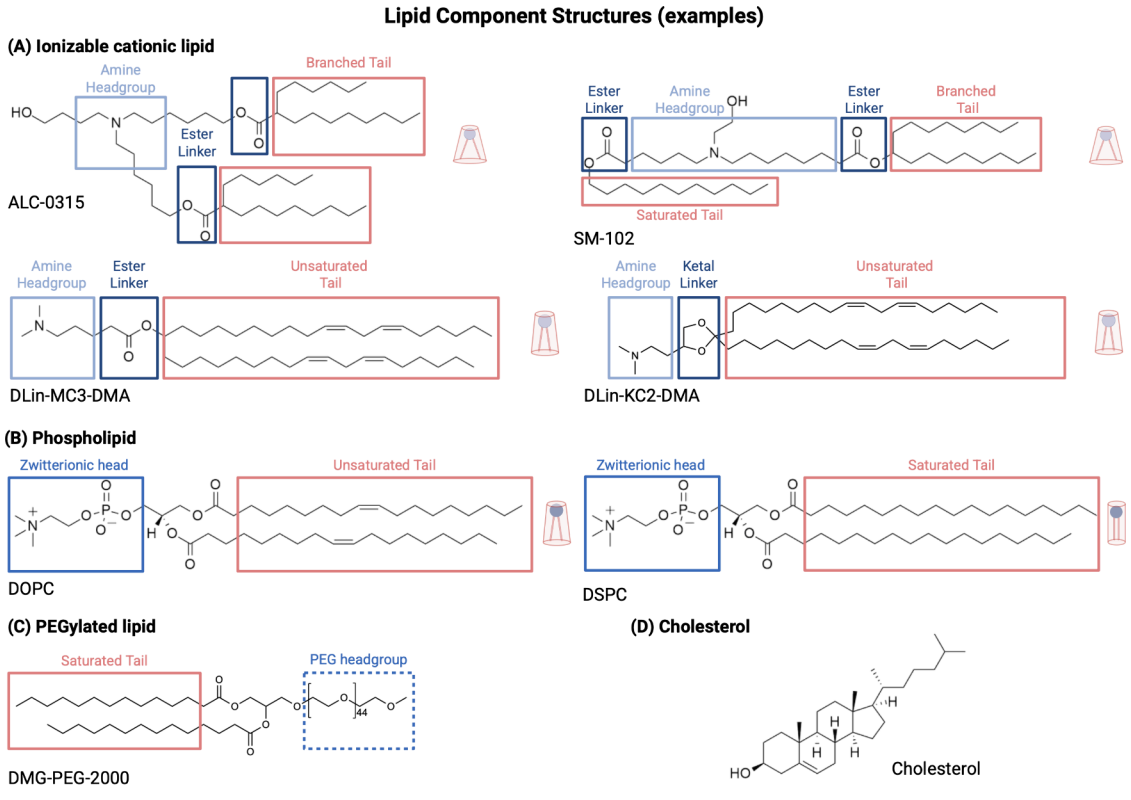

Typical formulation examples

	Onpattro	BNT162b (Comirnaty)	mRNA-1273 (Spikevax)	Lipid component structural / morphological function
Ionizable lipid	50% DLin-MC3-DMA	46.3% ALC-0315	50% SM-102	nucleic acid complexation, endosomal escape, adjuvant effect
Phospholipid	10% DSPC	9.4% DSPC	10% DSPC	lipid phase stabilization, improved stability
Cholesterol	38.5% cholesterol	42.7% cholesterol	38.5% cholesterol	lipid phase stabilization
PEGylated lipid	1.5% PEG2000-DMG	1.6% ALC-0159	1.5% PEG2000-DMG	size control, improved stability stealth effect

Figure 2. Chemical structures of typical lipid constituents used in benchmark LNP formulations: (A) Ionizable cationic lipids {e.g., ALC-0315 ([(4-hydroxybutyl)azanediyl]di(hexane-6,1-diyl) bis(2-hexyldecanoate)), SM-102 (9-heptadecanyl 8-(2-hydroxyethyl)[6-oxo-6-(undecyloxy)hexyl]aminooctanoate), DLin-MC3-DMA (4-(dimethylamino)butanoic acid, (10*Z*,13*Z*)-1-(9*Z*,12*Z*)-9,12-octadecadien-1-yl-10,13-nonadecadien-1-yl ester), and DLin-KC2-DMA (*N*,*N*-dimethyl-2,2-di(9*Z*,12*Z*)-9,12-octadecadien-1-yl-1,3-dioxolane-4-ethanamine)}. DLin-MC3-DMA is the IL used in the approved siRNA-loaded LNP, and SM-102 and ALC-0315 are the ILs used in the two approved mRNA vaccines.[18,80] It is shown whether the lipids exhibit cylindrical or cone-shaped molecular geometry.[57] (B) Phospholipids [e.g., DSPC (distearoylphosphatidylcholine), DOPC (dipalmitoylphosphatidylcholine)]. (C) PEGylated lipids [e.g., DMG-PEG2000 (1,2-dimyristoyl-*sn*-glycero-3-methoxypolyethylene glycol)] (D) Cholesterol. The lipid components in the three clinically approved formulations and their functions are shown in the table. Created with BioRender.com.

liposomes, LNPs incorporate ILs that regulate pH-dependent behavior, a key factor in facilitating efficient cargo delivery[36] (see Section 7.3). LNPs exhibit a "continuum of structures",[37−40] with multiple structures coexisting and evolving during the formulation process and during their subsequent application.[13,26,39,40] Beyond their temporal evolution, the wide variability in constituent components and assembly conditions—i.e., their design flexibility—further influences their structure, making it challenging to define thermodynamically stable organizations and the kinetic pathways leading to them.

While several reviews have discussed various aspects of LNP research,[7,10,12,13,15,18,34,41−56] a comprehensive overview specifically focusing on their structure and morphology is still lacking. Given the complexity and the rapid advancements in the field, a dedicated discussion is warranted. In this review, we present an overview of recent research related to the structural and morphological features of LNPs.

2. COMPONENTS OF THE LNP DELIVERY SYSTEM

In addition to the payload, FDA- and EMA-approved LNPs consist of four key components—cationic IL, cholesterol, PEGylated lipid, and zwitterionic phospholipid—each playing a specific role in determining both structure and efficacy.[13,18] Iterative formulation improvements have established a widely used recipe for nucleic acid delivery, with approximately 50:10:38.5:1.5 mol % for IL, phospholipid, cholesterol, and

https://doi.org/10.1021/acsnano.4c18274
ACS Nano XXXX, XXX, XXX−XXX

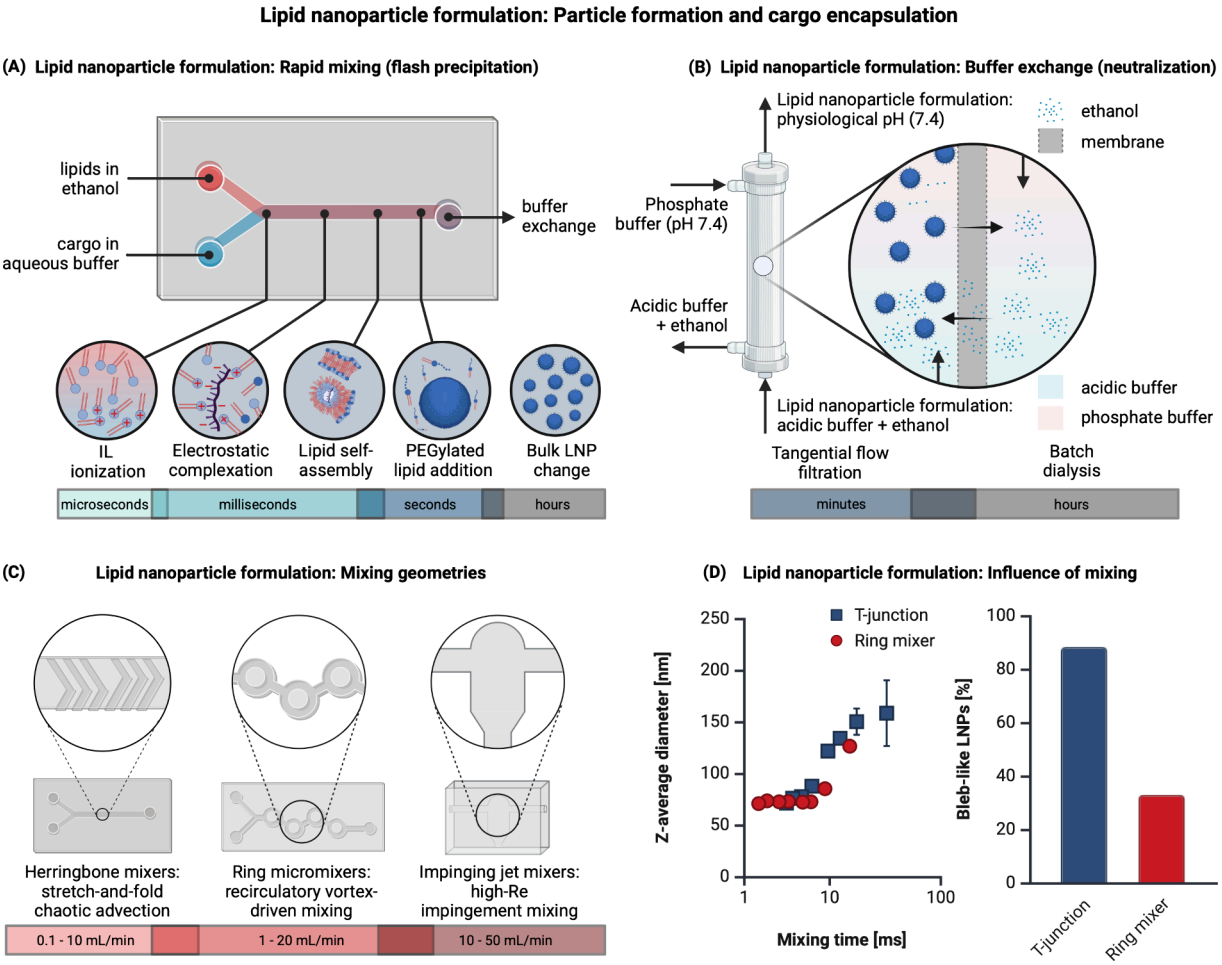

Figure 3. Schematic illustration of a typical LNP formulation as a two-step process consisting of particle formation, cargo encapsulation, and buffer exchange. (A) Formation shown as a flash precipitation process in a microfluidic mixer, where the particle self-assembly and structural evolution is shown at five different (estimated) time scales. (B) LNPs undergoing buffer exchange step for pH neutralization (physiological pH 7.4) and ethanol removal (ethanol ≤ 0.5%) employing TFF or batch membrane dialysis. The buffer exchange step is schematically illustrated here in a TFF setup. (C) Schematic representation of three commonly used mixing geometries—herringbone mixer, ring micromixers, and impinging-jet mixers—and the operating volumetric flow rates. (D) Influence of mixing time on the *z*-average diameter and morphology of LNPs formulated with T-junction and ring micromixers. Higher shear and turbulence in the T-junction (30 mL/min) resulted in a larger fraction of mRNA-loaded LNPs with blebs (a morphological feature) compared to LNPs formulated with the ring micromixer (12 mL/min) for the same micromixing time. Adapted with permission from ref 108. Copyright 2025 Elsevier. Created with BioRender.com.

PEGylated lipid, respectively.[13] Figure 2 shows a selection of lipid components used in benchmark LNP formulations. However, predicting LNP structure from composition alone remains challenging, as small variations in lipid components and cargo (whose selection is driven by its therapeutic properties) can significantly alter morphology and internal structure.[44] A wide variety of lipids have been employed in LNP formulations, each characterized by distinct chemical and structural properties. While this section highlights key features shared within the four major lipid classes used in LNPs, a more thorough discussions of lipid structures and their functional implications can be found in other reviews.[7,13,46,48,55,57−60]

2.1. Cationic ILs. ILs, the most abundant component of LNPs, are a fundamental building block developed through 25 years of research to optimize LNP formulations.[1,10,13,27] ILs are pH-sensitive lipids that consist of an amine headgroup, a linker, and a tail,[7,51] with each part serving different roles within the LNP.[59] Several thousand IL candidates [with different degrees of branching and saturation (i.e., double bonds)[61]] have been studied to identify IL formulations that are optimized for their ability to encapsulate the cargo and improve endosomal uptake and escape for a specific application.[23,62,63] ILs are preferred over permanently charged cationic lipids due to the latter's higher toxicity, potential immune response issues, and reduced endosomal escape efficiency.[64]

The ionization state of ILs, expressed as the apparent pK_a, is typically below 7.0—ideally between 6.2 and 6.7—ensuring they are positively charged at acidic pH and mostly neutral at physiological pH.[65−67] These pK_a values are the typical values reported in the literature and are based on experimental data from TNS binding assays, while alternative methods, such as theoretical calculations, may yield different pK_a estimates.[58] The dynamic charge switching is key to their role in both encapsulation (see Section 3.1) and release (see Section 7.3). During formulation at acidic pH, the cationic amine groups of ILs are protonated, allowing for electrostatic interactions with negatively charged nucleic acid cargo.[18] After buffer exchange (see Section 3), unbound ILs lose their charge. In the neutral pH of the bloodstream, ILs remain deprotonated, which helps to prevent the adsorption of negatively charged biomolecules.[68]

https://doi.org/10.1021/acsnano.4c18274
ACS Nano XXXX, XXX, XXX−XXX

Upon cellular uptake, the acidic endosomal environment reprotonates the ILs, facilitating endosomal escape and cargo release into the cytoplasm.[64] Apart from the headgroup chemistry also the lipid shape and packing, as discussed in Section 5.1, influences the final LNP structure and function.

2.2. Phospholipids. Phospholipids are a class of lipids consisting of a hydrophilic head that contains a phosphate group, and two hydrophobic tails, typically composed of alkyl chains.[61] Phospholipids are integral to the LNP, although their synthetic space has been far less explored than that of ILs. They stabilize LNP structures by influencing lipid-phase polymorphism (see Section 5.1) through stabilization or promotion of phase transitions.[69] For example, the neutral zwitterionic distearoylphosphatidylcholine (DSPC)—the most commonly used phospholipid and the main one utilized in clinical applications—supports bilayer formation and enhances LNP stability.[66,67,70] Phospholipids can also play other complex roles, which further impact the internal structure. Within the LNP core, phospholipids align between the IL chains interacting with both hydrophobic tails and hydrophilic heads, thereby reducing IL mobility.[71] In some cases, such as with DSPC, phospholipids can form ion pairs with ILs.[37] On the LNP surface, phospholipids enhance PEG chain flexibility, contributing to overall structural stability and functionality.[32,71]

2.3. Cholesterol. Cholesterol is a structural lipid that is often present in membranes and is typically used in LNP formulations. It is a neutral steroid with a bulky ring structure, that is added to LNP formulations to reduce membrane fluidity and increase bilayer thickness.[13] In some cases, cholesterol can also disrupt bilayer organization, promoting the formation of inverted micelles.[72] It integrates into the hydrophobic regions of both ILs and phospholipids, stabilizing the overall structure. For instance, in siRNA-loaded LNPs, cholesterol has been shown to enhance the stacked bilayer arrangement and reduce IL mobility.[71] While most formulations, and all clinical applications, rely on unmodified cholesterol, other sterols have been explored to improve LNP performance for both siRNA[73] and mRNA[26,27,74,75] delivery.

2.4. PEGylated Lipids. PEGylated lipids are hydrophobic lipids with alkyl chains attached to PEG chains. They play a crucial role in controlling the size and stability of LNPs. By creating a steric barrier, in the form of a hydrophilic shell (see Section 6.3) on the LNP surface, they prevent particle aggregation during formulation and maintain dispersion stability.[32,66,67,76] A high PEGylated lipid concentration[76,77] and long PEG-chain length[76] lead to smaller LNPs.

Though PEGylated lipids are primarily found on the outer surface, they can still influence internal structure. For example, PEG variants such as C16-PEG2000 were shown to create a more ordered core structure compared to DSPE-C18-PEG2000 in mRNA-loaded LNPs.[30] After intravenous injection, PEGylated lipids gradually leave the surface (see Section 7.2), allowing the LNPs to fuse with endosomal membranes and deliver their cargo.[66] During systemic circulation, PEG lipids with shorter lipid tails are more likely to leave the surface of LNPs than those with longer tails.[78,79]

2.5. Impurities. LNPs protect and transport NAT, in part to prevent physical and chemical degradation (see[81,82]). Lipid impurities from raw materials, degradation during synthesis/formulation, or storage (for example, cholesterol oxidation[75]) can also affect LNP structure. Lipid degradation is typically due to oxidation after exposure to light, oxygen, high temperatures, etc.[35]

Despite their potential impact, little research has addressed the effect of impurities on LNPs. Notably, Packer et al.[83] identified oxidative impurities, such as *N*-oxides, in ILs, which may alter the LNP structure and reduce efficacy even in small amounts. These impurities further hydrolyze into aldehydes undergo covalent addition with mRNA[83] and likely other NATs. Such mRNA−lipid adducts can be difficult to detect due to small changes in molecular mass they cause.[84] The lack of standardization in lipid raw material specifications and testing[85] results in inconsistent acceptance criteria, creating ambiguity about acceptable impurity levels and what thresholds are critical for ensuring product quality and safety. For example, impurity profiles of ALC-0315 (a common IL) vary significantly across suppliers, and some of the impurities were shown to carry over into the LNP formulations.[85]

3. LNP PRODUCTION

LNP production consists of particle formation and nucleic acid entrapment in the same step, as shown in Figure 3. Early methods such as thin-film hydration and ethanol injection were labor-intensive, had variability in output quality and lacked scalability and reproducibility.[12,34,67] We point the reader to existing reviews[86,87] for good summaries on the classic batch methods of LNP preparation. Today, loaded LNPs are produced continuously by rapid mixing of an organic lipid solution with an aqueous buffer containing nucleic acids under acidic pH conditions.[12,27,67,88,89] Microfluidic chips are used for screening purposes to reduce material cost, as they can provide rapid mixing even at low flow rates (see Section 3.4),[15,67,90−93] but are usually limited in throughput.[70] Successful scale-up to high volumetric throughput has been demonstrated;[94] however, achieving sustained clog-free operation over extended periods, such as 1 h, remains challenging. As a result, for larger scale production, impinging jet mixers, such as confined or multi-inlet vortex mixers, are used.[95−97] Formulations that can be successfully produced in microfluidic systems are not necessarily scalable to high-throughput manufacturing equipment. The cause of these challenges with scalability are discussed in Section 3.4.

After LNP particle formation, ethanol must be removed to preserve nanoparticle integrity[98] (ethanol disrupts hydrophobic regions of lipid bilayers and alters interlipid forces[69,98]) and to meet the final drug product requirements (ethanol $\leq$ 0.5%). To address this, a buffer exchange or solvent removal step is performed, shown in Figure 3, typically using dialysis or multiple centrifugation steps for small-scale applications or tangential flow filtration (TFF, using hollow fiber membranes) for larger scale applications.[99−101] During this buffer exchange the LNPs are brought to physiological pH (around 7.4), and excess lipids/nonencapsulated cargo is removed. While the buffer exchange's impact on LNP structure, size, and ζ potential is underexplored,[102] it is clear that pH shifts, buffer changes, and concentration alterations during dialysis significantly influence LNP properties (including size distribution, ζ potential, morphology, and structure).[38,102,103] Several studies[30,40,101,103] have shown that the LNP structure only fully matures after ethanol removal, emphasizing the need to integrate buffer exchange into early process design. Hammel et al.[30] demonstrated that structural differences between LNP formulations diminished following buffer exchange. In commercial processes, a filtration step is sometimes implemented to reduce bioburden. The last step in LNP production is sterile filtration.[84]

https://doi.org/10.1021/acsnano.4c18274
ACS Nano XXXX, XXX, XXX−XXX

One of the key advantages of using LNPs as a delivery vector is their manufacturing efficiency in terms of yield, production times, and material wastage. However, LNP manufacturing remains challenging due to difficulties with scale-up, reproducibility, and quality control. These challenges were highlighted during the COVID-19 pandemic, where LNP manufacturing was considered a bottleneck due to scale-up difficulties.[104] Substantial research and development efforts, both in academia and industry, aim to overcome the challenges and further optimize LNP manufacturing processes.

3.1. Self-Assembly Mechanism. The self-assembly of LNPs involves a series of steps that drive the organization of lipids and nucleic acids into stable, functional LNPs. Several hypotheses for LNP self-assembly center on rapid precipitation mechanisms—such as antisolvent or flash nanoprecipitation—and related phenomena like the Ouzo effect.[105−107] Rapid mixing (in the millisecond range; see Section 3.4) is important quickly achieve high supersaturation and ensure homogeneous formation, to produce a homogeneous and uniform distribution of LNPs.[84]

Lipids in ethanol—where no counterions are present and the IL remains unprotonated—are rapidly mixed with an aqueous buffer containing the cargo that acts as the antisolvent.[89] The addition of acidic buffer protonates the IL and causes a sharp drop in lipid solubility as ethanol can no longer effectively solvate the lipids.[89] This creates a supersaturated solution, triggering the self-assembly of lipids into structures like micelles, liposomes, or multilamellar vesicles (see Section 5.1). At the same time, positively charged ILs interact electrostatically with the anionic nucleic acid through interactions between the amine and phosphate groups. Lipids continue to assemble around the complex to further minimize energy and stabilize the structure, leading to the formation of a structure that continues to evolve into an LNP.

The fusion hypothesis[25,76,109] suggests that the formation of LNPs is a multistep process which involves a fusion stage where smaller lipid entities merge to form larger particles during the assembly (for instance during pH neutralization). This fusion process is regulated by the PEG-lipid content and is halted once PEGylated lipids on the surface reach a critical concentration, capping LNP growth and limiting their size.[76,77] The fusion hypothesis is based on experimental evidence showing the presence of small bilayer structures at pH 4, which evolve into larger structures with oily cores after buffer exchange to pH 7.4.[76,109] Fluorescence energy resonance transfer (FRET) experiments (see Section 4.5.2) with lipid tracers confirmed that lipid bilayer fusion occurs as the pH increases.[76] Apart from buffer exchange, fusion can also be induced by high buffer concentrations at acidic pH.[25] Under specific conditions of too acidic pH and high ionic strength, the fusion of siRNA-loaded LNPs slowed significantly, likely due to electrostatic shielding, osmotic stress, and PEGylated lipid condensation.[109] The fusion process occurs for LNPs loaded with various anionic cargoes [e.g., gold nanoparticles (GNPs) and siRNA].[76] Also other observations such as the increase in particle size when a hold time is introduced between mixing and buffer exchange[110] align with the fusion hypothesis. The fusion process impacts LNP structure and may be related to the formation of blebs (see Section 6.4)[25]

An overlooked area of research is the thermodynamic stability of LNPs (e.g., phase diagrams,[111,112] ideally with cargo). Typically metastable, LNPs can evolve based on composition and processing conditions even after formulation. Gindy et al.[113] observed that siRNA-loaded LNPs continued to anneal for up to 20 h under quiescent conditions before achieving lamellar ordering, indicating kinetic barriers that delay the system from reaching a more stable structure.

3.2. Critical Quality Attributes (CQAs). CQAs for LNPs are defined based on their ability to reach the target location and elicit the desired therapeutic effect.[102] The FDA identified composition, mean size and size distribution, shape, morphology, and stability as primary CQAs for nanomaterial drug products.[114] For liposomal systems, the FDA[115] included lamellarity, surface characteristics, net charge, integrity changes, among other attributes. LNP complexity raises questions about classifying lipid components as excipients or active ingredients, with some advocating for their recognition as active components in formulations.[116] An industrial perspective on the regulatory framework of lipids in LNPs provides an overview of different guidance documents and recommendations.[61]

The CQA typically assessed first is particle size. While the optimal size remains subject of debate[117] and varies depending on the application, the target size is usually below 200 nm with the polydispersity index (PDI) below 0.3. However, determining the optimal particle size is not always straightforward. The route of administration plays a significant role in determining efficacy, and *in vitro* LNP delivery does not always correlate with *in vivo* performance,[118−120] Additionally, the optimal particle size can vary significantly between species. For instance, Lam et al.[121] reported that smaller LNPs (∼60 nm) improved mRNA delivery in nonhuman primates, whereas larger particles were more effective in rodents. Hassett et al.[110] found that while 100 nm particles were optimal in mice, a broader range of 60−150 nm generated strong immune responses in nonhuman primates.

Apart from particle size, encapsulation efficiencies higher than 80%, and reasonable LNP stability (see Section 9) are desired.[94,122] For LNPs, the FDA also encourages further identification and characterization of quality attributes, such as structural features (e.g., lamellarity, surface properties), to enhance the understanding of safety, efficacy, and overall quality.[114,115] Additionally, drug release, surface charge (ζ potential), permeability, and targeting efficacy are relevant quality attributes.[102] The type of nucleic acid modality and the presence of drug-free LNPs also influence the attributes (see Section 6.5).

While structural attributes like morphology and lipid organization offer valuable insights into LNP behavior and function, most of the structural and morphological LNP features are not (yet) classified as CQAs (from a regulatory perspective), primarily due to measurement challenges, their distributed nature (e.g., blebs; see Section 6.4), and the fact that, while there is emerging research, generalizable rules linking these parameters to efficacy are still lacking and remain an area of active investigation.

3.3. Mapping CPPs to Quality Attributes. The most important critical process parameters (CPPs) influencing the physicochemical, structural, and morphological characteristics of LNPs include the flow rates and compositions of the aqueous and ethanol streams (such as lipid types and concentrations, cargo type and concentration, pH, buffer species and concentration, etc.).[102] While the underlying mechanisms of LNP formulation are grounded in established scientific principles, much of the process parameter optimization remains empirical, relying heavily on trial and error. The CPPs define a broad design space,[123] yet their selection is often inadequately justified in terms of their specific impact on LNP structure.

https://doi.org/10.1021/acsnano.4c18274
ACS Nano XXXX, XXX, XXX−XXX

Establishing a direct map between process parameters and quality attributes is difficult due to the vast design space and the nonlinear relationships between process parameters and product characteristics. To illustrate this point with one example, Okuda et al.[124] demonstrated that total flow rate (TFR), flow rate ratio (FRR), NaCl concentration, PEG content, total lipid concentration, and pH all significantly influence the LNP size. Section 6.8 discusses some generalizable conclusions regarding the influence of CPPs on the internal structure.

Some process parameters exhibit well-documented, predictable effects. Increasing TFR, up to a threshold, generally reduces particle size, lowers PDI, and enhances the encapsulation efficiency (EE).[125−127] Even small oscillations (5%) in the TFR can significantly affect the formation process, leading to larger sizes and reduced EE.[128] The effect related to TFR can be attributed to the influence of mixing, as discussed in Section 3.4. Likewise, a higher FRR typically decreases particle size and PDI while improving EE and stability (up to a certain extent, usually at around FRR = 3:1).[108,119,125−127] Even for these relatively well-characterized CPPs, their influence on LNP internal structure remains less clear.

Other process parameters, like the ionic environment, have more intricate effects. The pH must remain below the pK_a of the IL to ensure efficient complexation. The salt concentration and buffer species follow Hofmeister effects.[124] Higher ionic strength generally leads to larger (although sometimes negligibly so), less stable LNPs, and in some cases increasing salt concentration lowers both the ζ potential and EE.[109,124,129] Another study found that increasing citrate buffer molarity from 50 to 300 mM did not alter particle size but significantly impacted *in vitro* transfection efficiency.[129] Buffer molarity also affects the morphology (see Section 6.4).[25,129]

Some process parameters introduce trade-offs. Higher total lipid concentration likely enhances EE but also increases particle size.[127] Another parameter is the charge ratio (N/P ratio, which represents the ratio of protonatable nitrogen atoms in the IL headgroup to the anionic charges from the phosphate group on the nucleic acid backbone[15]), which affects the internal structure, EE, and electrostatic stability of LNPs.[15,44,122] The optimal N/P ratio typically ranges from 3 to 12 (i.e., an excess of IL) and is cargo-dependent (e.g., 6 for mRNA and 3 for siRNA).[18,53,93] Lowering the N/P ratio from 8 to 2 increased the particle size and reduced the EE, thereby decreasing the mRNA loading per LNP.[58] Haque et al.[53] noted that the N/P ratio effects also depend on the formulation process, adding another layer of complexity. The effect of the cargo itself is discussed in Section 6.6.

Lipid composition and molar ratios pose an even greater challenge in CPP-QA mapping due to their vast parameter space and their complex dependence on other process parameters. Additionally, the interplay between different lipid species[130] further complicates their effects on LNP properties. Changes in the lipid composition can affect the size, shape, morphology, structure, and other parameters of the LNPs.[7,57,77,130−132] A case in point is the behavior of the IL: DODMA and DODAP form heterogeneous structures, whereas DLin-KC2-DMA, DLin-MC3-DMA, and DLinDMA generate more uniform LNPs[58] (abbreviations defined at end of manuscript). Given these complexities, optimizing both lipid structure and molar ratios is crucial for achieving targeted quality attributes.[53]

Both formation and characterization are typically performed at room temperature (20−25 °C).[133] Gilbert et al.[103] reported subtle temperature-dependent changes in the internal LNP structure, likely due to temperature-driven fusion or aggregation processes.[134]

3.4. Mixing. Given the kinetic aspect of LNP self-assembly, as well as the relatively short times involved in this self-assembly, conditions within the mixers have a major impact on final product characteristics. Several studies have explored the impact of mixing on LNP formulation, but systematic investigations remain limited. This is further complicated by the large variety of continuous mixers used in LNP synthesis. Different mixers use qualitatively different fluid mechanical mechanisms to enact rapid mixing, which in turn means that the environment within which LNPs self-assemble is qualitatively different from one to the next, with different types of mixer warranting different analysis.

Mixers can roughly be categorized in three categories: microfluidic, millifluidic, and turbulent mixers. Older microfluidic mixers were based on hydrodynamic focusing systems,[135] which allows for extremely rapid mixing even in creeping flow regime. Such systems have been used for synthesizing liposomes[136] as well as polymeric nanoparticles,[137] but have fallen out of use as the high FRRs required for proper mixing lead to considerable waste of material. In more modern microfluidic methods, the alcohol and buffer streams are mixed in a simple T- or Y-junction, and then sent to a chaotic mixer such as herringbone mixers,[77,138−140] baffled mixer,[92] ring micromixer.[125] The main advantage of microfluidic methods is precise control over diffusion, owing to the laminar flow within them. Microfluidic platforms reproducibly yield tunable, small particle sizes (of the order of 20−100 nm), narrow particle size distributions (PSDs), and near 100% encapsulation.[90] Millifluidic mixers for LNP formulation have been introduced by Prud'homme and collaborators.[95,141,142] These works include confined impinging jet mixers,[95,141] as well as multi-inlet vortex mixers.[142,143] These systems exhibit higher throughput than microfluidic systems, but their adoption by research laboratories has been somewhat slow owing to their fabrication requiring precision micromachining, and the fact that they consume significantly more reagent than microfluidic methods. Protocols for synthesizing LNPs with these mixers have recently been presented,[96] achieving particle sizes in the 60−100 nm range. In 2014, Lim et al.[144] introduced a high-throughput system based on turbulent coaxial jets for the synthesis of various types of nanoparticles. Turbulent mixing allows this system to reach mixing times comparable to microfluidic systems, with much higher throughput. Such a system has been used to synthesize LNPs, with comparison to results from standard microfluidic methods.[84]

In all of the mixers mentioned above, higher flow rates generally correlate to faster mixing. Mixing time has generally been identified as the more important parameter determining the impact of fluid dynamics on LNP formulation. In general, faster mixing has been correlated with smaller resulting particle sizes, narrower PSDs, and better cargo encapsulation.[127] Mixing time can be determined experimentally using well-established ruler reactions,[145] or physical tracer tests based on colored dyes in the case of transparent mixers.[95] Mixing in microfluidic hydrodynamic focusing systems is determined by FRR, and can be determined using either simple 1D arguments[146] or more complete models for 2D transport in microfluidic systems.[147] Mixing time in chaotic "stretch-and-fold" mixers can be determined theoretically using the appropriate theory of mixing,[148] and mixing time scales in more turbulent mixers

https://doi.org/10.1021/acsnano.4c18274
ACS Nano XXXX, XXX, XXX−XXX

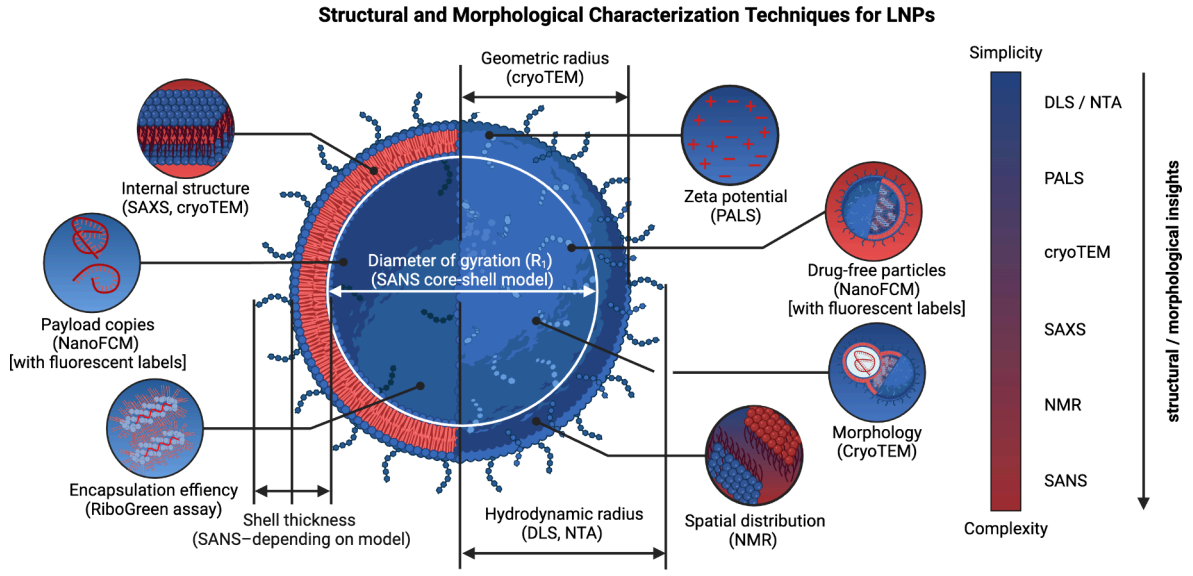

Figure 4. Schematic of the most commonly used structural and morphological characterization techniques for LNPs, highlighting the information each can provide, along with an assessment of their ease of use and operational complexity. The abbreviation SAXS stands for small-angle X-ray scattering, SANS for small-angle neutron scattering, DLS for dynamic light scattering, NTA for nanoparticle tracking analysis, NMR for nuclear magnetic resonance, PALS for phase analysis light scattering, and NanoFCM for nano-flow cytometry. Created with BioRender.com.

can be estimated using well-established turbulent mixing time scales.[149]

However, it is becoming increasingly clear that descriptions in terms of a single mixing rate, which are currently standard, are insufficient to fully predict output characteristics. Abstracting away the mixing process into a single mixing time is only truly valid if the speed of mixing is much faster than the kinetics of the self-assembly, which usually turns out not to be realized in practice. Indeed, experiments with microfluidic systems have shown that differences of the order of microsecond in the mixing steps to have an impact on output characteristics,[150] thus indicating the presence of a step of comparable time scale in the self-assembly process.

Besides mixing time, other aspects of the fluid mechanics within a mixer are likely to impact resulting LNP morphologies. The exact structure of concentration gradients and fluid shear within a mixer is likely to have an impact on the resulting particle distributions, as particles with a similar residence time may find themselves in different microenvironments within the same mixer. That will cause variation in product quality even in mixers that have the same average mixing time. Differences in shear stresses across mixers are also likely to impact self-assembly. Shear stresses have been shown to affect the morphology of lipid assembly in certain controlled conditions.[151] Additionally, turbulent mixers, either through shear or through inertial effects, may give rise to collision events which do not happen in laminar mixer, leading to qualitatively different growth processes and end products.[152] Finally, the more irregular conditions in turbulent mixers may also lead to the growth of lipid membranes with topological defects, which have been shown to affect the vesicle properties such as its curvature.[153]

A complete systematic study of the impact of fluid dynamics on LNP self-assembly is still missing, but we mention here a number of studies highlighting this effect. Even when different micromixers achieve comparable physicochemical properties, *in vitro* expression can still vary.[93] Work by Laramy et al.[84] compared LNPs produced in a microfluidic chip to LNPs produced using a turbulent coaxial jet mixer. They obtained smaller LNPs and narrower size distributions using the turbulent method, but noted poorer encapsulation, higher variation in internal structure, and higher incidence of irregularities such as blebs. This variation could be in part due to higher shear stresses at play in turbulent mixing.[84] Another study compared LNP formulation in a commercial T-junction with the bifurcating ring microreactor.[108] At comparable mixing times, the LNPs had a comparable particle size, but different percentage of LNPs with blebs[108] (see Section 6.4). More vortex formation resulted in more bleb-like structures.[108] An increase in the FRR of the aqueous to the organic phase resulted in larger particles,[108,140] with FRR of 1 leading to significantly larger particles even at comparable micromixing times.[108] The increase in the LNP size with an increase in FRR is attributed to higher lipid supersaturation[108] or slower ethanol dilution.[140] Another study[123] found that different LNP formulations require a unique mixing optimization.

Theoretical investigation of the impact of other critical parameters of the mixer on LNP formulation is currently being hampered by incomplete understanding of the self-assembly processes of LNPs (see Section 3.1). In the absence of well-established mechanisms, any tentative modeling ought to be backed by solid experimental results. Transferring the results from one group in a specific setup to a different setup is often difficult, given the combinatorially large number of different lipid formulations available and used by different groups. Very often, only the broadest trends transfer from one setup to the next, with the quantitative details depending on the specific parameters of the mixer and lipid formulation.

Given the factors discussed above, scaling up of production is also an important challenge. A large volume of research on LNPs is done in microfluidic systems, while large-scale production is often more conveniently achieved in larger-scale mixers, due to their higher throughput. However, since the fluid mechanics is significantly different, recipes rarely translate directly from the microfluidic screening to more turbulent large-scale production. This is a relatively unstudied problem, and should be an important area of research moving forward. One approach to the

https://doi.org/10.1021/acsnano.4c18274
ACS Nano XXXX, XXX, XXX−XXX

problem of scaling up is to attempt to match as many parameters (mixing time, maximum shear rate, variability of the concentration gradient, temperature gradients, vorticity) of the flow as possible, although this may not always be possible. Identification of the key parameters to match again requires a more complete understanding of LNP self-assembly kinetics, which is currently missing.

4. STRUCTURAL AND MORPHOLOGICAL CHARACTERIZATION

Characterizing LNPs is essential for ensuring therapeutic safety and efficacy, while also establishing structure−activity relationships to optimize formulations and to better understand CPPs. However, the field faces reproducibility challenges, to some extent caused by a lack of harmonization, and an analytical gap relative to the complex nature of LNPs. The FDA[114] recommends using orthogonal techniques for assessment of the CQAs (see Section 3.2) and has put some emphasis on structural and morphological characterization.[114,115] Most LNP characterization focuses on properties such as PSD, ζ potential, and EE.[30,44,103] While these properties are linked to structural features, a more detailed analysis is often limited by the accessibility and resource demands of advanced techniques,[30] along with the need for high spatial and temporal resolution.[154] Traditional LNP characterization relies on bulk measurements, which only provide static end point data without kinetic insight. Some common characterization techniques are illustrated in Figure 4. Recent developments in single-particle measurement platforms,[155−157] coupled with complementary techniques, such as cryogenic transmission electron microscopy (cryoTEM) and scattering methods (light, neutrons, X-rays), offer more precise characterization. Single-particle measurements can be used, for example, for assessing interparticle heterogeneity.[157,158] As no single technique can fully resolve LNP structure,[44] combining multiple multiscale methods through a robust analytical characterization train has proven most effective for understanding LNPs' complex structure and dynamics.[13,44,159−162]

4.1. Particle Size Distribution (PSD). While not all structural changes affect the PSD,[163] the mean size and PDI are routinely measured because they are straightforward and reliable quality indicators.[68] Caution is required when comparing sizing techniques,[164] particularly for multimodal or polydisperse samples, as different techniques rely on distinct principles and can yield different diameter measurements.

4.1.1. Dynamic Light Scattering (DLS). DLS is commonly used to measure the hydrodynamic diameter of NAT-loaded LNPs.[26,76,103,133] It is commonly used as the initial technique to validate the quality of an LNP formulation during early stage and high-throughput screening, helping to determine optimal process conditions. In a typical DLS setup, a dilute sample (around 1 mg/mL or lower[111]) is illuminated by a laser (600−660 nm range), and fluctuations in scattered light caused by Brownian motion are recorded at a high scattering angle (90° or 173°). The intensity fluctuations can be resolved to obtain the ensemble z-average diffusion coefficient (D_z), which is related to the z-average particle hydrodynamic diameter (D_h) by the Stokes−Einstein equation. The Stokes−Einstein equation assumes particles are monodisperse rigid spheres when determining D_h,[165] which may not apply to LNPs, especially those with irregular shapes such as blebs (see Section 6.4). More complex data analysis techniques, such as CONTIN and cumulant analysis, are used to determine the PSD and PDI. DLS results in intensity-weighted distributions, giving disproportionate emphasis to larger particles and aggregates. The hydrodynamic diameter is sensitive to factors such as pH, ionic strength, viscosity, and temperature, so LNPs should be diluted in the same buffer used for formulation[111]. Moreover, DLS has limited resolution, struggling to differentiate particle subpopulations with less than a 3-fold size difference.[166] Spatially resolved dynamic light scattering (SR-DLS) can be used as an alternative to conventional DLS for measuring LNP size in turbid and concentrated suspensions,[167,168] and can be exploited for real-time monitoring and control.[168]

4.1.2. Nanoparticle Tracking Analysis (NTA). NTA offers an alternative approach to DLS for measuring LNP hydrodynamic diameter-based size distributions.[38,169,170] NTA tracks nanoparticles' Brownian motion via laser-illuminated microscopy,[160,171] providing better resolution of distinct populations and determining absolute particle concentration.[166,169] Compared to DLS, NTA has lower detection limits, longer measurement times, and greater sensitivity to instrument settings.[160,166] In addition, NTA requires careful dilution of the sample[172] and background calibration for reliable measurement.[173]

4.1.3. Additional Techniques. CryoTEM (see Section 4.2.1) can measure number-based PSD and number-averaged mean size of LNPs using geometric diameters.[164] PEGylated lipids in brush conformations (~5 nm) are invisible in cryoTEM.[24,169] Unlike other size-measurement methods, cryoTEM also reveals structural details, including aspect ratio and shape features such as blebs.[26]

Atomic force microscopy (AFM; see Section 4.2.2) is sometimes used to determine the PSDs of LNPs,[174] alongside techniques such as multiangle light scattering (MALS),[175,176] Taylor dispersion analysis (TDA),[177] and small-angle neutron scattering (SANS).[103] DLS typically reports larger radii compared to methods like SANS or AFM, as it measures the hydrodynamic radius, including the counterion cloud, which most other methods do not capture.[174,178]

4.2. Structural and Morphological Features. *4.2.1. Cryogenic Transmission Electron Microscopy.* CryoTEM is widely used for imaging of LNPs, providing insights into the size, shape, and morphology.[26,30,38] In this method, concentrated LNP samples (~3 μL at a cargo concentration of ~100−500 ng/μL[38,104]) are vitrified within carbon film holes and then imaged. Proper vitrification and achieving optimal ice thickness is challenging.[179] It is important to image the entire carbon hole due to the ice thickness gradient, which can skew PSDs (i.e., the lens effect).[164,179] Through the use of automated vitrification[180] these disadvantages can be overcome, which results in better and more consistent sample preparation for LNPs. CryoTEM may not fully represent LNPs' behavior in solution[181] and offers limited quantitative insights, but can provide some descriptive information. There are some analysis challenges in distinguishing between LNP components such as lipids and nucleic acids due to their similar electron densities, making morphological features difficult to fully resolve.[44] CryoTEM can also be subject to interpretational bias. Some studies have addressed this by using negatively charged colloidal GNPs as tracers[76] or by selectively staining RNA with thionine to enhance contrast.[38] While cryoTEM offers low throughput,[164] this is compensated for by its small sample requirements.[179] Cryogenic electron tomography (cryoET) is another technique for visualizing LNP morphology and structure, similar to cryoTEM but with the added benefit of 3D reconstructions for better spatial context.[133]

https://doi.org/10.1021/acsnano.4c18274
ACS Nano XXXX, XXX, XXX−XXX

4.2.2. Atomic Force Microscopy (AFM). AFM has also been used to image NAT-loaded LNPs for structural and morphological characterization.[174,182−185] AFM measures interactions between a flexible cantilever tip and the sample surface.[183,184] AFM offers several advantages for structural characterization, including high-resolution surface imaging and the ability to generate surface interaction maps, but is limited by its small scanning area and challenging sample preparation (which involves immobilization on a substrate).[184] Drawbacks of AFM are the deformation of LNPs due to contact between the LNPs and the AFM tip[184] or destruction of LNPs on the substrate,[185] both of which can lead to inaccurate size and shape determination. The deformation can be minimized by intermittent contact[184] or by surface immobilization of the substrate.[185] LNP interaction with the AFM tip and deformation can also be exploited to probe LNPs' intermolecular interactions[174] and mechanical properties[183,186]

4.2.3. Small-Angle X-ray Scattering (SAXS). SAXS[187] is a technique used to analyze repeating structures in solution, resolving features from a few to several hundred nanometers.[103,188] SAXS has been applied to LNPs loaded with self-amplifying mRNA (SAM),[169] siRNA,[71,133] or mRNA,[24,189] to identify ordered internal structures within LNPs[13] and to determine the particle size [radius of gyration (R_g)].[169] Comparing SAXS with DLS (via the $2R_g/D_h$ ratio) yields a value around 0.78 for uniform spheres[140] and close to 0.5 for the presence of blebs.[29]

In SAXS, a dilute LNP suspension is placed in a glass capillary and exposed to a collimated X-ray beam (wavelength 0.01−0.2 nm), producing an isotropic scattering pattern (from interactions with electrons) captured by a detector.[190] To obtain the LNP scattering pattern, the radially averaged scattering intensity (I), with the solvent background subtracted, is plotted against the scattering vector (q). High polydisperse samples can affect data quality by masking key structural features. To address this, Graewert et al.[191] used asymmetrical-flow field-flow fractionation (AF4) coupled with SAXS for size-dependent fractionation and characterization of mRNA-loaded LNPs. High-throughput, time-resolved SAXS enables rapid screening of LNP structural characteristics.[30,103,192,193] Additionally, ultrasmall-angle X-ray scattering (USAXS) provides insights into LNP structures ranging from 100−1000 nm. Moreover, the integration of high-throughput SAXS workflows, as demonstrated by Hammel et al.,[30] offers an efficient approach for rapidly screening LNP formulations and elucidating structure−function relationships.

The low-q region of the SAXS profile corresponds the particle size, while the high-q region reveals the internal lipid organization.[190] Ordered lipid structures, such as inverse hexagonal, lamellar, or cubosome phases (see Section 5.1), have characteristic Braggs peaks which can be identified.[30,39,189] A sharp peak signifies a highly ordered structure, while a broad peak indicates disordered organization.[113] The length scale (d) of the unit cell can be determined by the relationship $q = 2\pi/d$.

Solution scattering data, such as SAXS, can be processed using the Density from Solution Scattering (DENSS) algorithm to reconstruct 3D electron density maps and complex particle shapes without predefined structural models.[194] When applied to mRNA-loaded LNPs, SAXS combined with DENSS has shown good agreement with cryoTEM and DLS data,[195] although further investigation is needed to address its limitations.

4.2.4. Small-Angle Neutron Scattering (SANS). SANS has been utilized for obtaining structural insights.[24,40,103,169,178,196] SANS operates similarly to SAXS, using a neutron beam (0.1−2 nm),[190] which interacts with atomic nuclei and differentiates between isotopes of different elements.[154] By adjustment of the H_2O/D_2O ratio, the isotopic contrast[190] and LNP scattering are manipulated. Enhanced contrast is achieved through deuterated lipids (e.g., cholesterol, phospholipids), which is exploited for precisely localizing different lipid components within LNPs.[71,196] LNP SANS data have been interpreted using different models.[24,40,133,169,178,188] For instance, a single shell−core model, (e.g.,[103,178]), a double shell−core model (e.g.,[24]), and a triple shell−core model (e.g.,[40]) have been fitted to SANS data to capture the LNP structural features. SANS assumes implicitly that every LNP contains cargo.[197] To overcome this limitation, Chen et al.[197] proposed two structural models: one for NAT-loaded LNPs and one for drug-free LNPs. Others[103] have used similar approaches to analyze SAXS data from mixtures of drug-free and loaded LNPs. By fitting the scattering length density (SLD) profiles, further detail on the water and lipid fractions within the core and shell can be obtained.[40,103,196] Some drawbacks of SANS are long acquisition times (several hours) and limited accessibility, hindering broader use.[190] The SAXS and SANS techniques complement each other effectively,[154] and can elucidate the internal lipid organization and the core−shell composition of the LNPs, respectively.

4.2.5. Techniques to Probe LNPs' Phase Behavior. LNPs can undergo phase transitions (see Sections 3.1 and 7.3). Apart from SAXS, cryoTEM, and nuclear magnetic resonance (NMR; see Section 4.5.1) several complementary techniques have been employed to probe the phase behavior of LNPs and their components. Differential scanning calorimetry (DSC) has been widely applied to characterize thermotropic phase transitions of both lipids and mRNA.[112,132,198] DSC measures the heat flow associated with thermal events in a sample relative to a reference, providing insights into material stability and phase behavior.[199] In mRNA-loaded LNPs, DSC thermograms have been used to evaluate the interactions between the nucleic acid cargo and lipid components. Shifts in thermal transitions can provide indirect insights into EE, lipid organization, and the overall structural stability of the formulation. Additionally, DSC has been employed to investigate mRNA unfolding in its free form.[132]

Circular dichroism (CD) spectroscopy is another valuable, nondestructive technique that measures the differential absorption of left- and right-handed circularly polarized light. It has been used to evaluate the tertiary structure of nucleic acids, like mRNA.[112,132] CD spectra originate from specific structural motifs—such as stem-loop regions in mRNA (see Section 5.2)—and can be monitored for spectral shifts that reflect conformational changes. For instance, CD has been used to detect pH-induced changes in mRNA structure when encapsulated within LNPs.[112]

Fourier transform infrared (FTIR) spectroscopy, which measures molecular vibrations to identify chemical bonds, has also been used to assess lipid and nucleic acid interactions within LNPs.[112,200] Lipid phase transitions result in changes in the molecular order and the conformational freedom, which can be detected using FTIR.[200]

4.3. EE and Payload Distribution. EE quantifies the percentage of NAT encapsulated by LNPs. The RiboGreen assay, the most common EE measurement method, employs a proprietary fluorescent dye (RiboGreen) to assess RNA

https://doi.org/10.1021/acsnano.4c18274
ACS Nano XXXX, XXX, XXX−XXX

fluorescence intensity before and after LNP disruption with surfactants (e.g., Triton X-100, Tween 20), releasing the encapsulated cargo.[201,202] The assay assumes minimal dye penetration into the LNP core, enabling calculation of accessible vs encapsulated RNA. Dye binding to mRNA occurs via both charge and hydrophobic interactions,[203] making pH and buffer molarity critical for consistent binding efficiency, necessitating identical buffer conditions between standards and samples. Crucially, the RiboGreen assay quantifies accessible RNA, which is often misinterpreted as free residual RNA; however, surface-bound RNA from incomplete encapsulation can also contribute to the fluorescent signal. While widely used, the RiboGreen assay cannot determine NATs per LNP or distinguish between drug-free and loaded LNPs. It also lacks the ability to assess RNA integrity, which necessitates the use of complementary techniques such as electrophoresis.[204] The surfactant concentration can influence the solubilization of LNPs and/or nucleic acid-dye interaction and, thus, underestimate the nucleic acid concentration and EE.[202] Despite these shortcomings, the RiboGreen assay remains the preferred technique for estimating EEs.

Analytical ultracentrifugation (AUC) is used to separate LNPs based on their density differences, particle size, and shape.[205−208] This can be exploited to estimate the drug loading and the fraction of drug-free LNPs.[204−206] AUC can yield more precise size distributions than DLS,[207,208] but demands expertise.[207] To address challenges like low-resolution fractionation caused by LNP diffusion and minimal density contrast,[204] the application of sucrose density gradients offers an effective solution.[209] Le Ru et al.[210] recently demonstrated scatter-free absorption spectroscopy (SFAS) as a faster and more precise alternative to RiboGreen assay to quantify the RNA concentration in RNA-loaded LNPs.

Bulk techniques are not suited for estimating payload heterogeneity in LNPs (see Section 6.5). Recent advances in microscopy techniques coupled with fluorescently labeled formulation components have enabled the characterization of EE and nucleotide loading at the single-particle level. Li et al.[156,211] developed multilaser cylindrical illumination confocal spectroscopy (CICS), which can distinguish between drug-free LNPs, free nucleotide, and loaded LNPs. By tagging nucleotides and lipids with fluorescent markers, this technique could quantify mRNA payload capacity at single-particle resolution.[156,211] Sych et al.[201] used single-particle profiling (SPP) with confocal microscopy to determine the loading of fluorescently labeled mRNA-loaded LNPs, resolving individual intensity peaks of diffusing particles. Kamanzi et al.[109,155] applied convex lens-induced confinement (CLiC) microscopy to study size and loading of siRNA-LNPs, focusing on formulation, pH, and drug loading. Münter et al.[212] employed confocal microscopy with Cy3-labeled mRNA and fluorescent lipids to quantify the fraction of drug-free LNPs. De Peña et al.[213] developed and employed an electrophoretic microfluidic characterization platform to quantify payload in NAT-loaded LNPs. Ueda et al.[71] and Chen et al.[197] employed nano-flow cytometry (NanoFCM) with fluorescently tagged cargo to quantify the fraction of drug-free LNPs and payload copy per LNP.

While single-particle and molecular interaction techniques can provide valuable insights, they often require the use of fluorescently labeled components. Aside from being costly and impractical for larger-scale studies, labeled cargoes or lipids can alter the interactions between the cargo and the lipids or even modify the lipid structure itself. This means that these systems may not accurately reflect the characteristics of the unlabeled formulation, leading to a potential mismatch between model and real-world formulations.

4.4. Surface Characterization. The ζ potential is the electrical potential at the boundary of an electric double layer,[214] which separates freely moving fluid around a charged particle from fluid attached to its surface. This attached layer consists of bound counterions (the Stern layer) and a surrounding region of loosely bound ions.[214] It is often measured to give an indication of LNPs' surface characteristics using light scattering techniques.[160,214,215] When an electric field is applied, charged particles migrate with a velocity proportional to the ζ potential.[214,215] The change in velocity is measured through shifts in the frequency (in electrophoretic light scattering, ELS) or phase (in phase analysis light scattering, PALS) of a reference laser beam.[214,215] ζ potentials above 30 mV [positive or negative (preferred)] are typically desired for long-term LNP stability to prevent aggregation.[160] However, lower ζ potentials do not necessarily imply aggregation, as steric stabilization by PEGylated lipids also plays a role.[214] ζ potential is highly dependent on pH, ionic strength, and temperature,[214] so LNPs should be measured in the same solvent used in their final formulation for accurate results.

Tunable resistive pulse sensing (TRPS) is a single-particle technique that employs the Coulter counter principle to measure surface charge and size simultaneously.[216−218] TRPS features a conical tunable elastomeric pore mounted horizontally between two electrolyte reservoirs, with the sample in one of the reservoirs.[216] As particles pass through the pore, electrolyte displacement causes a current drop, which correlates with nanoparticle size and surface charge. TRPS provides more precise ζ potential measurements compared to PALS and allows for ζ potential distribution across the nanoparticle population.[217]

Cryogenic X-ray photoelectron spectroscopy (cryo-XPS) has also been employed to probe surface-specific information, typically within the top few nanometers, particularly regarding the PEGylated lipid layer in mRNA-loaded LNPs.[219] One promising label-free analytical technique is single-particle automated Raman trapping analysis (SPARTA), which is effective for studying the functionalization of LNPs.[220] Additionally, SPARTA enables the investigation of chemical composition differences between individual LNPs, revealing sample heterogeneity[220]

4.5. Molecular Interactions. *4.5.1. Nuclear Magnetic Resonance (NMR).* NMR spectroscopy is a powerful analytical technique commonly used to investigate organic molecules. By applying a strong magnetic field and radiofrequency radiation, NMR probes the local environment of specific atomic nuclei, such as hydrogen (^{1}H), nitrogen (^{15}N), carbon (^{13}C), and phosphorus (^{31}P), providing detailed structural information on individual molecules. NMR spectroscopy is particularly valuable for characterizing LNPs, enabling the assessment of LNP size distributions, lipid and mRNA distribution within the nanoparticles, and the uniformity of different formulation processes.[130,221−223]

^{1}H NMR is an essential tool for accurately profiling the surface characteristics of LNPs. It can be used to determine the lipid composition, surface density, and the conformation of PEG side chains of PEGylated lipids.[224] Additionally, NMR is capable of studying the pK_a of ionizable water-soluble lipid analogues, with results that closely match theoretical predictions.[58] ^{1}H NMR

https://doi.org/10.1021/acsnano.4c18274
ACS Nano XXXX, XXX, XXX−XXX

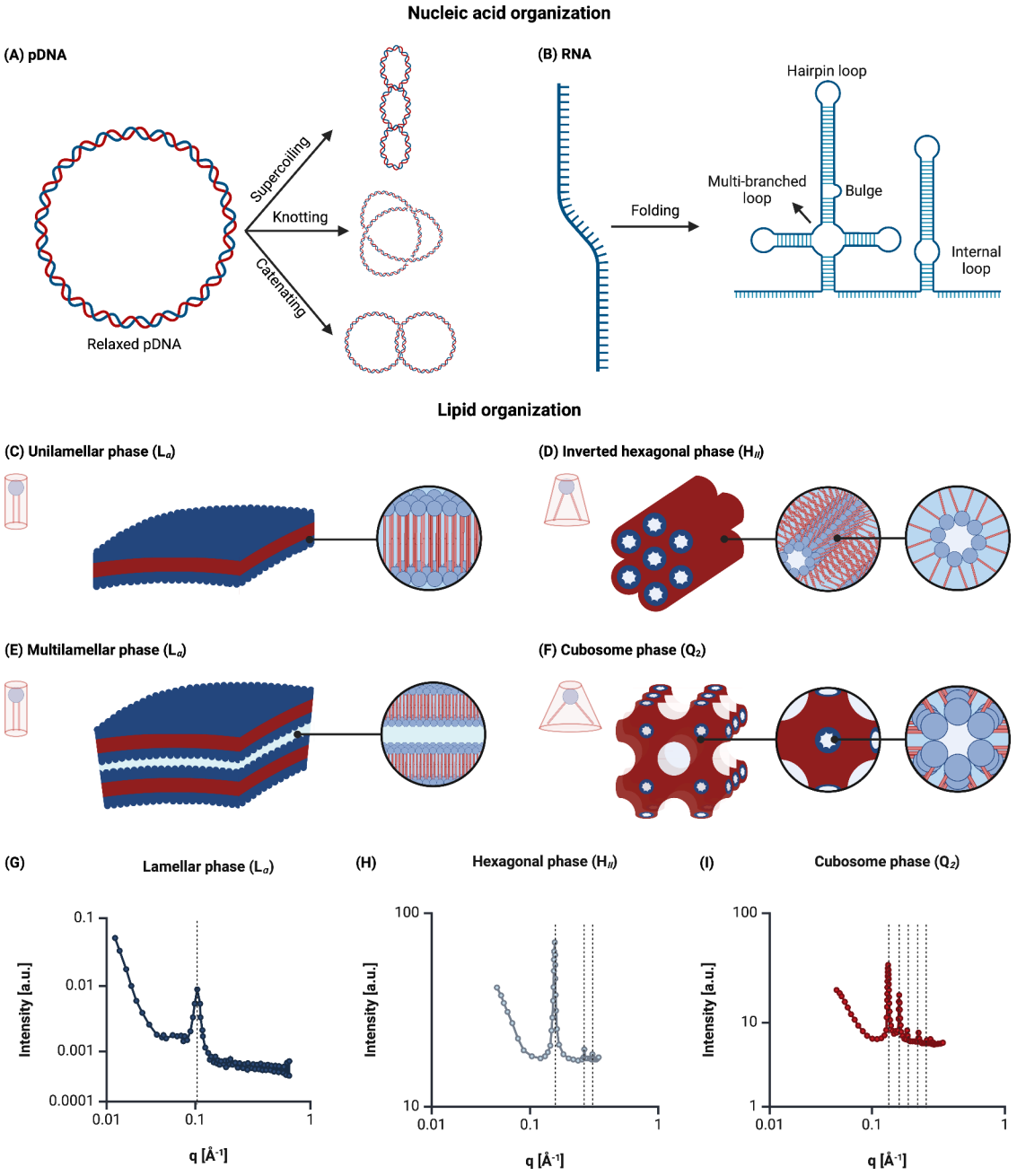

Figure 5. Schematic of NATs and lipids' structures. Interactions of the nucleotides can lead to secondary/tertiary structures in (A) pDNA and (B) RNA. (C−I) Representative lipid phases that appear in LNPs and can form from ILs, either alone or in combination with phospholipid: Cylindrical-shaped lipids tend to form (C) unilamellar or (E) multilamellar phases (L_α). Cone-shaped lipids tend to form nonbilayer inverted phases, such as (D) hexagonal H_{II} phases or (F) cubosome phases (Q_2). (G) SAXS profile of LNPs with a characteristic lamellar phase. Adapted with permission from ref 133 under the Creative Commons Attribution 4.0 International License. (H and I) SAXS profiles of particles with a characteristic hexagonal and cubosome phase. Adapted with permission from ref 235. Copyright 2016 American Chemical Society. Created with BioRender.com.

relaxometry has been applied to study the effects of lipids such as DSPC and cholesterol on the structural and physicochemical properties of siRNA-loaded LNPs.[71] Dynamic nuclear polarization-enhanced (DNP) NMR has provided insights into the layered architecture of LNPs.[225] ^{31}P NMR has been used to analyze phospholipids within LNPs, providing information on structural homogeneity, the assembly of the lipid layer, and potentially a method to assess batch-to-batch reproducibility.[226]

4.5.2. Fluorescence-Based Techniques. FRET is mostly employed to investigate the coalescence of the LNPs after dialysis or buffer exchange[25,37,76,109,133] and study the intracellular and *in vivo* biofate of LNPs.[227,228] For FRET, LNPs are formulated with a donor probe (e.g., DiO Ex 484 nm, Em 501 nm[76]) and an acceptor probe (e.g., Dil Ex 549 nm, Em 565 nm[76]). When the donor probe is excited and is in close proximity of the acceptor probe, the fluorescence from the acceptor probe confirms the fusion of the LNPs/membranes. Zhao et al.[229] formulated LNPs with a pH-sensitive dye-based DNA probe and used FRET to determine the internal pH of LNPs.

https://doi.org/10.1021/acsnano.4c18274
ACS Nano XXXX, XXX, XXX−XXX

The TNS (used to determine LNP pK_a[230]) and RiboGreen assays (used to determine EE; see Section 4.3) are two commonly employed fluorescent-based assays for characterizing LNP formulations. Various studies have utilized fluorescent binders for mRNA (e.g., thionine[38]), fluorescent tags for mRNA (e.g., Cy5-tagged mRNA[156]) or fluorescent lipids (e.g., Cy5-PEGylated lipid[211]) for mRNA localization in LNPs[38] or payload characterization of LNP formulations.[156,201,211−213] Some limitations of fluorescence-based techniques are difficult interpretability, poor scalability due to cost, and potential interference of binders/tags with laser-based characterization techniques (e.g., in DLS the fluorescence signal may interfere with scattering). In addition, the fluorescent labels might affect the LNP structure/dynamics.

5. STRUCTURAL FEATURES OF INDIVIDUAL COMPONENTS

5.1. Lipid Organization. Lipids, the primary components of LNPs, self-assemble into lyotropic mesostructures in aqueous solutions due to their amphiphilic nature—polar heads and hydrophobic tails—forming closed structures to shield their tails from water.[231] These mesostructures are also commonly found in LNPs, with the most prevalent being: lamellar (L_α), hexagonal (H_{II}), and cubic (Q_2);[232] see Figure 5. The lamellar phase consists of lipids arranged into planar bilayers, which consist of two layers of lipids with their hydrophobic tails facing inward and hydrophilic heads facing outward toward the aqueous environment.[231] Multiple bilayers separated by an aqueous region is called multilamellar organization. In the hexagonal phase, lipids form inverted cylindrical micelles,[231] where hydrophobic tails face outward, that result in inverted water-filled tubules. The cubic phase is even more complex, consisting of highly ordered 3D networks where lipids form curve bilayers that create intricate, periodic structures, as shown in Figure 5. Phospholipids are known to organize more into lamellar phases, whereas ILs generally prefer to assemble into the hexagonal phase.[70,230]

Lipid organization in aqueous systems, whether pure or mixed, is conceptually predicted using the packing parameter[51,231]

$$P = V/al \quad (1)$$

with V the tail (or hydrocarbon) volume, a the effective area per molecule at the interface, and l the surfactant tail length. P is thus considered a measure for the preferred curvature. This way, the lipids' "shape property" (e.g., cylindrical vs cone-shaped) dictates their preferred phases.[231,232] For $P > 1$ nanostructures with negative curvature are formed, like the inverted hexagonal phase (H_{II}). For $P \approx 1$ lamellar (L_α) structures (no curvature) are adopted. For $P \ll 1$ lipids assembly into micelles. Lipids with saturated hydrocarbon tails, such as DSPC, are classified as cylindrical lipids.[13,44,48] Due to their lower intrinsic membrane curvature, they tend to form LNPs with stable lamellar structures.[13,48] In contrast, lipids with unsaturated tails (e.g., DOPE) or branched tails (e.g., ALC-0315, SM-102) exhibit higher membrane curvature and a cone-shaped geometry, favoring the formation of LNPs with more "fusogenic" inverted hexagonal (H_{II}) phase.[13,44,48]

Apart from the IL structure, also the helper phospholipids play a role in facilitating specific lipid organizations.[55,111,233] Lipid phase behavior also depends on temperature, pH, ionic strength, hydration, composition, and intermolecular factors such as association interactions, steric hindrance, and packing constraints.[39,231] The packing parameter offers a simplified framework but lacks explicit treatment of these variables. Comprehensive characterization requires high-resolution structural tools such as SAXS and cryoTEM.

Lipid packing directly influences membrane curvature, local chemical environment, and apparent pK_a, thereby modulating LNP internal structure.[36,163] Crucially, certain mesophases—such as inverse hexagonal and cubic symmetries—enhance nucleic acid delivery efficiency[11,30,31,39,44,189,234] (see Section 7.3).

5.2. Nucleic Acid Cargo Structure. Nucleic acids, including different types of RNA and DNA, are polyanionic macromolecules made up of negatively charged nucleotides (NTs) linked by a sugar−phosphate backbone. Their structure is defined at four levels: primary (linear nucleotide sequence), secondary (base pairing), tertiary (long-range interactions between base-paired regions), and quaternary (higher order folding), resulting in structures such as duplexes, hairpins, and junctions.[236,237] The cargo in LNPs can be different types of nucleic acid chains, such as siRNA, mRNA, ASO, SAM, and pDNA. The cargo vary significantly in size and structure (Figure 5), influencing LNP formation. siRNA typically has 20−24 base pairs, is double-stranded, and has a well-defined structure. mRNA is single-stranded, much larger at about 1000 nucleotides long, with variability in size and structure depending on the mRNA type. Antisense oligonucleotides (ASOs), which are designed to bind to specific mRNA sequences, are typically even shorter than siRNA, ranging from 10 to 30 nucleotides in length. SAM, capable of generating new mRNA copies, ranges from 9000 to 15000 nucleotides. pDNA typically exists as a circular strand ranging from hundreds to thousands of nucleotides, though linear forms of pDNA can also be used.

Unlike the fully connected, hydrogen-bonded double helix structure of DNA, which arises from the perfect alignment of complementary sequences (A-T, C-G), RNA is a single strand, with siRNA intentionally synthesized as a double-stranded molecule as an exception. This single-stranded form gives RNA greater flexibility, allowing it to fold into complex secondary and tertiary structures provided the chain is long enough. Both siRNA and ASO are, for example, vulnerable to degradation due to their minimal or lack of secondary structure, with ASOs being particularly susceptible.[68] In the case of mRNA, the secondary and tertiary structure influences the behavior and properties of the LNPs.[236] The primary base pairings in RNA are A-U and G-C base pairs (also known as Watson−Crick base pairs), along with the less stable G-U interaction, known as the wobble base pair.[238,239] Additionally, noncanonical base pairs, base triples, and pseudoknots are three other types of special base pairs that also occur in RNA secondary structures.[240] RNA's secondary structure is composed of short helical regions that form when complementary sections of the RNA sequence pair. These helical regions typically consist of 2 to 10 base pairs, as single isolated pairs are generally unstable, and helices with more than 10 continuous base pairs are uncommon.[239] Given that an RNA sequence does not have perfect pairing throughout, the secondary structure also features various single-stranded regions that interrupt the helices, forming distinctive motifs such as hairpin loops, bulges, internal loops, and multibranched loops (Figure 5). To determine RNA secondary structure from its sequence, comparative sequence analysis[241] combined with score-based methods such as RNAalifold,[242,243] have been extensively used over the past decades. In recent years, machine learning-based methods have also gained popularity.[238] The 3D

https://doi.org/10.1021/acsnano.4c18274
ACS Nano XXXX, XXX, XXX−XXX

shape of RNA (tertiary structure) has been studied less extensively than that of proteins, primarily due to the challenges involved in RNA crystallization. The prevailing view of RNA folding is hierarchical, where stable secondary structures form first, followed by the bending of the RNA around flexible single-stranded regions to form the tertiary structure.[132,236,239]

pDNA is a stable, circular, double-stranded helical structure. While the topological state of circular pDNA may begin as an isolated, unknotted closed curve, its length often leads to the emergence of various topologies (Figure 5). A pDNA molecule can form knots with itself or undergo positive or negative supercoiling, inducing stress and spatial deformations in the helix. Additionally, pDNA molecules can undergo catenation or hemicatenation, resulting in interlinked structures between two separate pDNA molecules.[244] These various topological forms of plasmids can affect their interaction with the LNPs.

The extent to which these RNA and pDNA structures can maintain their native folding within an LNP remains an open question. Inside LNPs, large nucleic acid chains must adapt to the nanoparticle's shape, with coarse-grained simulations suggesting that mRNA may adopt an inverted morphology.[245] AFM data show that mRNA is coiled, with surrounding lipids screening surface charges.[174] Due to mRNA's large size, it may not fit into smaller LNPs (60−150 nm) without folding into dense loops or coils.[182]

Although traditionally seen as simple carriers of genetic information, mRNA secondary and tertiary structures are crucial for their function.[246] For instance, the mRNA start codon must remain single-stranded to align properly within the ribosomal preinitiation complex for translation initiation, with misfolding potentially disrupting this process.[247] The therapeutic efficacy of nucleic acid cargos in LNP formulations is thus influenced by their higher-order structures and microenvironment within the LNP.[132]

6. STRUCTURAL AND MORPHOLOGICAL LNP FEATURES

LNPs are multicomponent supramolecular assemblies whose structure combines features from the pure lipid phase (including the lipid mesostructures) with emergent features such as structural heterogeneity, phase separation, and dynamic transitions arising from component interplay.

6.1. Structural LNP Models. Several structural models have been proposed for LNPs,[13,18,130,224,225] accompanied by a wide range of illustrative representations—rarely to scale,[182] often oversimplified, and primarily descriptive rather than quantitative. These visualizations reflect the ongoing uncertainties and misconceptions surrounding LNP internal architecture—often ignoring structural heterogeneity while overemphasizing uniformity and sphericity.

The multilamellar vesicle (MLV) model proposes that LNPs consist of concentric lipid bilayers, forming an "onion-like" structure with uniformly distributed components.[26,182,225] However, this model fails to align with experimental findings,[18,225] particularly cryoTEM images, which reveal an electron-dense hydrophobic core rather than a neatly layered architecture.[225] A more accurate representation thus describes LNPs as core−shell structures,[37,40,103,178] where the therapeutic cargo is housed within a protective compartment.[1] This structural organization occurs regardless of cargo type—whether siRNA,[37,122,164] mRNA,[24] pDNA,[40] or even in the absence of cargo.[37] The inner compartment consists of an electron-dense, lipid-rich core surrounded by one or more concentric lipid shells.[24,37,122,164] This contrasts with liposomes, which lack such an electron-dense core.[248] Within core−shell models, a distinction can be made between nanostructured cores,[178,225] which feature complex internal organization (possibly with different lipid phases), and homogeneous (isotropic) cores,[18,225] in which components are homogeneously distributed. Both experimental and computational studies indicate an asymmetric distribution between the core and shell,[24,37,178,225,249] suggesting that the nanostructured core models are physically more accurate.

6.2. Core Composition and Cargo Localization. Three key questions persist in the debate surrounding LNP cores: First, how does the lipid composition vary between the core and shell, as well as between the inner and outer leaflets of the membrane, given its nonuniform distribution. These composition differences are challenging to identify due to the similar elemental composition of the lipid components.[161] Second, what is the internal structure of the core, and where exactly is the cargo located within it? Third, how many copies of the cargo are present in a single LNP?

In terms of composition, ILs are nearly twice as concentrated in the core compared to the shell.[178] Protonated ILs complex with the cargo, with the cargo acting almost as glue between the lipid layers.[230] For example, siRNA cargo within an inverted micelle (see further) exhibits reduced mobility compared to its free tumbling in an aqueous environment.[37] Excess neutral ILs (after buffer exchange) that are not complexed with the cargo contribute to the electron-dense core, by separating from the phospholipids, forming an oily phase (which is different from the ordered phases in the core).[37,40,122,223] These oil droplets can be stabilized by a lipid monolayer,[122] typically including some of the phospholipids. The core likely also contains some small amounts of cholesterol (see Section 6.3). An example of the core and shell composition, determined using SANS, after dialysis for a benchmark LNP formulation is shown in Figure 10. While cargo size has minimal impact on core/shell composition, excess IL at high N/P ratios may increasingly localize to the shell, lowering the relative IL molar fraction in the core[40,103] and a decrease in the solvent volume fraction in the core.[103] In addition, drug-free LNPs and LNPs dialyzed to neutal pH have more ILs in the shell, likely due to the absence of IL−mRNA complexation.[196,197]

Table 1 illustrates that lipids in the core organize, at least partially, into either inverted hexagonal or lamellar phases, or a combination of both (an example is shown in Figure 8 and a schematic is shown in Figure 6). Alongside these ordered regions, there can also be completely disordered lipid phases, especially at low N/P ratios, that are structural precursors to the inverse H_{II} phase.[30] The internal lipid organization has an important impact on the endosomal escape efficiency, as discussed in Section 7.3.

The nucleic acid cargo resides in the aqueous core (for example in small 3−9 nm pockets),[37] despite the water content in the core being potentially as low as 5 wt %.[250] An additional point of interest is whether the cargo preferentially resides within the inverted micelles (for siRNA[37] or is intercalated, sandwiched between the lamellar lipid bilayers (for siRNA,[27,71,122] or mRNA[251]). Yanez Arteta et al.[24] found that, in the absence of mRNA, LNPs form a regular inverse H_{II} phase. However, in the presence of mRNA, this order is disrupted, leading to a disordered H_{II} phase or wormlike inverse micelles (current scattering theories are not able to discriminate between

https://doi.org/10.1021/acsnano.4c18274
ACS Nano XXXX, XXX, XXX−XXX

Table 1. Representative Internal Structures and Cargo Locations for Nucleic Acid Therapeutics-Loaded LNPs Reported in the Literature

method	cargo	internal structure	cargo location	
SAXS	drug-free	H_{II}	N/A	24
SAXS	polyA	H_{II}	aqueous core	39
cryoTEM	ASO	H_{II}, L_{α}, disorder	aqueous region	30
cryoTEM and SAXS	siRNA	H_{II}, L_{α}, Q_2	aqueous region	189
cryoTEM and SAXS	siRNA	H_{II}, L_{α}	aqueous region	133
cryoTEM and SAXS	siRNA	H_{II}, L_{α}	aqueous core	122
SAXS	mRNA	disordered H_{II}	aqueous region	24
cryoTEM and SAXS	mRNA	H_{II}, L_{α}, Q_2	aqueous region	189
cryoTEM	mRNA	oily core	aqueous bleb	38, 227
SAXS	mRNA	L_{α}	aqueous core	39
cryoTEM and SAXS	mRNA	H_{II}, L_{α}	aqueous core	252
cryoTEM and SAXS	mRNA	L_{α}, disordered	aqueous core	26
cryoTEM	saRNA	oily core	aqueous bleb	169

the two). The presence of cubosomes for siRNA- and mRNA-loaded LNPs is mentioned far less.[189]

Another aspect of interest is the number of copies of the cargo in a single LNP. Short-chain nucleic acid cargoes, such as siRNA, have a large number of copies in a single LNP.[155] For larger cargoes, such as mRNA, the average number of copies in a single LNP ranges from 1 to 5.[156,196,197,201] An increase in the pH and number of nucleotides in the cargo and a decrease in the N/P ratio and PEG lipid molar fraction usually results in a higher average number of copies of payload in an LNP.[58,156,196] All these findings highlight the complexity of the LNP core, with variations in reported composition likely arising from differences in formulation, preparation, and storage conditions. Ultimately, LNPs cannot be categorized into a single structural type.

6.3. Shell Composition. LNP shells consist of lamellar structures primarily made of hydrophobic lipid aggregates.[37] These shells can form as a monolayer, bilayer, or multilamellar layer (Figure 5),[37] with most LNPs believed to have bilayer shells.[44,178] In other studies, SANS data corresponded well to a monolayer, roughly 2.4 nm in size.[24] Several studies[24,169,178,225] have confirmed that phospholipids are enriched on the LNP surface. This enrichment could be attributed to the formation of an unfavorable IL−cargo structure in the core, causing the phospholipid to segregate away from it. Recent research[130] has shown that also ILs can coexist in the lipid envelope and interact with the PEGylated lipids.

The distribution of cholesterol within LNPs remains debated. Molecular simulations suggest cholesterol is evenly distributed between the core and shell[37] and experimental studies confirm its presence in both regions.[169,178] However, due to cholesterol's low solubility in ILs, other research suggests that cholesterol cannot be uniformly distributed,[44] as excess cholesterol leads to crystallization or demixing, creating local cholesterol-rich

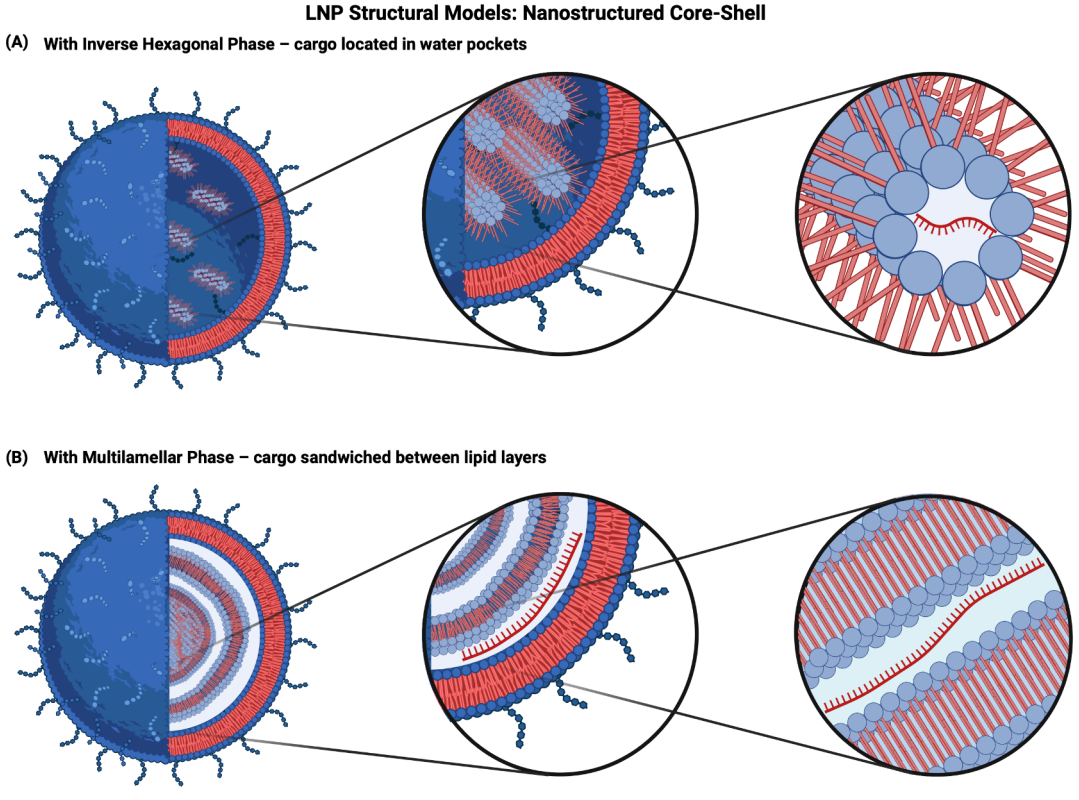

Figure 6. Nanostructured core−shell LNP model: (A) LNP with an inverse hexagonal phase (H_{II}) in the core with nucleic acid cargo located in the water pockets and (B) LNP with a multilamellar phase (L_{α}) with nucleic acid cargo sandwiched in the aqueous layers between two lipid layers. Adapted with permission from ref 225. Copyright 2019 American Chemical Society. The nanostructured core model is widely regarded as the most realistic depiction of LNP internal organization based on current evidence. These schematic representations are not to scale, and significant differences in cargo size exist across various LNPs. Created with Biorender.com.

https://doi.org/10.1021/acsnano.4c18274
ACS Nano XXXX, XXX, XXX−XXX

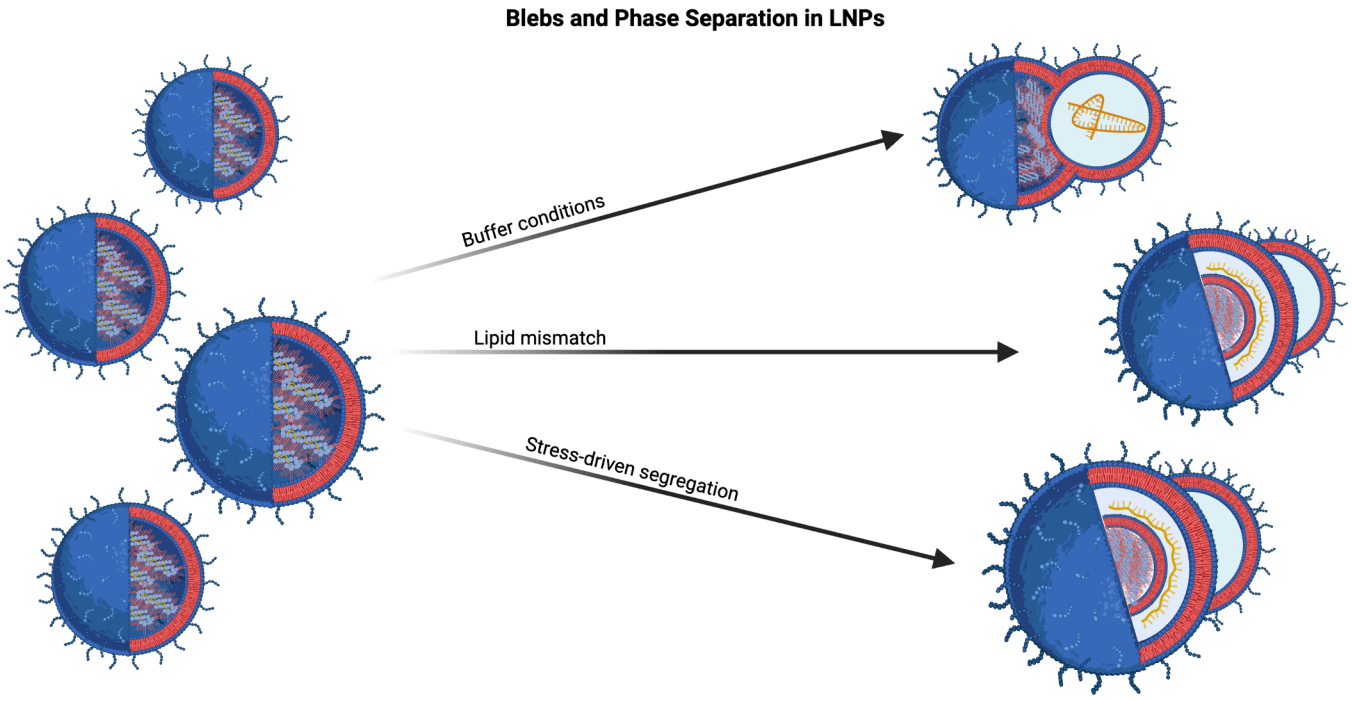

Figure 7. Formulation and postformulation factors contributing to bleb and phase separation in LNPs. Created with BioRender.com.

zones.[71,253] These studies state that the LNP shell is cholesterol-rich, with concentrations 2−4 times higher than in the core.[24,178,254]

The outermost layer of LNPs is coated with a relatively homogeneous layer of PEGylated lipids,[37] which can adopt either a mushroom-like (sparsely packed) or brush-like (densely packed) conformation based on the packing density.[224] The latter affects the hydration number of the PEG molecules.[255] Yanez Arteta et al.[24] describe a mushroom-like arrangement of PEGylated lipids, approximately 4 nm in size (based on SANS), as an outer shell.

6.4. Blebs and Phase Separation. LNPs are often assumed to be spherical. However, many studies have imaged LNPs with highly nonspherical morphologies[26,37,38,169] showing protruding structures, aka "blebs", which (often but not necessarily) consist of an aqueous core surrounded by a lipid bilayer.[42,70,132] An example of such a bleb-like particle is shown in Figure 8. Bleb formation is caused by phase separation (or segregation) of the IL and other lipids present in the LNPs (primarily the phospholipids).[37,42,132] In more extreme cases, the aqueous structures can completely engulf the electron-dense part of the LNP.[119,131] For a detailed discussion specifically on blebs, we refer to ref 42.

Blebs often appear grainy[38,182] and are debated as structural defects.[42] Compelling evidence, however, links bleb-like features to enhanced transfection efficiencies,[25,131,256] possibly due to the enhanced integrity of the cargo. However, excessive cargo loading—often accompanied by bleb formation (see further)—compromises *in vivo* efficacy.[204] In LNPs, blebs may be aqueous—resembling liposomal substructures—or cargo-containing, especially when mottled.[38,132] They are more prevalent in mRNA- than siRNA-loaded LNPs (see Section 6.6),[132] with extreme bleb-dominated, cylindrical morphologies observed in SAM-loaded systems.[169]

Several factors can induce phase separation in LNPs (Figure 7). Spontaneous phase separation may arise from lipid incompatibility,[131,257,258] such as mismatches in molecular geometry, unfavorable packing, lipid immiscibility, or local asymmetries induced by the presence of cargo, or even overloading of cargo. Both the structure and the local concentration of the different lipids matter. Increasing the phospholipid content to 40 mol % yielded LNPs with a diminished core and an internal aqueous compartment enclosed by a lipid bilayer.[131] LNP fractions with lower mRNA loading levels (payload) exhibited smaller and fewer blebs (as shown in Figure 9).[204] Environmental conditions also play a key role:[25,113,129,257] shifts in the pH can alter IL protonation, while changes in the buffer molarity may lead to charge screening—both of which disrupt lipid organization and promote instability. Similarly, conducting formulation at lower FRRs (i.e., higher ethanol content) can result in the formation of additional liposomal lipid layers around the LNP core.[119] Higher ionic strength promotes morphological heterogeneity: mRNA-loaded LNPs formulated in 300 mM citrate exhibited 76% bleb formation vs 2% at 25 mM.[25] This is attributed to enhanced IL-mediated fusion, which increases the number of aqueous compartments available for mRNA loading during buffer exchange (see Sections 3.1 and 4). Finally, stress-induced rearrangements, particularly mechanical stresses during formulation[108] or lyophilization,[259,260] can also contribute to phase separation.

6.5. Drug-Free Particles. There are some concerns about the homogeneity of LNPs, particularly in terms of cargo (payload).[212] A key question is whether all LNPs in a formulation encapsulate cargo or if many particles remain drug-free, and how this affects the efficacy. These particles are often referred to as "empty" to denote the absence of cargo rather than the actual emptiness of their structure. The presence of drug-free LNPs is not without consequence, as they have been shown to induce increased inflammation compared to loaded LNPs.[261]

For smaller NAT such as siRNA, one LNP can encapsulate hundreds of siRNA molecules.[155,161] Henrickson et al.[205] reported no measurable drug-free LNPs for siRNA (20

https://doi.org/10.1021/acsnano.4c18274
ACS Nano XXXX, XXX, XXX−XXX

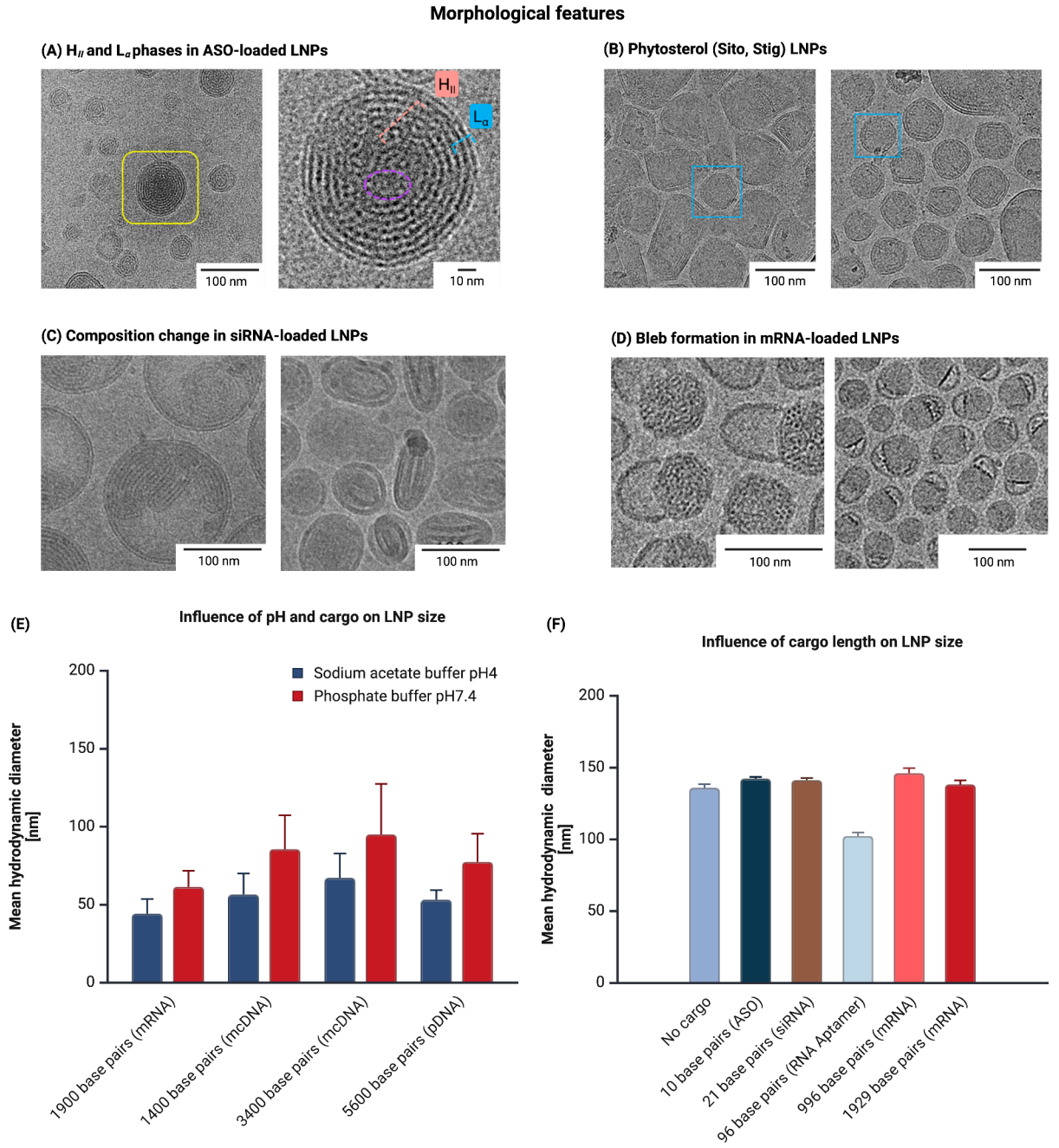

Figure 8. Overview of key morphological features relevant to LNPs: CryoTEM images showcasing different LNP morphologies. (A) ASO-loaded LNPs (N/P = 2) displaying both the H_{II} (orange) and L_α (blue) lipid phases, with a disordered phase marked by the purple circle. These lipid phases were identified using SAXS. Adapted with permission from ref 30 under the Creative Commons Attribution 4.0 International License. (B) LNPs incorporating phytosterols in place of cholesterol, resulting in nonspherical morphology. The blue box highlights a clear multilamellar structure. Adapted with permission from ref 26 under the ACS public use license. (C) Morphological effects of composition changes in siRNA-loaded LNPs, with varying IL, phospholipid, and cholesterol ratios (left and right panels). Concentric bilayer LNPs are observed. Adapted with permission from ref 254. Copyright 2019 Royal Society of Chemistry. (D) Bleb-like morphology in mRNA-loaded LNPs. Adapted with permission from ref 38 under the Creative Commons Attribution 4.0 International License. (E) Effect of buffer exchange on the LNPs' particle size with different cargoes. Adapted with permission from ref 76. Copyright 2019 Royal Society of Chemistry. (F) Influence of the cargo length on the LNPs' particle size. Adapted with permission from ref 68 under the Creative Commons Attribution 4.0 International License. Created with BioRender.com.

nucleotides). Other reports suggest a low fraction (<20%) of drug-free LNPs for siRNA encapsulation.[211,212] However, for LNPs encapsulating larger cargoes, such as mRNA (900−5000 nucleotides), payload variability increases, often resulting in a higher fraction of drug-free LNPs.[197,201,206,212] This is in line with other research, as Kulkarni et al.[76] demonstrated via cryoTEM that LNPs loaded with GNPs contained drug-free particles, with the fraction varying based on GNP size—approximately 75% for 5 nm GNPs and 25% for 12 nm GNPs. It has been suggested[103] that LNPs have a maximum mass limit, which could potentially limit the amount of encapsulated cargo, though this remains invalidated.

https://doi.org/10.1021/acsnano.4c18274
ACS Nano XXXX, XXX, XXX−XXX

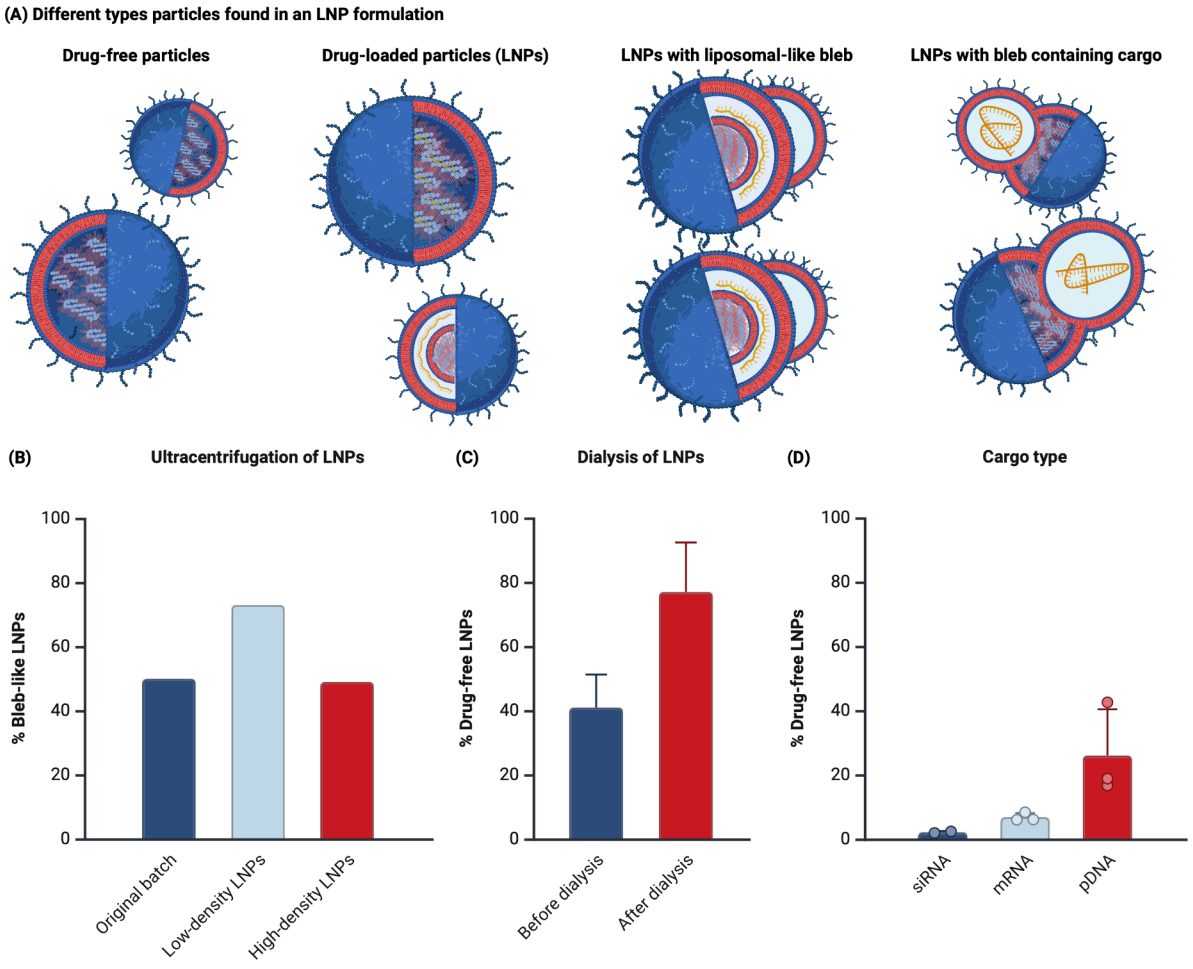

Figure 9. (A) Different types of particles that can be found in an LNP formulation: drug-free LNP, drug-loaded LNP, LNP with liposomal-like bleb, and LNP with bleb containing mRNA. (B) Quantification of bleb-like LNPs based on density fractions determined by AUC. Data extracted from Liao et al.[204] (C) Fraction of drug-free LNPs before and after dialysis. Data extracted from Li et al.[156] (D) Effect of the cargo type on the fraction of drug-free LNPs. Adapted with permission from ref 212 under the Creative Commons Attribution 4.0 International License. Created with BioRender.com.

Table 2 gives an overview of different reported fraction in the literature. Higher N/P ratio results in a lower fraction of drug-free LNPs.[156,201] Discrepancies in reported values can stem not only from variations in formulation components, conditions, and cargo, but also from differences in measurement sensitivity, sample preparation artifacts, and the ability to accurately distinguish truly empty LNPs from those with low payload content. Additionally, the accuracy of novel measurement techniques can be difficult to evaluate, making direct comparisons challenging. These challenges make it difficult to establish generally applicable heuristics, highlighting the importance of interpreting reported values with caution.

How the absence of cargo affects the internal structure of LNPs is challenging to assess, as most structural measurements typically provide an average of both loaded and drug-free particles. One study found that in terms of lipid distribution and shell thickness, both mRNA-loaded and drug-free LNPs where found to be similar, although the solvent content is lower in the drug-free LNPs.[197] Variations in the payload per LNP do lead to a heterogeneous distribution of LNPs with differing charge ratios,[204] which may affect the efficacy.[58] Typically loaded LNPs are larger than drug-free LNPs with a smaller PDI,[24,26,68] with some exceptions.[68] Liao et al.[204] found no variation in lipid composition across different LNP subpopulations, but did observe that fractions with higher mRNA loading were the least potent both *in vitro* and *in vivo*.

Figure 10 shows the internal structural organization of mRNA-loaded LNPs for a benchmark formulation. The presence of drug-free LNPs results in broad or distinct peaks (representing loaded and drug-free subpopulations) in SAXS signals.[29,103,234] Specifically, Iscaro et al.[234] observed an increase in the Q_2 peak, corresponding to drug-free LNPs, with higher N/P ratios, suggesting an increasing fraction of drug-free LNPs. Analyzing peak intensity may prove to be a useful approach for estimating drug-free LNP fractions.

6.6. Impact of Cargo. Despite being described as a "platform technology", this does not imply that LNPs are entirely cargo-independent. Indeed, concerns persist that formulations tailored for one cargo may not readily translate to another.[68] Such adaptation challenges are particularly evident for the two most commonly encapsulated cargoes: siRNA and mRNA.[178]

Some direct comparisons between LNPs with different cargo sizes have been reported,[68,70,103,262] with a specific example shown in Figure 10. A general trend is that larger and more structurally complex cargo molecules—such as mRNA compared to siRNA—tend to induce more pronounced structural features that deviate from the typical spherical LNP

https://doi.org/10.1021/acsnano.4c18274
ACS Nano XXXX, XXX, XXX−XXX

Table 2. Reported Fractions of Drug-Free Particles in the Literature, Measured Using Various Techniques and Different Encapsulated Cargoes[a]

method	cargo	drug-free fraction	
single LNP heterogeneity assay	siRNA (21 nucleotides)	5.8 ± 3.8%	212
single LNP heterogeneity assay	mRNA (996 nucleotides)	12.1 ± 2.0%	212
single LNP heterogeneity assay	mRNA (2700 basepairs)	26.4 ± 14.3%	212
NanoFCM	mRNA (2856 nucleotides)	27.6 ± 2.9%	197
NanoFCM	mRNA	4.5−21.0%	101
NanoFCM	mRNA	13−32.7%	101
single-particle profiling	mRNA (1800 nucleotides)	59.3 ± 4%	201
CICS	siRNA	26.3 ± 6.4%	211
CICS	mRNA (996 nucleotides)	66.5 ± 5.8%	156
CICS	mRNA (1929 nucleotides)	77.0 ± 8.0%	156

[a]The percentages represent the fraction of empty particles after dialysis to neutral pH. Prior to dialysis, a drug-free fraction of 41 ± 10% was reported in ref 156. For ref 101, the first value corresponds to the drug-free fraction measured after one-step TFF, while the second reflects the fraction after a two-step purification process.

model. However, whether this is due to their size, double-stranded nature, higher diffusivity (which enhances mixing during assembly), or a combination of these factors remains unclear. The most important observations related to the effect of cargo are summarized in Table 3.

6.7. Impact of Lipid Composition. The overarching factor that governs LNP structure is the chemistry of the individual components, along with their molar ratios. An example of how a change in the lipid composition can affect the LNP morphology is shown in Figure 8. Research efforts have been focused on designing "fusogenic" LNPs with desired internal structures and morphologies in part by tuning the molar fraction of the four principal lipid components.

The lipid structure has an impact on the final morphology (see Section 5.1). By substituting the cylindrical lipids with cone-shaped lipids or by increasing the cone-shaped lipids molar fraction, the blebs fraction can be reduced[70] and the H_{II} internal structure is promoted.[133] In addition, increasing the molar fraction of cylindrical phospholipid results in an increase in the bleb fraction, with 30% resulting or more in bilayer LNPs.[37,122,131]

Beyond lipid structure, the relative molar ratios significantly influence LNP properties. Given the four-component system, a large number of permutations are possible. Rather than exhaustively detailing how each relative change affects the system, we provide a few representative examples in Table 4. From these, some generalizable trends become apparent: Changing the phospholipid-to-cholesterol ratio or the PEGylated lipid concentration[30,254] influences on the morphology. Cholesterol plays a crucial role in shaping LNP structures.[26,27,71,164] Excessive cholesterol can lead to deformed structures and high contrast in cryoTEM images.[71] Crawford et al.[164] observed that LNPs with low PEGylated lipid and high cholesterol content tend to be more spherical, while high PEGylated lipid and low cholesterol formulations produce less spherical particles. Altering cholesterol derivatives during formulation was shown to lead to various structural changes, such as bilamellar, multilamellar, and polymorphic shapes[26] and to tune the LNP elasticity.[186] For instance, replacing cholesterol with C-24 alkyl phytosterols—a class of cholesterol analogues—results in LNPs with more faceted, polyhedral structures, potentially due to phase separation (e.g., due to crystallization) or differences in membrane rigidity.[26,27] Other analogues had varying effects; for example,[27] those with a modified tail incorporating a fifth ring showed low encapsulation efficiencies. This distinct external morphology may enhance transfection efficiency, though the internal structure remains unchanged.[27] An example of LNPs with cholesterol analogues is shown in Figure 8. In addition, increasing either the molar fraction of the PEGylated lipid or the PEG chain length has resulted in lower bleb fraction[254] and highly disordered structure.[30]

6.8. Mapping CPPs to Structural Features. Section 3.3 explores the relationship between CPPs and various LNP quality attributes. While deriving generalizable conclusions about the effects of specific CPPs on LNP structure is challenging, certain observations can be made regarding CPPs that govern the physicochemical environment during LNP self-assembly. In particular, those parameters that influence electrostatic and protonation-dependent interactions between the nucleic acid cargo and ILs play a significant role in governing the internal structure. These include the N/P ratio, buffer species, buffer molarity, and pH.

Lowering the formulation buffer pH can induce the LNP internal structure transition from the L_α to H_{II} or Q_2 structure.[39,111,193,234] The transition is driven by an increase in the packing density.[193,234] Cullis' group[25,109] has demonstrated that higher buffer molarity promotes fusion of LNPs, leading to a higher fraction of bleb-like particles.[25] Higher buffer molarity favors highly ordered internal structure with a higher membrane curvature. For instance, higher buffer molarity for sodium acetate enhances the H_{II} signal in the SAXS profile.[263] Compared to sodium acetate, LNPs formulated with sodium citrate buffer, a trivalent buffer, have a higher-order internal structure (as evidenced by a sharp SAXS signal), higher-packing density structure (H_{II}), a larger fraction of bleb-like particles,[25,263] and larger blebs.[257] Overall, the protonation state of the IL headgroup, modulated by the ionic species and ionic strength, governs the structural and morphological characteristics of the LNPs.

Apart from the buffer, increasing the charge (N/P) ratio results in an higher-order internal structure for siRNA-loaded LNPs[70,133,264] and ASO-loaded LNPs.[30] A higher N/P ratio for mRNA promotes formation of bleb-like particles and an increase in the bleb count per-particle and the bleb size.[204]

In contrast, other CPPs, like the TFR, have been reported to not influence the internal structure, irrespective of the particle size.[125] Ethanol (the amount is controlled by the FRR) has been shown to disrupt or hinder the structured lipid organization in the LNP core. Structural reorganization typically happens over time, either due to ethanol removal[103] or due to annealing.[113] Apart from modulating the ethanol content other effects of FRR on the internal structure remain unclear.

7. POSTFORMULATION STRUCTURAL EVOLUTION

7.1. During Handling and Storage. LNPs often exhibit limited physical (e.g., particle size and surface charge) and chemical (e.g., mRNA and lipid integrity, due to hydrolysis and oxidation) stability, sometimes lasting only hours at room temperature (e.g., COVID-19 vaccines).[35] Significant morpho-

https://doi.org/10.1021/acsnano.4c18274
ACS Nano XXXX, XXX, XXX−XXX

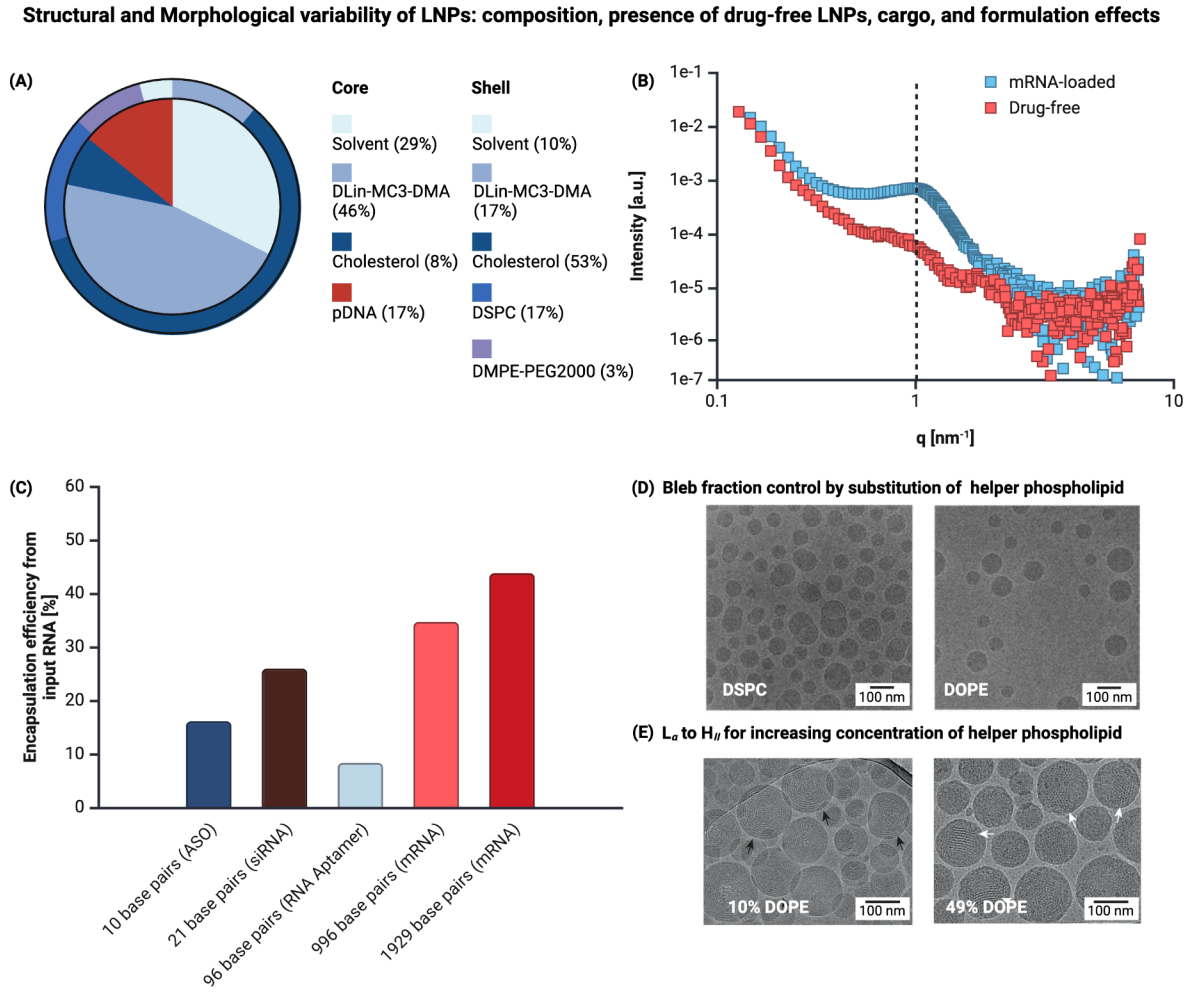

Figure 10. Structural and morphological variability of LNPs: composition, presence of drug-free LNPs, cargo, and formulation effects for different benchmark LNP formulations. (A) Lipid composition of the core and shell in pDNA-loaded LNPs, determined via SANS, after dialysis to neutral pH. Adapted with permission from ref 103 under the Creative Commons Attribution 4.0 International License. (B) SAXS characterization of drug-free and mRNA-loaded LNPs, highlighting the presence of a distinct internal structure for LNPs with encapsulated mRNA. Data extracted with permission from Yanez Arteta et al.[24] (C) EE, defined as the ratio of encapsulated RNA to input RNA concentration, for various cargo types using a modified RiboGreen assay. Adapted with permission from ref 68 under the Creative Commons Attribution 4.0 International License. (D) Influence of helper phospholipids on the bleb-like particle morphology of mRNA-loaded LNPs. Adapted with permission from ref 70. Copyright 2015 American Chemical Society. (E) Transformation from L_α to H_{II} on the increasing the molar fraction of DOPE in the lipid composition for siRNA-loaded LNPs. The black arrows indicate the L_α structure and the white arrows indicate the H_{II} structure in the LNP core. Adapted with permission from ref 133 under the Creative Commons Attribution 4.0 International License. Created with Biorender.com.

Table 3. Comparison of Different Structural and Morphological Aspects When Changing from siRNA-Loaded to mRNA-Loaded LNPs, Highlighting the Impact of Cargo Size and Complexity[a]

aspect	siRNA	mRNA	
particle size	similar	similar	68
EE	lower	higher	68
optimal N/P	lower	higher	18
phase separation	low degree	high degree	70, 132
internal structure disorder	lower	higher	24
drug-free fraction	lower	higher	212
packing density	higher	lower	68
stability	better	worse	103
core composition	similar	similar	103

[a]The stability effect and core composition mentioned is extrapolated from results reported in ref 103.

logical changes have been observed after storage: mRNA-loaded LNPs stored at 4 °C for 1 day displayed increased size, shape heterogeneity, and rougher surfaces compared to the smooth, spherical appearance of freshly prepared LNPs.[182] Subjecting LNPs to various forms of stress (like shaking or freeze−thaw cycles) may result in aggregation, the formation of liposomes, or the release of mRNA.[38] As a result, storage measures, typically involving ultracold temperatures, are employed to preserve their structure. Various strategies are being explored to enhance the long-term stability and shelf life of LNPs,[35] including water removal techniques such as freeze-drying[265] (or more advanced techniques like spin-freeze-drying,[260] thin-film freezing and drying[266,267]) and spray-drying.[268] While a comprehensive discussion of storage and postformulation handling is beyond the scope of this review, some key considerations are highlighted.

https://doi.org/10.1021/acsnano.4c18274
ACS Nano XXXX, XXX, XXX−XXX

Table 4. Summary of the Influence of the Lipid Composition on the LNP Structure and Morphology[a]

formulation	molar fraction (%)	cargo	structure	morphology	
MC3:Chol:ESM:DMG-PEG	50:38.5:10:1.5	mRNA	oily core	spherical	131
MC3:Chol:ESM:DMG-PEG	38.5:30:30:1.5	mRNA	oily core	blebs and bilayer structure	131
MC3:Chol:ESM:DMG-PEG	27.25:21.25:50:1.5	mRNA	oily core	bilayer structure	131
MC3:Chol:DSPC:DMG-PEG	50:38.5:10:1.5	mRNA	unilamellar (L_α) and oily core	spherical	7
MC3:Sito:DSPC:DMG-PEG	50:38.5:10:1.5	mRNA	multilamellar (L_α) and oily core	polymorphic and flaceted	7
MC3:Fuco:DSPC:DMG-PEG	50:38.5:10:1.5	mRNA	multilamellar (L_α) and disordered	blebs	7
KC2:Chol:DSPC:DMG-PEG2000	50:38.5:10:1.5	siRNA (N/P = 1)	multilamellar (L_α, concentric rings)	spherical	122
KC2:Chol:DSPC:DMG-PEG2000	50:38.5:10:1.5	siRNA (N/P = 6)	unilamellar (L_α)	spherical	122
DODAP:Chol:DOPE:DMG-PEG2000	50:39:10:1	siRNA	multilamellar (L_α)	spherical	133
DODAP:Chol:DOPE:DMG-PEG2000	50:0:49:1	siRNA	H_{II}	spherical	133
KC2:Chol:DSPC:DMA-PEG	50:37.5:11.5:1	mRNA	oily core	blebs	70
KC2:Chol:DOPE:DMA-PEG	50:37.5:11.5:1	mRNA	oily core	spherical	70
MC3:Chol:DSPC:DMG-PEG	50:38.5:10:1.5	mRNA	oily core	blebs (76%)	25
SM-102:Chol:DSPC:DMG-PEG	50:38.5:10:1.5	mRNA	oily core	blebs (21%)	25
MC3:Chol:DSPC:DMG-PEG2000	40:39:10:1	ASO	H_{II}, L_α, and disordered (small fraction)	spherical	30
MC3:Chol:DSPC:DMG-PEG2000	40:35:10:5	ASO	highly disordered and H_{II}, L_α	spherical	30
SM-102:Chol:MO	50:0:50	PolyA	multilamellar (L_α) and Q_2	N/A	234
SM-102:Chol:MO	50:40:10	PolyA	multilamellar (L_α)	N/A	234

[a]The "formulation" column depicts the IL, cholesterol (or cholesterol derivatives), phospholipid, and PEGylated lipid employed in the formulation. The "molar fraction" column shows the % molar fraction of IL:cholesterol:phospholipid:PEGylated lipid used. MC3 refers to IL DLin-MC3-DMA, KC2 to IL DLin-KC2-DMA, Chol to cholesterol, Stig to stigmastanol, Fuco to fucosterol, ESM to egg sphingomyelin, MO to monoolein, and DMG-PEG to PEGylated lipid.

The freezing process can induce structural changes resulting in LNPs that differ considerably from the ones after formulation. For example, during the freezing stage, fusion between LNPs can occur,[195] which may lead to the formation of blebs, depending on the presence of buffers[260] (Figure 11). Another study showed that thawed mRNA vaccine LNPs developed electron-dense semicircular caps—likely phospholipid bilayers—that were absent in freshly prepared formulations.[182] The buffer composition plays a crucial role in the structure and stability of LNPs during postformulation handling.[35,259,260,269] The use of a phosphate-buffered saline (PBS) appears to be problematic for LNP stability, leading to aggregation, structural heterogeneity, and phase transitions (from amorphous toward multilamellar), especially under freeze−thaw or long-term storage conditions.[35,259,260,269] PBS-stored LNPs displayed a heterogeneous internal organization and liposomal-like structures, whereas HEPES-stored LNPs formed hourglass-shaped particles.[259] Buffers like Tris and HEPES act as cryoprotectants and provide better structural preservation and stability.[259,260] Beyond buffer selection, other factors such as formulation (N/P ratio,[260] lipid composition[266]), the addition of cryoprotectants and excipients[35,270] can be optimized to further enhance LNP stability.

Also mechanical stress can induce instability problems. The stability of Comirnaty COVID-19 vaccines was assessed by subjecting them to various shear forces, including shaking, vortexing, dropping from different heights, and needle drawing/injection.[271] While no significant differences in the LNP size or PDI were observed between gently handled and vaccines subjected to height drops, physical stability was compromised when shaken or repeatedly drawn through a needle,[271] as shown in Figure 11. Other studies have also reported that the size distribution of NAT-loaded LNPs is altered upon shear,[167,207,272,273] sometimes accompanied by a decrease in EE.[167,272]

7.2. Behavior in Physiological Conditions. Beyond storage stability, LNPs must also be able to respond to the interactions with the complex biological milieu in which they are administered. Studies have shown that LNPs' performance *in vivo* is strongly influenced by interactions with components of the biological environment,[274] such as plasma proteins, including opsonins, which mark the particles for clearance by the immune system. The complex interactions between nanoparticles and the biological environment may explain unexpectedly poor *in vivo* performance.[275]

The LNP stability in physiological conditions is typically correlated with the size and ζ potential[274] but is also strongly influenced by their structural characteristics. The most significant structural alteration upon exposure to biological fluids, such as blood, is the formation of a protein corona—an interfacial layer formed by the adsorption of proteins and biomolecules onto the LNP surface.[54,276] This complex biological coating can impact the LNP's physicochemical properties, biodistribution, and overall therapeutic and pathophysiological behavior.[54,276] The impact of a specific protein, Apolipoprotein E, present in the blood and its binding to the surface of LNPs has been extensively studied.[178] It has been demonstrated that upon interaction, not only does the LNP surface undergo changes, but the lipid components within the nanoparticle also undergo significant internal reorganization.[178]

The inclusion of PEGylated lipids in LNP formulations helps form a hydrophilic steric barrier that limits protein corona formation, reduces opsonization, and prolongs circulation time.[54,277] However, mobile PEG on the LNP surface can also negatively impact therapeutic efficacy by limiting cellular uptake or altering the release of the encapsulated drug.[78,277] A portion of the PEG leaves the LNP surface following intravenous administration, partially counteracting this issue and allowing for improved performance.[78,277]

Other structural changes in LNPs upon interaction with biological environments include pH-induced changes (discussed in Section 7.3) as well as LNP fusion or agglomeration and degradation, which in extreme cases can even lead to

https://doi.org/10.1021/acsnano.4c18274
ACS Nano XXXX, XXX, XXX−XXX

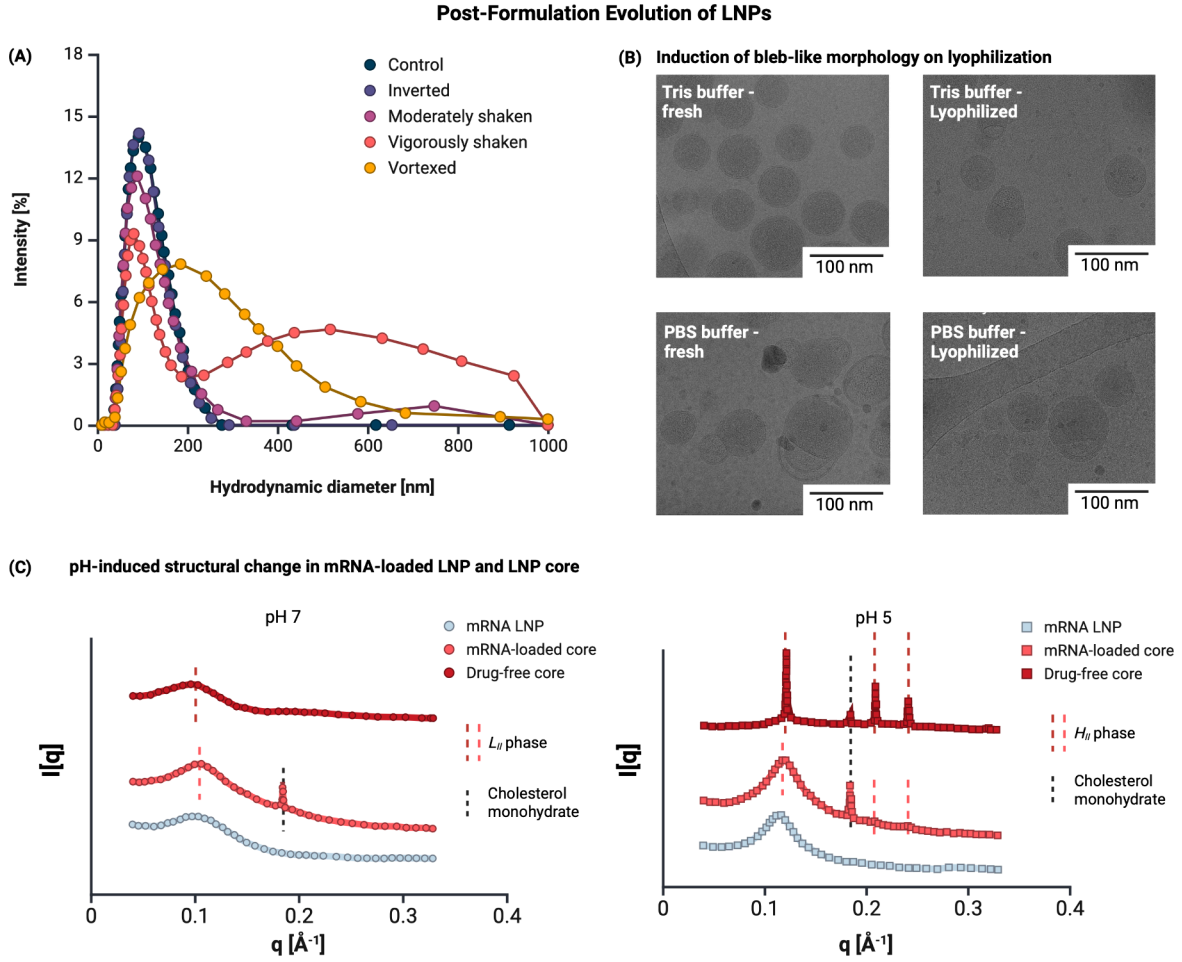

Figure 11. Postformulation structural evolution of LNPs. (A) PSDs determined using DLS for Comirnaty vaccines after different types of mixing during postformulation handling. Adapted with permission from ref 271 under the Creative Commons Attribution 4.0 International License. (B) Morphology of mRNA-loaded LNPs pre- and postlyophilization in Tris buffer and PBS. Adapted with permission from ref 260. Copyright 2023 Elsevier. (C) pH-induced structural transition of mRNA-loaded LNP, mRNA-loaded core (DLin-MC3-DMA/cholesterol/mRNA), and drug-free core (DLin-MC3-DMA/cholesterol). At neutral pH (pH 7), the LNP and the core have a L_{II} structure, which transitions to a H_{II} structure upon acidification to pH 5. Adapted from ref 39 under the Creative Commons Attribution 4.0 International License. Created with Biorender.com.

complete LNP disassembly.[274] For instance, a study on the interaction between LNPs and phospholipase D—an endogenous enzyme that cleaves choline headgroups from phospholipids—revealed that the enzyme can fully penetrate the LNP structure and convert the encapsulated phospholipids into negatively charged lipids.[158]

7.3. Endosomal Acidification. When an LNP enters a cell through endocytosis, it is enclosed in an early endosome that matures over time into late endosomes and then lysosomes.[11,278] Efficient delivery requires the release of the cargo into the cytosol before maturation into lysosomes.[11] During intracellular trafficking, the pH surrounding the LNP drops progressively due to protonation—from neutral (7.4) in the extracellular fluid to 6.8−6.1 in early endosomes, 6.0−4.8 in late endosomes, and eventually 4.5 in lysosomes.[278] Due to the pH sensitivity of the IL, this process can trigger structural changes in the LNP. Although the mechanism through which cargo escapes from the endosome is subject of debate[11]—two possible mechanisms are shown in Figure 1—it is clear that the internal structure of the LNP has an impact. The propensity to form inverse hexagonal (H_{II}) or cubosome (Q_2) phases has been strongly correlated with enhanced endosomal escape.[11,30,31,39,44,189,234]

Lowering the pH can trigger mesophase transitions in LNP lipids, typically evolving from inverse micellar to inverse hexagonal (H_{II}) and then to other structured phases[31,36,39,40,111,193,263,279] on the millisecond[193] or hour[112] time scale. A key focus in LNP research is developing formulations that respond to physiological pH and temperature (37 °C) cues by adopting internal structures—such as the H_{II} phase—that promote membrane fusion and enhance endosomal escape.

Even within the same lipid family, ILs can display markedly different packing behaviors along the pH trajectory—for instance, nearest-neighbor packing can differ by up to 30% between DLin-MC3-DMA and DLin-DMA.[39] The presence of cargo, like RNA, has a strong impact on the lipid ionization[36] and the lipid organization. In the presence of polyA, a complexed H_{II} nucleic acid phase has been observed which coexists with other mesophases.[39] Apart from such internal structural evolutions, Li et al.[40] showed that acidification induces a 46.6% volume expansion (from 467 to 530 Å) in pDNA-loaded LNPs, attributed to osmotic water influx due to incomplete complexation by newly protonated ILs. Lipid redistribution from shell to core was also observed.[40] LNPs formulated in

https://doi.org/10.1021/acsnano.4c18274
ACS Nano XXXX, XXX, XXX−XXX

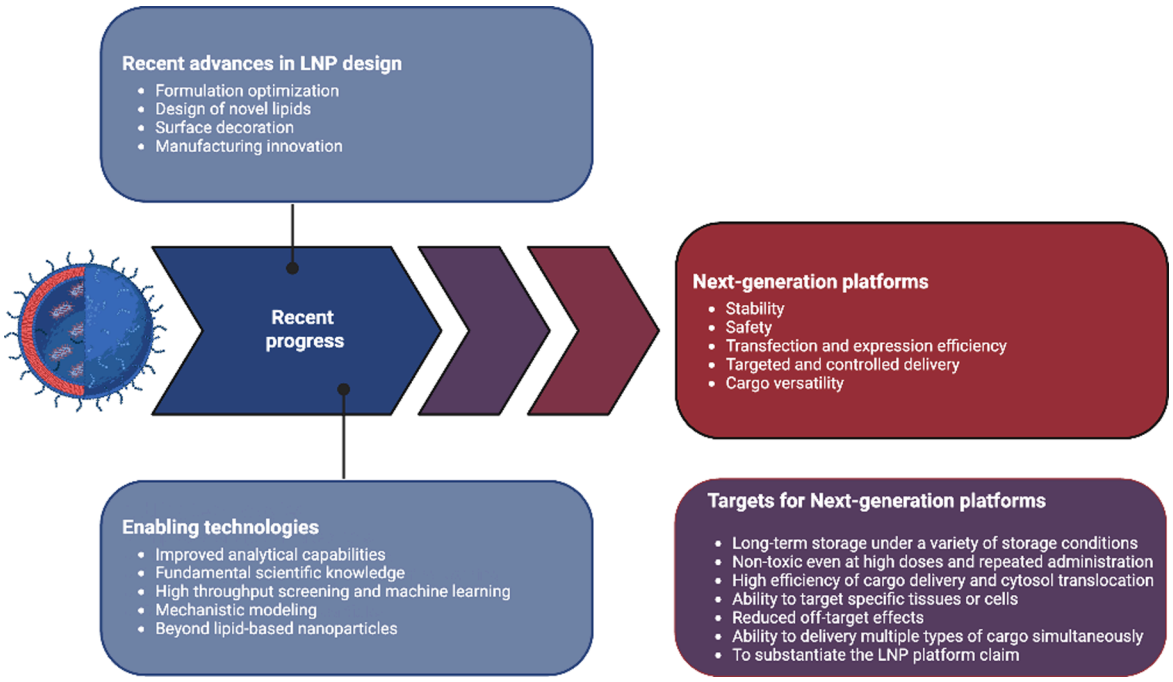

Figure 12. Overview of recent advancements in the development of next-generation NAT-loaded LNPs, emphasizing innovations in LNP design and enabling technologies. Potential high-level targets for the development of next-generation LNP platforms, aimed at enhancing therapeutic efficacy, broadening application potential, and improving safety, are listed. Created with BioRender.com.

citrate buffers show enhanced *in vitro* expression compared to phosphate or acetate, likely because citrate promotes the H_{II} phase, while phosphate and acetate stabilize the inverse lamellar phase and require lower pH to induce the inverse hexagonal transition.[263]

8. OPEN QUESTIONS IN CURRENT-GENERATION LNPS

Despite all the research outlined in this review, many aspects of the LNP structure and behavior remain unresolved. Key open questions include the following:

- Thermodynamics and kinetics of self-assembly, including unresolved aspects of phase behavior and phase separation
- Lipid localization and interactions, particularly how different lipids distribute and influence each other within the LNP
- Lipid dynamics, both at the molecular level and in terms of larger-scale processes such as fusion
- Interplay between lipid composition, process parameters, and structural organization, which remains highly complex and nontrivial to predict
- Precise role of certain internal structures on the stability of LNPs
- How to reliably predict *in vivo* LNP behavior based on structural attributes and physiochemical characteristics

9. TOWARD THE DESIGN OF NEXT-GENERATION PLATFORMS

9.1. Goals for Next-Generation Platforms. A significant amount of research and development by academia and industry is actively underway, employing a variety of sophisticated and creative approaches, to develop the next generation of nanoparticulate delivery systems for nucleic acid therapeutics. An overview of this path forward is provided in Figure 12. Thematically, these efforts can be categorized into (a) developing a deeper understanding of NAT delivery systems (its production, structure, and/or function) and (b) developing delivery systems that improve key functionalities. The main goals that are being pursued in the next generation of NAT delivery technologies are (in no particular order) as follows:

- **Product Safety** NAT-loaded LNPs and their constituents/metabolites can have undesirable immunogenic effects and can pose toxicity concerns that need to be better understood and mitigated.[280] A key target for next-generation LNPs is to minimize toxicity and adverse immunogenicity while maximizing therapeutic efficacy, to enable high-dose therapies and/or repeated aministration.
- **Product Stability** Ensuring the integrity of the nucleic acid cargo and that other CQAs are in spec is important for ensuring the efficacy of the drug product. Long-term shelf-stability of NAT-loaded LNPs, preferably at room temperature and under different storage conditions, will improve access to NATs at lower costs.[281,282]
- **Transfection and Expression Efficiency** Current nucleic acid delivery platforms have low endosomal escape efficiency ($\leq 10\%$).[283,284] With new therapeutic applications potentially requiring significantly higher dosages, improving the transfection efficacy and the therapeutic effect per unit of cargo administered (e.g., protein expression) is an important target for next-generation LNPs.
- **Targeted and Controlled Delivery** Delivery systems with enhanced targeting capabilities toward specific cells and/or tissues can enable the treatment of conditions where conventional NAT-loaded LNPs biodistribution limits its efficacy. In addition, targeted delivery can help improve transfection efficiency while minimizing off-target effects and dose-related toxicity concerns.

https://doi.org/10.1021/acsnano.4c18274
ACS Nano XXXX, XXX, XXX−XXX

- **Cargo Versatility** The ability for the delivery system to function as a platform technology i.e., the system can be adapted with minimal effort to effectively deliver a variety of nucleic acid constructs would accelerate drug discovery and development. Co-delivery of multiple nucleic acid constructs is also of interest for the development of multivalent vaccines and gene therapies.[283,285]

Approaching nucleic acid delivery as a systems challenge, there are two layers to consider in the formulation−structure−activity relationship. The first layer consists of the mapping between manufacturing process conditions and the physicochemical attributes of the relevant species to the delivery vector structure and quality attributes, while the second layer relates the delivery vector structure and quality attributes to its efficacy. As next-generation platforms are likely to become increasingly sophisticated with more complex constituents, it is also likely that particle structures and properties are going to become more complex, underscoring the need for a deeper understanding of both layers of the formulation−structure−activity relationship to enable optimization.

9.2. Recent Advances in LNP Design. In the pursuit of producing LNPs that can better achieve the various objectives listed above, a variety of approaches have been considered:

- **Formulation Optimization** Tuning the LNP formulation, involving both the selection of the constituents and their relative ratio, is one of the most commonly carried out LNP optimization procedures and is performed in view of some or all of the objectives listed above. In the context of targeted delivery, we refer the reader to the recent review by Vasileva et al.[46] which outlines developments in LNP formulation and lipid design to facilitate targeted delivery.
- **Novel Lipid Design** Often carried out in parallel with formulation optimization, the identification of novel lipids to achieve the various objectives is of high interest. Both high-throughput screening and rational design approaches have yielded novel lipids that are reported to improve various properties such as transfection efficacy,[286] desirable adjuvant effects,[287] and targeted delivery.[46,288] While considerable attention has been directed toward the IL (and modifications/substitutions thereof), the engineering of other lipid components such as cholesterol[27] and the PEGylated lipid[289,290] are also being explored. A novel approach was recently developed based on ionizable phospholipids (iPhos), which incorporate a pH-responsive zwitterionic headgroup and three hydrophobic tails to enhance endosomal escape and enable organ-selective delivery.[291] When formulated with helper lipids, iPhos-based LNPs preferentially targeted the spleen, liver, or lungs, depending on the composition. A complementary strategy to expand tissue-specific delivery is the Selective ORgan Targeting (SORT) system, which introduces a fifth component (i.e., a SORT molecule) into conventional four-component LNP formulations.[54,292] SORT molecules are lipids with defined charge properties (e.g., permanently cationic, anionic, or ionizable) that are incorporated in controlled molar ratios to modulate LNP surface characteristics and protein corona. The SORT system enabled predictable redirection of LNP biodistribution to organs beyond the liver, including the lungs, spleen, and kidneys, offering a promising avenue for organ- and cell-type-specific delivery.[293−296] The primary rationale behind the novel lipid design is to modulate the pK_a and tail branching to promote the formation of H_{II} phase, thereby enhancing endosomal escape.
- **Surface Decoration** One of the primary routes for enabling targeted delivery currently being explored is the functionalization of the LNP surface with moieties that bind to receptors expressed on the desired cell populations.[296,297] Typically, small-molecule ligands, peptides, or monoclonal antibodies are conjugated to the surface of LNPs for this purpose.[45,54] Functionalization of LNPs with mannose ligands led to selective delivery to liver sinusoidal endothelial cells and minimal uptake by hepatocytes, which are instead predominantly targeted by naive LNP formulations.[298] LNPs conjugated with antibodies that bind to the platelet-endothelial cell adhesion molecule (PECAM-1) delivered mRNA to the lungs with a 200-fold increase compared to nontargeted LNPs.[299] Hematopoietic stem cell-targeted LNPs, conjugated with antibodies against CD117, demonstrated the ability to deliver mRNA to hematopoietic stem cells *in vivo*.[300] Notably, *in vivo* generation of chimeric antigen receptor (CAR) T cells entirely inside the body was recently achieved by delivering mRNA cargo to T lymphocytes through LNPs decorated with CD5-targeted antibodies.[301] Although advantageous for targeted delivery, surface functionalization can influence the internal lipid organization by modulating lipid curvature and packing near the interface — an aspect often neglected in formulation studies.
- **Manufacturing Process Optimization and Innovation** As outlined in Section 3.3, the manufacturing process can have a profound impact on various CQAs and therapeutic efficacy of the drug product. This can be seen as a double-edged sword: On the one hand, it is clear that robust controls and process optimization are crucial for producing efficacious NAT-loaded LNPs. On the other hand, the manufacturing process can be seen as a degree of freedom that is available for LNP optimization. For example, the same production process can be adapted to generate LNPs of various size distributions for different applications. In addition, as NAT-loaded LNPs drug products become more complex, it is likely that innovations in the manufacturing process may become necessary to support the development and scale-up of these products such as novel rapid mixing protocols.[302]

9.3. Enabling Technologies for the Design of Next-Generation Platforms. It should be recognized that LNP optimization is a challenging multiobjective optimization problem with an incredibly large design space. In that context, the synergistic and holistic optimization of LNPs (i.e., systematically exploring all possible avenues for optimization ranging from construct optimization all the way to process development) is necessary for achieving efficacious nucleic acid delivery. In light of the complexity of this task, a range of enabling technologies, of varying technological maturity, have emerged to support this endeavor:

- **Improved Analytical and Characterization Capabilities** As outlined in Section 4, there are a diverse and growing range of analytical capabilities for characterizing LNP systems. As these techniques and know-how for using and interpreting the results mature, the availability of rich data

https://doi.org/10.1021/acsnano.4c18274
ACS Nano XXXX, XXX, XXX−XXX

sets will increase, facilitating a deeper understanding of LNP systems and support product and process development.

- **Fundamental Biochemistry and Pharmacokinetics/Dynamics** With increasing amounts of fundamental research and clinical studies, we are progressively developing a deeper understanding of the biology and biochemistry of the LNPs, their constituents, and their uptake by cells for a variety of indications. This insight can be used to guide novel design choices and improve LNP efficacy significantly. For example, advances in targeted LNPs have leveraged tissue or cell-specific environmental conditions, such as pH or hypoxia, to design stimuli-responsive formulations for improved RNA delivery.[303,304] For instance, LNPs incorporating acid-degradable lipids have led to formulations that rapidly hydrolyze within endosomes, delivering mRNA to multiple organs with higher efficiency compared to conventional LNPs.[286] Another example is the development of biphosphonate-functionalized lipid-like materials for LNPs which enabled the delivery of mRNA cargo to the bone microenvironment,[288] leveraging the insight that biphosphonates can chelate strongly with the calcium in bones.
- **High-Throughput Screening and Machine Learning** Data-driven approaches using machine learning in conjunction with high-throughput screening have emerged as a viable method for optimizing LNP formulations, identifying novel lipids, and characterizing important process and material attributes. The input features to the model (which depend on the purpose of the model) typically include molecular descriptors of the various species present and/or the formulation/process operating conditions. Such approaches have been successfully applied to model various parts of the relationship such as that between IL types and efficacy (e.g., transfection efficacy/immune response),[22,23,305,306] LNP formulation/process conditions and LNP product quality attributes,[307−309] and a combination thereof.[310,311] The use of sparse machine learning methods and/or techniques that facilitate the interpretation of machine learning models [e.g., SHapley Additive exPlanations (SHAP)] have enabled the identification of significant features that provides insights on material and process property−structure−function relationships, and consequently a means by which LNPs can be optimized. The interested reader is referred to the recent review by[312] which provides a comprehensive overview of commonly used methods and strategies for incorporating machine learning to augment the development and characterization of LNPs.

In terms of novel lipid design and structure−function relationships, machine learning has demonstrated its utility in identifying efficacious novel lipids such as IL 119−23, which contains an adamantyl group in the linker, and demonstrates comparable if not superior mRNA expression in *in vivo* mice models with the ability to target multiple key organs such as the lungs with a 5 component SORT formulation.[23] Other studies have also yielded insight regarding groups and structural features in the IL that guide design such as the advantage of having phenol groups in the lipid functional head or that there the length of the linker and tail needs to be optimized with there being trade-off between lipid membrane stability and efficacy.[310] Machine learning has also found utility in developing process models relating various formulation and manufacturing inputs such as the N/P ratio and FRR/TFR to LNP quality attributes such as size and ζ potential with the machine learning model capturing trends observed experimentally such as an increase in the FRR leading to a smaller particle size.[307] The ability of these machine learning models to capture the complex trends in LNP production engenders the possibility of employing advanced optimization methods such as Bayesian optimization for formulation optimization and process development.[312]

The selection of the optimal formulations in a high-throughput screening workflow is typically based on *in vitro* testing on model cell lines,[313,314] although a poor correlation between *in vivo* and *in vitro* delivery performance has been documented for several targets.[118,119] High-throughput screening incorporating *in vivo* testing data can potentially overcome this limitation[315] though it can be costly if done naively. A novel strategy employing peptide-encoded mRNA barcodes enabled the rapid evaluation of over 400 LNP formulations in just nine mice, optimizing a biodegradable LNP for liver-targeted mRNA delivery.[315]

- **Mechanistic Modeling for LNP Optimization** Mechanistic/first-principles modeling of LNPs (in the context of nucleic acid therapeutics) is still in its nascent phase, but in view of its success in other complex pharmaceutical and chemical applications,[316,317] we anticipate that it will be a powerful enabling technology for NAT-loaded LNP development going forward. A detailed discussion of mechanistic modeling approaches for LNPs for nucleic acid delivery is beyond the scope of this review, but additional information can be found in a recent perspective article.[318]

The majority of physics-based modeling work thus far has been centered on applying molecular simulation methods such as molecular dynamics (both coarse-grained and atomistic) to probe the LNP structure,[33,36,37,98,223,245,249,253,319−321] as recently reviewed by Paloncýová et al.[322] While molecular dynamics-based approaches provide detailed molecular insights into LNPs, they remain severely restricted in studying larger scale systems (e.g., multiple particles/longer time scales/larger nucleic acid constructs) due to their high computational cost. At larger length and time scales such as at the reactor scale, mechanistic modeling approaches such as computational fluid dynamics and population balance models have been used to optimize the mixer design (e.g., see refs 323 and 324) and model related (albeit simpler) nanoparticulate systems (e.g., see ref 325).

- **Beyond Lipid-Based Nanoparticles** Lipid-based nanoparticles have demonstrated the most significant clinical success in nonviral delivery of NATs.[326] However, researchers have extensively explored alternative nanoparticle delivery platforms, including inorganic[327,328] and polymeric[329−332] systems. Among polymeric approaches, cell-penetrating peptide-based nanoparticles have emerged as particularly promising vectors, characterized by low immunogenicity and design flexibility that enable high targeting capabilities.[330,333−335] The unprecedented success of LNPs provides a valuable blueprint for advancing the other nanoparticle systems, especially for increasing their transfection efficiency. Key optimization strategies include modulating surface charge and hydro-

https://doi.org/10.1021/acsnano.4c18274
ACS Nano XXXX, XXX, XXX−XXX

phobicity to enhance cellular uptake and endosomal escape, as well as developing robust payload protection mechanisms. Further, the development of novel structural configurations of polymer−lipid hybrid nanoparticles represents a critical research avenue for creating systems with enhanced targeting capabilities, reduced immunogenicity, increased payload capacity, and controlled release properties.[328,336,337]

10. CONCLUSIONS

Nucleic acid therapeutics offer immense potential for groundbreaking treatments. LNPs are at the forefront of enabling such breakthrough therapies as the most advanced delivery system currently available. This review highlights the current understanding of LNP structural and morphological features, emphasizing their complexity and the challenges that remain. Despite significant advancements and widespread recognition of the importance of LNP structure, its dynamic and multifaceted features remain elusive. This is largely due to the vast array of parameters—including lipid composition, cargo size, formulation conditions, and environmental factors—that govern the LNP structure. Compounding these challenges is the difficulty of structural characterization, which is time- and resource-intensive. As a result, few studies provide a comprehensive view of LNP structure, often focusing instead on isolated features.

This has left the relationships between formulation, structure, and activity poorly understood, with few generalizable principles established. Addressing these gaps will require refined and more accessible tools and methodologies for characterizing LNP morphology and behavior across their life-cycle (from formulation until use). Such tools could help answer key questions, such as the origins of bleb-like structures or the implications of cargo-free particles on therapeutic efficacy. Greater standardization in formulation and characterization practices could also mitigate some of the variability that hinders progress. At the same time, maintaining flexibility to screen for and develop more effective formulations remains essential.

Despite these challenges, the field is advancing rapidly and continues to improve. Embracing the inherent complexity of LNP systems will enable the design of more precise and reliable delivery vectors, leveraging a vast parameter space to optimize outcomes. Such an approach will be pivotal in driving the development of next-generation nucleic acid−based therapies.

AUTHOR INFORMATION

Corresponding Author

Allan S. Myerson − *Department of Chemical Engineering, Massachusetts Institute of Technology, Cambridge, Massachusetts 02139, United States;* orcid.org/0000-0002-7468-8093; Email: myerson@mit.edu

Authors

Aniket Udepurkar − *Department of Chemical Engineering, Massachusetts Institute of Technology, Cambridge, Massachusetts 02139, United States;* orcid.org/0000-0001-9958-412X

Cedric Devos − *Department of Chemical Engineering, Massachusetts Institute of Technology, Cambridge, Massachusetts 02139, United States;* orcid.org/0000-0002-8154-4872

Peter Sagmeister − *Department of Chemical Engineering, Massachusetts Institute of Technology, Cambridge, Massachusetts 02139, United States;* orcid.org/0000-0002-4326-1775

Francesco Destro − *Department of Chemical Engineering, Massachusetts Institute of Technology, Cambridge, Massachusetts 02139, United States;* orcid.org/0000-0002-0977-0672

Pavan Inguva − *Department of Chemical Engineering, Massachusetts Institute of Technology, Cambridge, Massachusetts 02139, United States;* orcid.org/0000-0001-6216-296X

Soroush Ahmadi − *Department of Chemical Engineering, Massachusetts Institute of Technology, Cambridge, Massachusetts 02139, United States*

Etienne Boulais − *Department of Chemical Engineering, Massachusetts Institute of Technology, Cambridge, Massachusetts 02139, United States*

Yufeng Quan − *Department of Chemical Engineering, Massachusetts Institute of Technology, Cambridge, Massachusetts 02139, United States*

Richard D. Braatz − *Department of Chemical Engineering, Massachusetts Institute of Technology, Cambridge, Massachusetts 02139, United States*

Complete contact information is available at: https://pubs.acs.org/10.1021/acsnano.4c18274

Author Contributions

†A.U., C.D., and P.S. contributed equally to this work.

Notes

The authors declare no competing financial interest.

ACKNOWLEDGMENTS

This research was supported by the U.S. Food and Drug Administration under the FDA BAA-22-00123 program, Award Number 75F40122C00200.

VOCABULARY

lipid nanoparticle (LNP) A nanosized particle composed of a combination of four main lipids: ionizable cationic lipid, phospholipid, cholesterol, and PEGylated lipid. It features a core−shell structure designed to encapsulate therapeutic molecules, such as nucleic acids (e.g., mRNA), for delivery into target cells. LNPs are commonly used in gene therapy and vaccine development due to their stability, biocompatibility, and efficiency in cellular uptake.

https://doi.org/10.1021/acsnano.4c18274
ACS Nano XXXX, XXX, XXX−XXX

nucleic acid therapeutic (NAT) A class of therapeutics that uses nucleic acids, such as DNA or RNA, to treat diseases by modulating gene expression or protein production. This category includes modalities like mRNA, siRNA, ASOs, and pDNA. These molecules can be used to either replace defective genes, silence harmful genes, or promote the production of therapeutic proteins, offering potential treatments for genetic disorders, cancers, and infectious diseases.

structure The internal architecture of an LNP, including how and which individual components are organized at a molecular level. This encompasses the arrangement of lipid molecules, the encapsulation of nucleic acids, and the presence of distinct lipid phases, such as lamellar, micellar, or disordered core−shell formations.

morphology The external shape and surface features of an LNP. This includes their overall size, geometry (e.g., spherical or bleb-like), surface smoothness or roughness, and other observable traits identified through imaging techniques.

formulation The process and composition used to create LNPs. It mostly refers to the selection of lipid components, nucleic acids, solvents, and buffers, as well as the specific conditions under which they are combined. It directly influences the structure, morphology, and functional properties of the resulting LNPs.

ionizable lipid (IL) A specialized and typically the most abundant lipid component within LNP. It contains a functional group capable of undergoing protonation or deprotonation depending on the pH of the surrounding environment. This allows ILs to transition between neutral and charged states, which can be exploited to complexate with the anionic cargo.

LIST OF ABBREVIATIONS

AF4	asymmetric-flow field-flow fractionation
AFM	atomic force microscopy
ASOs	antisense oligonucleotides
AUC	analytical ultracentrifugation
CAR	chimeric antigen receptor
CLiC microscopy	convex lens-induced confinement microscopy
COVID-19	coronavirus disease 2019
CPPs	critical process parameters
CQAs	critical quality attributes
cryoET	cryogenic electron tomography
cryoTEM	cryogenic transmission electron microscopy
cryo-XPS	cryogenic X-ray photoelectron spectroscopy
(Q2)	cubic
DENSS	density from solution scattering
DLS	dynamic light scattering
DNAs	deoxyribonucleic acids
EE	encapsulation efficiency
EMA	European Medicines Agency
FDA	Food and Drug Administration
FRET	fluorescence energy resonance transfer
GNPs	gold nanoparticles
HEPES	2-[4-(2-hydroxyethyl)piperazin-1-yl]-ethanesulfonic acid
(H_{II})	hexagonal
IL	ionizable cationic lipid
(L_{α})	lamellar
LNPs	lipid nanoparticles
MALS	multiangle light scattering
MLV model	multilamellar vesicle model
mRNA	messenger ribonucleic acid
NAT	nucleic acid therapeutics
NMR	nuclear magnetic resonance
NTA	Nanoparticle tracking analysis
PBS	phosphate-buffered saline
PDI	polydispersity index
pDNA	plasmid DNA
PECAM-1	latelet-endothelial cell adhesion molecule
PEGylated lipids	polyethylene glycolated lipids
PSD	particle size distribution
RNAs	ribonucleic acids
SAM	self-amplifying mRNA
SANS	small-angle neutron scattering
SAXS	small-angle X-ray scattering
SFAS	scatter-free absorption spectroscopy
siRNA	small interfering RNA
SLD	scattering length density
SPARTA	single-particle automated Raman trapping analysis
SPP	single-particle profiling
TDA	Taylor dispersion analysis
TFF	tangential flow filtration
Tris	tris(hydroxymethyl)aminomethane
TRPS	tunable resistive pulse sensing
USAXS	ultrasmall-angle X-ray scattering

Lipids

ALC-0315	[(4-hydroxybutyl)azanediyl]di(hexane-6,1-diyl) bis(2-hexyldecanoate)
DLin-DMA	*N*,*N*-dimethyl-2,3-bis[(9*Z*,12*Z*)-9,12-octadecadien-1-yloxy]-1-propanamine

https://doi.org/10.1021/acsnano.4c18274
ACS Nano XXXX, XXX, XXX−XXX

DLin-KC2-DMA	*N*,*N*-dimethyl-2,2-di(9*Z*,12*Z*)-9,12-octadecadien-1-yl-1,3-dioxolane-4-ethanamine
DLin-MC3-DMA	(6*Z*,9*Z*,28*Z*,31*Z*)-heptatriaconta-6,9,28,31-tetraen-19-yl 4-(dimethylamino)butanoate
DMG-PEG2000	1,2-dimyristoyl-*sn*-glycero-3-methoxypolyethylene glycol.
DODAP	1,2-dioleoyl-3-dimethylammonium propane
DODMA	1,2-dioleyloxy-3-(dimethylamino)propane
DOPC	dipalmitoylphosphatidylcholine
DSPC	distearoylphosphatidylcholine
SM-102	9-heptadecanyl 8-(2-hydroxyethyl)[6-oxo-6-(undecyloxy)hexyl]aminooctanoate

REFERENCES

(1) Kulkarni, J. A.; Witzigmann, D.; Thomson, S. B.; Chen, S.; Leavitt, B. R.; Cullis, P. R.; Van Der Meel, R. The current landscape of nucleic acid therapeutics. *Nat. Nanotechnol.* **2021**, *16*, 630−643.

(2) Hamilton, A. G.; Swingle, K. L.; Mitchell, M. J. Biotechnology: Overcoming biological barriers to nucleic acid delivery using lipid nanoparticles. *PLOS Biology* **2023**, *21*, No. e3002105.

(3) Paunovska, K.; Loughrey, D.; Dahlman, J. E. Drug delivery systems for RNA therapeutics. *Nat. Rev. Genet.* **2022**, *23*, 265−280.

(4) Yin, H.; Kanasty, R. L.; Eltoukhy, A. A.; Vegas, A. J.; Dorkin, J. R.; Anderson, D. G. Non-viral vectors for gene-based therapy. *Nat. Rev. Genet.* **2014**, *15*, 541−555.

(5) Mitchell, M. J.; Billingsley, M. M.; Haley, R. M.; Wechsler, M. E.; Peppas, N. A.; Langer, R. Engineering precision nanoparticles for drug delivery. *Nat. Rev. Drug Discovery* **2021**, *20*, 101−124.

(6) Dammes, N.; Peer, D. Paving the Road for RNA Therapeutics. *Trends Pharmacol. Sci.* **2020**, *41*, 755−775.

(7) Eygeris, Y.; Gupta, M.; Kim, J.; Sahay, G. Chemistry of Lipid Nanoparticles for RNA Delivery. *Acc. Chem. Res.* **2022**, *55*, 2−12.

(8) Buck, J.; Grossen, P.; Cullis, P. R.; Huwyler, J.; Witzigmann, D. Lipid-Based DNA Therapeutics: Hallmarks of Non-Viral Gene Delivery. *ACS Nano* **2019**, *13*, 3754−3782.

(9) Wang, C.; Pan, C.; Yong, H.; Wang, F.; Bo, T.; Zhao, Y.; Ma, B.; He, W.; Li, M. Emerging non-viral vectors for gene delivery. *J. Nanobiotechnol.* **2023**, *21*, 272.

(10) Cullis, P. R.; Felgner, P. L. The 60-year evolution of lipid nanoparticles for nucleic acid delivery. *Nat. Rev. Drug Discovery* **2024**, *23*, 709−722.

(11) Chatterjee, S.; Kon, E.; Sharma, P.; Peer, D. Endosomal escape: A bottleneck for LNP-mediated therapeutics. *Proc. Natl. Acad. Sci. U.S.A.* **2024**, *121*, No. e2307800120.

(12) Hou, X.; Zaks, T.; Langer, R.; Dong, Y. Lipid nanoparticles for mRNA delivery. *Nature Reviews Materials* **2021**, *6*, 1078−1094.

(13) Hald Albertsen, C.; Kulkarni, J. A.; Witzigmann, D.; Lind, M.; Petersson, K.; Simonsen, J. B. The role of lipid components in lipid nanoparticles for vaccines and gene therapy. *Adv. Drug Delivery Rev.* **2022**, *188*, 114416.

(14) Campani, V.; Giarra, S.; De Rosa, G. Lipid-based core-shell nanoparticles: Evolution and potentialities in drug delivery. *OpenNano* **2018**, *3*, 5−17.

(15) Ferhan, A. R.; Park, S.; Park, H.; Tae, H.; Jackman, J. A.; Cho, N.-J. Lipid Nanoparticle Technologies for Nucleic Acid Delivery: A Nanoarchitectonics Perspective. *Adv. Funct. Mater.* **2022**, *32*, 2203669.

(16) Wang, F.; Zuroske, T.; Watts, J. K. RNA therapeutics on the rise. *Nat. Rev. Drug Discovery* **2020**, *19*, 441−442.

(17) Damase, T. R.; Sukhovershin, R.; Boada, C.; Taraballi, F.; Pettigrew, R. I.; Cooke, J. P. The Limitless Future of RNA Therapeutics. *Frontiers in Bioengineering and Biotechnology* **2021**, *9*, 628137.

(18) Schoenmaker, L.; Witzigmann, D.; Kulkarni, J. A.; Verbeke, R.; Kersten, G.; Jiskoot, W.; Crommelin, D. J. mRNA-lipid nanoparticle COVID-19 vaccines: Structure and stability. *Int. J. Pharm.* **2021**, *601*, 120586.

(19) Graván, P.; Aguilera-Garrido, A.; Marchal, J. A.; Navarro-Marchal, S. A.; Galisteo-González, F. Lipid-core nanoparticles: Classification, preparation methods, routes of administration and recent advances in cancer treatment. *Adv. Colloid Interface Sci.* **2023**, *314*, 102871.

(20) https://www.ema.europa.eu/en/medicines/human/EPAR/kostaive (accessed on 11-03-2025).

(21) https://www.fda.gov/vaccines-blood-biologics/vaccines/mresvia (accessed on 11-03-2025).

(22) Xu, Y.; Ma, S.; Cui, H.; Chen, J.; Xu, S.; Gong, F.; Golubovic, A.; Zhou, M.; Wang, K. C.; Varley, A.; Lu, R. X. Z.; Wang, B.; Li, B. AGILE platform: a deep learning powered approach to accelerate LNP development for mRNA delivery. *Nat. Commun.* **2024**, *15*, 6305.

(23) Li, B.; Raji, I. O.; Gordon, A. G. R.; Sun, L.; Raimondo, T. M.; Oladimeji, F. A.; Jiang, A. Y.; Varley, A.; Langer, R. S.; Anderson, D. G. Accelerating ionizable lipid discovery for mRNA delivery using machine learning and combinatorial chemistry. *Nat. Mater.* **2024**, *23*, 1002−1008.

(24) Yanez Arteta, M.; Kjellman, T.; Bartesaghi, S.; Wallin, S.; Wu, X.; Kvist, A. J.; Dabkowska, A.; Székely, N.; Radulescu, A.; Bergenholtz, J.; Lindfors, L. Successful reprogramming of cellular protein production through mRNA delivered by functionalized lipid nanoparticles. *Proc. Natl. Acad. Sci. U.S.A.* **2018**, *115*, E3351−E3360.

(25) Cheng, M. H. Y.; Leung, J.; Zhang, Y.; Strong, C.; Basha, G.; Momeni, A.; Chen, Y.; Jan, E.; Abdolahzadeh, A.; Wang, X.; Kulkarni, J. A.; Witzigmann, D.; Cullis, P. R. Induction of Bleb Structures in Lipid Nanoparticle Formulations of mRNA Leads to Improved Transfection Potency. *Adv. Mater.* **2023**, *35*, 2303370.

(26) Eygeris, Y.; Patel, S.; Jozic, A.; Sahay, G. Deconvoluting Lipid Nanoparticle Structure for Messenger RNA Delivery. *Nano Lett.* **2020**, *20*, 4543−4549.

(27) Patel, S.; Ashwanikumar, N.; Robinson, E.; Xia, Y.; Mihai, C.; Griffith, J. P.; Hou, S.; Esposito, A. A.; Ketova, T.; Welsher, K.; Joyal, J. L.; Almarsson, Ö.; Sahay, G. Naturally-occurring cholesterol analogues in lipid nanoparticles induce polymorphic shape and enhance intracellular delivery of mRNA. *Nat. Commun.* **2020**, *11*, 983.

(28) Heyes, J.; Palmer, L.; Bremner, K.; MacLachlan, I. Cationic lipid saturation influences intracellular delivery of encapsulated nucleic acids. *J. Controlled Release* **2005**, *107*, 276−287.

(29) Chen, X.; Li, M.; Jiang, F.; Hong, L.; Liu, Z. Revealing a Correlation between Structure and in vitro activity of mRNA Lipid Nanoparticles. *bioRxiv* **2024**. DOI: 10.1101/2024.09.01.610730

(30) Hammel, M.; Fan, Y.; Sarode, A.; Byrnes, A. E.; Zang, N.; Kou, P.; Nagapudi, K.; Leung, D.; Hoogenraad, C. C.; Chen, T.; Yen, C.-W.; Hura, G. L. Correlating the Structure and Gene Silencing Activity of Oligonucleotide-Loaded Lipid Nanoparticles Using Small-Angle X-ray Scattering. *ACS Nano* **2023**, *17*, 11454−11465.

(31) Yu, H.; Iscaro, J.; Dyett, B.; Zhang, Y.; Seibt, S.; Martinez, N.; White, J.; Drummond, C. J.; Bozinovski, S.; Zhai, J. Inverse Cubic and Hexagonal Mesophase Evolution within Ionizable Lipid Nanoparticles Correlates with mRNA Transfection in Macrophages. *J. Am. Chem. Soc.* **2023**, *145* (45), 24765−24774.

(32) Sabnis, S.; Kumarasinghe, E. S.; Salerno, T.; Mihai, C.; Ketova, T.; Senn, J. J.; Lynn, A.; Bulychev, A.; McFadyen, I.; Chan, J.; Almarsson, Ö.; Stanton, M. G.; Benenato, K. E. A Novel Amino Lipid Series for mRNA Delivery: Improved Endosomal Escape and Sustained Pharmacology and Safety in Non-human Primates. *Molecular Therapy* **2018**, *26*, 1509−1519.

(33) Gindy, M. E.; Feuston, B.; Glass, A.; Arrington, L.; Haas, R. M.; Schariter, J.; Stirdivant, S. M. Stabilization of Ostwald Ripening in Low Molecular Weight Amino Lipid Nanoparticles for Systemic Delivery of siRNA Therapeutics. *Mol. Pharmaceutics* **2014**, *11*, 4143−4153.

(34) Tenchov, R.; Bird, R.; Curtze, A. E.; Zhou, Q. Lipid Nanoparticles-From Liposomes to mRNA Vaccine Delivery, a Landscape of Research Diversity and Advancement. *ACS Nano* **2021**, *15*, 16982−17015.

(35) Oude Blenke, E.; Örnskov, E.; Schöneich, C.; Nilsson, G. A.; Volkin, D. B.; Mastrobattista, E.; Almarsson, Ö.; Crommelin, D. J. The Storage and In-Use Stability of mRNA Vaccines and Therapeutics: Not A Cold Case. *J. Pharm. Sci.* **2023**, *112*, 386−403.

(36) Tesei, G.; Hsiao, Y.-W.; Dabkowska, A.; Grönberg, G.; Yanez Arteta, M.; Ulkoski, D.; Bray, D. J.; Trulsson, M.; Ulander, J.; Lund, M.;

https://doi.org/10.1021/acsnano.4c18274
ACS Nano XXXX, XXX, XXX−XXX

Lindfors, L. Lipid shape and packing are key for optimal design of pH-sensitive mRNA lipid nanoparticles. *Proc. Natl. Acad. Sci. U. S. A.* **2024**, *121*, No. e2311700120.
(37) Leung, A. K. K.; Hafez, I. M.; Baoukina, S.; Belliveau, N. M.; Zhigaltsev, I. V.; Afshinmanesh, E.; Tieleman, D. P.; Hansen, C. L.; Hope, M. J.; Cullis, P. R. Lipid Nanoparticles Containing siRNA Synthesized by Microfluidic Mixing Exhibit an Electron-Dense Nanostructured Core. *J. Phys. Chem. C* **2012**, *116*, 18440−18450.
(38) Brader, M. L.; Williams, S. J.; Banks, J. M.; Hui, W. H.; Zhou, Z. H.; Jin, L. Encapsulation state of messenger RNA inside lipid nanoparticles. *Biophys. J.* **2021**, *120*, 2766−2770.
(39) Philipp, J.; Dabkowska, A.; Reiser, A.; Frank, K.; Krzysztoń, R.; Brummer, C.; Nickel, B.; Blanchet, C. E.; Sudarsan, A.; Ibrahim, M.; Johansson, S.; Skantze, P.; Skantze, U.; Östman, S.; Johansson, M.; Henderson, N.; Elvevold, K.; Smedsrød, B.; Schwierz, N.; Lindfors, L.; Rädler, J. O. pH-dependent structural transitions in cationic ionizable lipid mesophases are critical for lipid nanoparticle function. *Proc. Natl. Acad. Sci. U.S.A.* **2023**, *120*, No. e2310491120.
(40) Li, Z.; Carter, J.; Santos, L.; Webster, C.; Van Der Walle, C. F.; Li, P.; Rogers, S. E.; Lu, J. R. Acidification-Induced Structure Evolution of Lipid Nanoparticles Correlates with Their *In Vitro* Gene Transfections. *ACS Nano* **2023**, *17*, 979−990.
(41) De Jesus, M. B.; Zuhorn, I. S. Solid lipid nanoparticles as nucleic acid delivery system: Properties and molecular mechanisms. *J. Controlled Release* **2015**, *201*, 1−13.
(42) Simonsen, J. B. A perspective on bleb and empty LNP structures. *J. Controlled Release* **2024**, *373*, 952−961.
(43) Kulkarni, J. A.; Cullis, P. R.; Van Der Meel, R. Lipid Nanoparticles Enabling Gene Therapies: From Concepts to Clinical Utility. *Nucleic Acid Therapeutics* **2018**, *28*, 146−157.
(44) Cárdenas, M.; Campbell, R. A.; Yanez Arteta, M.; Lawrence, M. J.; Sebastiani, F. Review of structural design guiding the development of lipid nanoparticles for nucleic acid delivery. *Curr. Opin. Colloid Interface Sci.* **2023**, *66*, 101705.
(45) Witten, J.; Hu, Y.; Langer, R.; Anderson, D. G. Recent advances in nanoparticulate RNA delivery systems. *Proc. Natl. Acad. Sci. U.S.A.* **2024**, *121*, No. e2307798120.
(46) Vasileva, O.; Zaborova, O.; Shmykov, B.; Ivanov, R.; Reshetnikov, V. Composition of lipid nanoparticles for targeted delivery: application to mRNA therapeutics. *Front. Pharmacol.* **2024**, *15*, 1466337.
(47) Alfutaimani, A. S.; Alharbi, N. K.; Alahmari, A. S.; Alqabbani, A. A.; Aldayel, A. M. Exploring the landscape of Lipid Nanoparticles (LNPs): A comprehensive review of LNPs types and biological sources of lipids. *Int. J. Pharm.: X* **2024**, *8*, 100305.
(48) Tang, X.; Zhang, Y.; Han, X. Ionizable Lipid Nanoparticles for mRNA Delivery. *Adv. NanoBiomed. Res.* **2023**, *3*, 2300006.
(49) Hourdel, L.; Lebaz, N.; Peral, F.; Ripoll, M.; Briançon, S.; Bensaid, F.; Luthra, S.; Cogné, C. Overview on LNP-mRNA encapsulation unit operation: Mixing technologies, scalability, and influence of formulation & process parameters on physico-chemical characteristics. *Int. J. Pharm.* **2025**, *672*, 125297.
(50) Samaridou, E.; Heyes, J.; Lutwyche, P. Lipid nanoparticles for nucleic acid delivery: Current perspectives. *Adv. Drug Delivery Rev.* **2020**, *154*−*155*, 37−63.
(51) Rietwyk, S.; Peer, D. Next-Generation Lipids in RNA Interference Therapeutics. *ACS Nano* **2017**, *11*, 7572−7586.
(52) Moss, K. H.; Popova, P.; Hadrup, S. R.; Astakhova, K.; Taskova, M. Lipid Nanoparticles for Delivery of Therapeutic RNA Oligonucleotides. *Mol. Pharmaceutics* **2019**, *16*, 2265−2277.
(53) Haque, M. A.; Shrestha, A.; Mikelis, C. M.; Mattheolabakis, G. Comprehensive analysis of lipid nanoparticle formulation and preparation for RNA delivery. *International Journal of Pharmaceutics: X* **2024**, *8*, 100283.
(54) Dilliard, S. A.; Siegwart, D. J. Passive, active and endogenous organ-targeted lipid and polymer nanoparticles for delivery of genetic drugs. *Nature Reviews Materials* **2023**, *8*, 282−300.
(55) Mrksich, K.; Padilla, M. S.; Mitchell, M. J. Breaking the final barrier: Evolution of cationic and ionizable lipid structure in lipid nanoparticles to escape the endosome. *Adv. Drug Delivery Rev.* **2024**, *214*, 115446.
(56) Xu, L.; Wang, X.; Liu, Y.; Yang, G.; Falconer, R. J.; Zhao, C.-X. Lipid Nanoparticles for Drug Delivery. *Adv. NanoBiomed. Res.* **2022**, *2*, 2100109.
(57) Binici, B.; Rattray, Z.; Zinger, A.; Perrie, Y. Exploring the impact of commonly used ionizable and pegylated lipids on mRNA-LNPs: A combined in vitro and preclinical perspective. *J. Controlled Release* **2025**, *377*, 162−173.
(58) Carrasco, M. J.; Alishetty, S.; Alameh, M.-G.; Said, H.; Wright, L.; Paige, M.; Soliman, O.; Weissman, D.; Cleveland, T. E.; Grishaev, A.; Buschmann, M. D. Ionization and structural properties of mRNA lipid nanoparticles influence expression in intramuscular and intravascular administration. *Commun. Biol.* **2021**, *4*, 956.
(59) Hashiba, K.; Sato, Y.; Taguchi, M.; Sakamoto, S.; Otsu, A.; Maeda, Y.; Shishido, T.; Murakawa, M.; Okazaki, A.; Harashima, H. Branching Ionizable Lipids Can Enhance the Stability, Fusogenicity, and Functional Delivery of mRNA. *Small Sci.* **2023**, *3*, 2200071.
(60) Zhang, Y.; Sun, C.; Wang, C.; Jankovic, K. E.; Dong, Y. Lipids and Lipid Derivatives for RNA Delivery. *Chem. Rev.* **2021**, *121*, 12181−12277.
(61) O'Brien Laramy, M.; Foley, D. A.; Pak, R. H.; Lewis, J. A.; McKinney, E.; Egan, P. M.; Yerabolu, R.; Dane, E.; Dirat, O.; Saunders Gorka, L.; Martinelli, J. R.; Moussa, E. M.; Barthuet, J. Chemistry, manufacturing and controls strategies for using novel excipients in lipid nanoparticles. *Nat. Nanotechnol.* **2025**, *20*, 331.
(62) Miao, L.; Li, L.; Huang, Y.; Delcassian, D.; Chahal, J.; Han, J.; Shi, Y.; Sadtler, K.; Gao, W.; Lin, J.; Doloff, J. C.; Langer, R.; Anderson, D. G. Delivery of mRNA vaccines with heterocyclic lipids increases anti-tumor efficacy by STING-mediated immune cell activation. *Nat. Biotechnol.* **2019**, *37*, 1174−1185.
(63) Xue, L.; Zhao, G.; Gong, N.; Han, X.; Shepherd, S. J.; Xiong, X.; Xiao, Z.; Palanki, R.; Xu, J.; Swingle, K. L.; Warzecha, C. C.; El-Mayta, R.; Chowdhary, V.; Yoon, I.-C.; Xu, J.; Cui, J.; Shi, Y.; Alameh, M.-G.; Wang, K.; Wang, L.; Pochan, D. J.; Weissman, D.; Vaughan, A. E.; Wilson, J. M.; Mitchell, M. J. Combinatorial design of siloxane-incorporated lipid nanoparticles augments intracellular processing for tissue-specific mRNA therapeutic delivery. *Nat. Nanotechnol.* **2025**, *20*, 132.
(64) Chen, J.; Xu, Y.; Zhou, M.; Xu, S.; Varley, A. J.; Golubovic, A.; Lu, R. X. Z.; Wang, K. C.; Yeganeh, M.; Vosoughi, D.; Li, B. Combinatorial design of ionizable lipid nanoparticles for muscle-selective mRNA delivery with minimized off-target effects. *Proc. Natl. Acad. Sci. U.S.A.* **2023**, *120*, No. e2309472120.
(65) Cullis, P. R.; Hope, M. J. Lipid Nanoparticle Systems for Enabling Gene Therapies. *Molecular Therapy* **2017**, *25*, 1467−1475.
(66) Semple, S. C.; Akinc, A.; Chen, J.; Sandhu, A. P.; Mui, B. L.; Cho, C. K.; Sah, D. W. Y.; Stebbing, D.; Crosley, E. J.; Yaworski, E.; Hafez, I. M.; Dorkin, J. R.; Qin, J.; Lam, K.; Rajeev, K. G.; Wong, K. F.; Jeffs, L. B.; Nechev, L.; Eisenhardt, M. L.; Jayaraman, M.; Kazem, M.; Maier, M. A.; Srinivasulu, M.; Weinstein, M. J.; Chen, Q.; Alvarez, R.; Barros, S. A.; De, S.; Klimuk, S. K.; Borland, T.; Kosovrasti, V.; Cantley, W. L.; Tam, Y. K.; Manoharan, M.; Ciufolini, M. A.; Tracy, M. A.; De Fougerolles, A.; MacLachlan, I.; Cullis, P. R.; Madden, T. D.; Hope, M. J. Rational design of cationic lipids for siRNA delivery. *Nat. Biotechnol.* **2010**, *28*, 172−176.
(67) Evers, M. J. W.; Kulkarni, J. A.; Van Der Meel, R.; Cullis, P. R.; Vader, P.; Schiffelers, R. M. State-of-the-Art Design and Rapid-Mixing Production Techniques of Lipid Nanoparticles for Nucleic Acid Delivery. *Small Methods* **2018**, *2*, 1700375.
(68) Schober, G. B.; Story, S.; Arya, D. P. A careful look at lipid nanoparticle characterization: analysis of benchmark formulations for encapsulation of RNA cargo size gradient. *Sci. Rep.* **2024**, *14*, 2403.
(69) Sun, G. Y.; Sun, A. Y. Ethanol and Membrane Lipids. *Alcoholism: Clinical and Experimental Research* **1985**, *9*, 164−180.
(70) Leung, A. K. K.; Tam, Y. Y. C.; Chen, S.; Hafez, I. M.; Cullis, P. R. Microfluidic Mixing: A General Method for Encapsulating Macromolecules in Lipid Nanoparticle Systems. *J. Phys. Chem. B* **2015**, *119*, 8698−8706.

https://doi.org/10.1021/acsnano.4c18274
ACS Nano XXXX, XXX, XXX−XXX

(71) Ueda, K.; Sakagawa, Y.; Saito, T.; Fujimoto, T.; Nakamura, M.; Sakuma, F.; Kaneko, S.; Tokumoto, T.; Nishimura, K.; Takeda, J.; Arai, Y.; Yamamoto, K.; Ikeda, Y.; Higashi, K.; Moribe, K. Molecular-Level Structural Analysis of siRNA-Loaded Lipid Nanoparticles by ^{1}H NMR Relaxometry: Impact of Lipid Composition on Their Structural Properties. *Mol. Pharmaceutics* **2023**, *20*, 4729−4742.
(72) Cullis, P.; De Kruijff, B. Lipid polymorphism and the functional roles of lipids in biological membranes. *Biochim. Biophys. Acta (BBA): Rev. Biomembr.* **1979**, *559*, 399−420.
(73) Paunovska, K.; Gil, C. J.; Lokugamage, M. P.; Sago, C. D.; Sato, M.; Lando, G. N.; Gamboa Castro, M.; Bryksin, A. V.; Dahlman, J. E. Analyzing 2,000 in vivo Drug Delivery Data Points Reveals Cholesterol Structure Impacts Nanoparticle Delivery. *ACS Nano* **2018**, *12*, 8341−8349.
(74) Paunovska, K.; Da Silva Sanchez, A. J.; Sago, C. D.; Gan, Z.; Lokugamage, M. P.; Islam, F. Z.; Kalathoor, S.; Krupczak, B. R.; Dahlman, J. E. Nanoparticles Containing Oxidized Cholesterol Deliver mRNA to the Liver Microenvironment at Clinically Relevant Doses. *Adv. Mater.* **2019**, *31*, 1807748.
(75) Park, S. A.; Hwang, D.; Kim, J. H.; Lee, S.-Y.; Lee, J.; Kim, H. S.; Kim, K.-A.; Lim, B.; Lee, J.-E.; Jeon, Y. H.; Oh, T. J.; Lee, J.; An, S. Formulation of lipid nanoparticles containing ginsenoside Rg2 and protopanaxadiol for highly efficient delivery of mRNA. *Biomaterials Science* **2024**, *12*, 6299−6309.
(76) Kulkarni, J. A.; Witzigmann, D.; Leung, J.; Van Der Meel, R.; Zaifman, J.; Darjuan, M. M.; Grisch-Chan, H. M.; Thöny, B.; Tam, Y. Y. C.; Cullis, P. R. Fusion-dependent formation of lipid nanoparticles containing macromolecular payloads. *Nanoscale* **2019**, *11*, 9023−9031.
(77) Belliveau, N. M.; Huft, J.; Lin, P. J.; Chen, S.; Leung, A. K.; Leaver, T. J.; Wild, A. W.; Lee, J. B.; Taylor, R. J.; Tam, Y. K.; Hansen, C. L.; Cullis, P. R. Microfluidic Synthesis of Highly Potent Limit-size Lipid Nanoparticles for In Vivo Delivery of siRNA. *Molecular Therapy - Nucleic Acids* **2012**, *1*, No. e37.
(78) Wilson, S. C.; Baryza, J. L.; Reynolds, A. J.; Bowman, K.; Keegan, M. E.; Standley, S. M.; Gardner, N. P.; Parmar, P.; Agir, V. O.; Yadav, S.; Zunic, A.; Vargeese, C.; Lee, C. C.; Rajan, S. Real Time Measurement of PEG Shedding from Lipid Nanoparticles in Serum via NMR Spectroscopy. *Mol. Pharmaceutics* **2015**, *12*, 386−392.
(79) Ambegia, E.; Ansell, S.; Cullis, P.; Heyes, J.; Palmer, L.; MacLachlan, I. Stabilized plasmid−lipid particles containing PEG-diacylglycerols exhibit extended circulation lifetimes and tumor selective gene expression. *Biochimica et Biophysica Acta (BBA) - Biomembranes* **2005**, *1669*, 155−163.
(80) Suzuki, Y.; Ishihara, H. Difference in the lipid nanoparticle technology employed in three approved siRNA (Patisiran) and mRNA (COVID-19 vaccine) drugs. *Drug Metabolism and Pharmacokinetics* **2021**, *41*, 100424.
(81) Houseley, J.; Tollervey, D. The Many Pathways of RNA Degradation. *Cell* **2009**, *136*, 763−776.
(82) Pogocki, D.; Schöneich, C. Chemical Stability of Nucleic Acid−Derived Drugs. *J. Pharm. Sci.* **2000**, *89*, 443−456.
(83) Packer, M.; Gyawali, D.; Yerabolu, R.; Schariter, J.; White, P. A novel mechanism for the loss of mRNA activity in lipid nanoparticle delivery systems. *Nat. Commun.* **2021**, *12*, 6777.
(84) O'Brien Laramy, M. N.; Costa, A. P.; Cebrero, Y. M.; Joseph, J.; Sarode, A.; Zang, N.; Kim, L. J.; Hofmann, K.; Wang, S.; Goyon, A.; Koenig, S. G.; Hammel, M.; Hura, G. L. Process Robustness in Lipid Nanoparticle Production: A Comparison of Microfluidic and Turbulent Jet Mixing. *Mol. Pharmaceutics* **2023**, *20*, 4285−4296.
(85) Birdsall, R. E.; Han, D.; DeLaney, K.; Kowalczyk, A.; Cojocaru, R.; Lauber, M.; Huray, J. L. Monitoring stability indicating impurities and aldehyde content in lipid nanoparticle raw material and formulated drugs. *Journal of Chromatography B* **2024**, *1234*, 124005.
(86) Mehnert, W.; Mäder, K. Solid lipid nanoparticles. *Adv. Drug Delivery Rev.* **2012**, *64*, 83−101.
(87) Duong, V.-A.; Nguyen, T.-T.-L.; Maeng, H.-J. Preparation of Solid Lipid Nanoparticles and Nanostructured Lipid Carriers for Drug Delivery and the Effects of Preparation Parameters of Solvent Injection Method. *Molecules* **2020**, *25*, 4781.
(88) Ball, R.; Bajaj, P.; Whitehead, K. Achieving long-term stability of lipid nanoparticles: examining the effect of pH, temperature, and lyophilization. *Int. J. Nanomed.* **2017**, *12*, 305−315.
(89) Buschmann, M. D.; Carrasco, M. J.; Alishetty, S.; Paige, M.; Alameh, M. G.; Weissman, D. Nanomaterial Delivery Systems for mRNA Vaccines. *Vaccines* **2021**, *9*, 65.
(90) Maeki, M.; Kimura, N.; Sato, Y.; Harashima, H.; Tokeshi, M. Advances in microfluidics for lipid nanoparticles and extracellular vesicles and applications in drug delivery systems. *Adv. Drug Delivery Rev.* **2018**, *128*, 84−100.
(91) Carvalho, B. G.; Ceccato, B. T.; Michelon, M.; Han, S. W.; De La Torre, L. G. Advanced Microfluidic Technologies for Lipid Nano-Microsystems from Synthesis to Biological Application. *Pharmaceutics* **2022**, *14*, 141.
(92) Kimura, N.; Maeki, M.; Sato, Y.; Note, Y.; Ishida, A.; Tani, H.; Harashima, H.; Tokeshi, M. Development of the iLiNP Device: Fine Tuning the Lipid Nanoparticle Size within 10 nm for Drug Delivery. *ACS Omega* **2018**, *3*, 5044−5051.
(93) Jürgens, D. C.; Deßloch, L.; Porras-Gonzalez, D.; Winkeljann, J.; Zielinski, S.; Munschauer, M.; Hörner, A. L.; Burgstaller, G.; Winkeljann, B.; Merkel, O. M. Lab-scale siRNA and mRNA LNP manufacturing by various microfluidic mixing techniques − an evaluation of particle properties and efficiency. *OpenNano* **2023**, *12*, 100161.
(94) Shepherd, S. J.; Warzecha, C. C.; Yadavali, S.; El-Mayta, R.; Alameh, M.-G.; Wang, L.; Weissman, D.; Wilson, J. M.; Issadore, D.; Mitchell, M. J. Scalable mRNA and siRNA Lipid Nanoparticle Production Using a Parallelized Microfluidic Device. *Nano Lett.* **2021**, *21*, 5671−5680.
(95) Devos, C.; Mukherjee, S.; Inguva, P.; Singh, S.; Wei, Y.; Mondal, S.; Yu, H.; Barbastathis, G.; Stelzer, T.; Braatz, R. D.; Myerson, A. S. Impinging jet mixers: A review of their mixing characteristics, performance considerations, and applications. *AIChE J.* **2025**, *71*, No. e18595.
(96) Subraveti, S. N.; Wilson, B. K.; Bizmark, N.; Liu, J.; Prud'homme, R. K. Synthesizing Lipid Nanoparticles by Turbulent Flow in Confined Impinging Jet Mixers. *J. Visualized Exp.* **2024**, *67047*. DOI: 10.3791/67047
(97) Misra, B.; Hughes, K. A.; Pentz, W. H.; Samart, P.; Geldenhuys, W. J.; Bobbala, S. Flash nanoprecipitation assisted self-assembly of ionizable lipid nanoparticles for nucleic acid delivery. *Nanoscale* **2024**, *16*, 6939−6948.
(98) Hardianto, A.; Muscifa, Z. S.; Widayat, W.; Yusuf, M.; Subroto, T. The Effect of Ethanol on Lipid Nanoparticle Stabilization from a Molecular Dynamics Simulation Perspective. *Molecules* **2023**, *28*, 4836.
(99) Sakurai, Y.; Hada, T.; Harashima, H. Scalable preparation of poly(ethylene glycol)-grafted siRNA-loaded lipid nanoparticles using a commercially available fluidic device and tangential flow filtration. *Journal of Biomaterials Science, Polymer Edition* **2017**, *28*, 1086−1096.
(100) Liu, H.-W.; Hu, Y.; Ren, Y.; Nam, H.; Santos, J. L.; Ng, S.; Gong, L.; Brummet, M.; Carrington, C. A.; Ullman, C. G.; Pomper, M. G.; Minn, I.; Mao, H.-Q. Scalable Purification of Plasmid DNA Nanoparticles by Tangential Flow Filtration for Systemic Delivery. *ACS Appl. Mater. Interfaces* **2021**, *13*, 30326−30336.
(101) Geng, C.; Zhou, K.; Yan, Y.; Li, C.; Ni, B.; Liu, J.; Wang, Y.; Zhang, X.; Wang, D.; Lv, L.; Zhou, Y.; Feng, A.; Wang, Y.; Li, C. A preparation method for mRNA-LNPs with improved properties. *J. Controlled Release* **2023**, *364*, 632−643.
(102) Vargas, R.; Romero, M.; Berasategui, T.; Narváez-Narváez, D. A.; Ramirez, P.; Nardi-Ricart, A.; García-Montoya, E.; Pérez-Lozano, P.; Suñe-Negre, J. M.; Moreno-Castro, C.; Hernández-Munain, C.; Suñe, C.; Suñe-Pou, M. Dialysis is a key factor modulating interactions between critical process parameters during the microfluidic preparation of lipid nanoparticles. *Colloid and Interface Science Communications* **2023**, *54*, 100709.
(103) Gilbert, J.; Sebastiani, F.; Arteta, M. Y.; Terry, A.; Fornell, A.; Russell, R.; Mahmoudi, N.; Nylander, T. Evolution of the structure of lipid nanoparticles for nucleic acid delivery: From in situ studies of

https://doi.org/10.1021/acsnano.4c18274
ACS Nano XXXX, XXX, XXX−XXX

formulation to colloidal stability. *J. Colloid Interface Sci.* **2024**, *660*, 66−76.
(104) Shepherd, S. J.; Han, X.; Mukalel, A. J.; El-Mayta, R.; Thatte, A. S.; Wu, J.; Padilla, M. S.; Alameh, M.-G.; Srikumar, N.; Lee, D.; Weissman, D.; Issadore, D.; Mitchell, M. J. Throughput-scalable manufacturing of SARS-CoV-2 mRNA lipid nanoparticle vaccines. *Proc. Natl. Acad. Sci. U.S.A.* **2023**, *120*, No. e2303567120.
(105) Lepeltier, E.; Bourgaux, C.; Couvreur, P. Nanoprecipitation and the "Ouzo effect": Application to drug delivery devices. *Adv. Drug Delivery Rev.* **2014**, *71*, 86−97.
(106) Ganachaud, F.; Katz, J. L. Nanoparticles and Nanocapsules Created Using the Ouzo Effect: Spontaneous Emulsification as an Alternative to Ultrasonic and High-Shear Devices. *ChemPhysChem* **2005**, *6*, 209−216.
(107) Roger, K.; Shcherbakova, N.; Raynal, L. Nanoprecipitation through solvent-shifting using rapid mixing: Dispelling the Ouzo boundary to reach large solute concentrations. *J. Colloid Interface Sci.* **2023**, *650*, 2049−2055.
(108) Chen, D.; Liu, Z.; Guo, L.; Yang, L.; Zhao, Y.; Yang, M. Controlled preparation of lipid nanoparticles in microreactors: Mixing time, morphology and mRNA delivery. *Chemical Engineering Journal* **2025**, *505*, 159318.
(109) Kamanzi, A.; Zhang, Y.; Gu, Y.; Liu, F.; Berti, R.; Wang, B.; Saadati, F.; Ciufolini, M. A.; Kulkarni, J.; Cullis, P.; Leslie, S. Quantitative Visualization of Lipid Nanoparticle Fusion as a Function of Formulation and Process Parameters. *ACS Nano* **2024**, *18*, 18191−18201.
(110) Hassett, K. J.; Higgins, J.; Woods, A.; Levy, B.; Xia, Y.; Hsiao, C. J.; Acosta, E.; Almarsson, Ö.; Moore, M. J.; Brito, L. A. Impact of lipid nanoparticle size on mRNA vaccine immunogenicity. *J. Controlled Release* **2021**, *335*, 237−246.
(111) Yu, H.; Dyett, B.; Kirby, N.; Cai, X.; Mohamad, M. E.; Bozinovski, S.; Drummond, C. J.; Zhai, J. pH-Dependent Lyotropic Liquid Crystalline Mesophase and Ionization Behavior of Phytantriol-Based Ionizable Lipid Nanoparticles. *Small* **2024**, *20*, 2309200.
(112) Larson, N. R.; Hu, G.; Wei, Y.; Tuesca, A. D.; Forrest, M. L.; Middaugh, C. R. pH-Dependent Phase Behavior and Stability of Cationic Lipid−mRNA Nanoparticles. *J. Pharm. Sci.* **2022**, *111*, 690−698.
(113) Gindy, M. E.; DiFelice, K.; Kumar, V.; Prud'homme, R. K.; Celano, R.; Haas, R. M.; Smith, J. S.; Boardman, D. Mechanism of Macromolecular Structure Evolution in Self-Assembled Lipid Nanoparticles for siRNA Delivery. *Langmuir* **2014**, *30*, 4613−4622.
(114) FDA. Drug Products, Including Biological Products, that Contain Nanomaterials. Technical Report, Center for Drug Evaluation and Research, 2018.
(115) FDA. Guidance for Industry: Liposome drug products. Technical Report, Center for Drug Evaluation and Research, 2018.
(116) Hemmrich, E.; McNeil, S. Active ingredient vs excipient debate for nanomedicines. *Nat. Nanotechnol.* **2023**, *18*, 692−695.
(117) Kong, W.; Wei, Y.; Dong, Z.; Liu, W.; Zhao, J.; Huang, Y.; Yang, J.; Wu, W.; He, H.; Qi, J. Role of size, surface charge, and PEGylated lipids of lipid nanoparticles (LNPs) on intramuscular delivery of mRNA. *J. Nanobiotechnol.* **2024**, *22*, 553.
(118) Paunovska, K.; Sago, C. D.; Monaco, C. M.; Hudson, W. H.; Castro, M. G.; Rudoltz, T. G.; Kalathoor, S.; Vanover, D. A.; Santangelo, P. J.; Ahmed, R.; Bryksin, A. V.; Dahlman, J. E. A Direct Comparison of in Vitro and in Vivo Nucleic Acid Delivery Mediated by Hundreds of Nanoparticles Reveals a Weak Correlation. *Nano Lett.* **2018**, *18*, 2148−2157.
(119) McMillan, C.; Druschitz, A.; Rumbelow, S.; Borah, A.; Binici, B.; Rattray, Z.; Perrie, Y. Tailoring lipid nanoparticle dimensions through manufacturing processes. *RSC Pharmaceutics* **2024**, *1*, 841−853.
(120) Whitehead, K. A.; Matthews, J.; Chang, P. H.; Niroui, F.; Dorkin, J. R.; Severgnini, M.; Anderson, D. G. *In Vitro* − *In Vivo* Translation of Lipid Nanoparticles for Hepatocellular siRNA Delivery. *ACS Nano* **2012**, *6*, 6922−6929.
(121) Lam, K.; Schreiner, P.; Leung, A.; Stainton, P.; Reid, S.; Yaworski, E.; Lutwyche, P.; Heyes, J. Optimizing Lipid Nanoparticles for Delivery in Primates. *Adv. Mater.* **2023**, *35*, 2211420.
(122) Kulkarni, J. A.; Darjuan, M. M.; Mercer, J. E.; Chen, S.; Van Der Meel, R.; Thewalt, J. L.; Tam, Y. Y. C.; Cullis, P. R. On the Formation and Morphology of Lipid Nanoparticles Containing Ionizable Cationic Lipids and siRNA. *ACS Nano* **2018**, *12*, 4787−4795.
(123) Strelkova Petersen, D. M.; Chaudhary, N.; Arral, M. L.; Weiss, R. M.; Whitehead, K. A. The mixing method used to formulate lipid nanoparticles affects mRNA delivery efficacy and organ tropism. *Eur. J. Pharm. Biopharm.* **2023**, *192*, 126−135.
(124) Okuda, K.; Sato, Y.; Iwakawa, K.; Sasaki, K.; Okabe, N.; Maeki, M.; Tokeshi, M.; Harashima, H. On the size-regulation of RNA-loaded lipid nanoparticles synthesized by microfluidic device. *J. Controlled Release* **2022**, *348*, 648−659.
(125) Ripoll, M.; Martin, E.; Enot, M.; Robbe, O.; Rapisarda, C.; Nicolai, M.-C.; Deliot, A.; Tabeling, P.; Authelin, J.-R.; Nakach, M.; Wils, P. Optimal self-assembly of lipid nanoparticles (LNP) in a ring micromixer. *Sci. Rep.* **2022**, *12*, 9483.
(126) Roces, C. B.; Lou, G.; Jain, N.; Abraham, S.; Thomas, A.; Halbert, G. W.; Perrie, Y. Manufacturing Considerations for the Development of Lipid Nanoparticles Using Microfluidics. *Pharmaceutics* **2020**, *12*, 1095.
(127) Maeki, M.; Fujishima, Y.; Sato, Y.; Yasui, T.; Kaji, N.; Ishida, A.; Tani, H.; Baba, Y.; Harashima, H.; Tokeshi, M. Understanding the formation mechanism of lipid nanoparticles in microfluidic devices with chaotic micromixers. *PLoS One* **2017**, *12*, No. e0187962.
(128) Dasaro, S. R.; Singh, A.; Vlachos, P.; Ristroph, K. D. Mechanistic insights into how mixing factors govern polyelectrolyte-surfactant complexation in RNA lipid nanoparticle formulation. *J. Colloid Interface Sci.* **2025**, *678*, 98−107.
(129) Binici, B.; Borah, A.; Watts, J. A.; McLoughlin, D.; Perrie, Y. The influence of citrate buffer molarity on mRNA-LNPs: Exploring factors beyond general critical quality attributes. *Int. J. Pharm.* **2025**, *668*, 124942.
(130) Li, M.; Schroder, R.; Ozuguzel, U.; Corts, T. M.; Liu, Y.; Zhao, Y.; Xu, W.; Ling, J.; Templeton, A. C.; Chaudhuri, B.; Gindy, M.; Wagner, A.; Su, Y. Molecular Insight into Lipid Nanoparticle Assembly from NMR Spectroscopy and Molecular Dynamics Simulation. *Mol. Pharm/* **2025**, *22*, 2193.
(131) Chander, N.; Basha, G.; Yan Cheng, M. H.; Witzigmann, D.; Cullis, P. R. Lipid nanoparticle mRNA systems containing high levels of sphingomyelin engender higher protein expression in hepatic and extra-hepatic tissues. *Molecular Therapy - Methods & Clinical Development* **2023**, *30*, 235−245.
(132) Kloczewiak, M.; Banks, J. M.; Jin, L.; Brader, M. L. A Biopharmaceutical Perspective on Higher-Order Structure and Thermal Stability of mRNA Vaccines. *Mol. Pharmaceutics* **2022**, *19*, 2022−2031.
(133) Pattipeiluhu, R.; Zeng, Y.; Hendrix, M. M.; Voets, I. K.; Kros, A.; Sharp, T. H. Liquid crystalline inverted lipid phases encapsulating siRNA enhance lipid nanoparticle mediated transfection. *Nat. Commun.* **2024**, *15*, 1303.
(134) Wang, H.; Pestre, H.; Tan, E.-K. N.; Wedemann, L.; Schuhmacher, J. S.; Schuhmacher, M.; Stellacci, F. Facile lipid nanoparticle size engineering approach via controllable fusion induced by depletion forces. *J. Colloid Interface Sci.* **2025**, *691*, 137334.
(135) Knight, J. B.; Vishwanath, A.; Brody, J. P.; Austin, R. H. Hydrodynamic Focusing on a Silicon Chip: Mixing Nanoliters in Microseconds. *Phys. Rev. Lett.* **1998**, *80*, 3863−3866.
(136) Jahn, A.; Vreeland, W. N.; DeVoe, D. L.; Locascio, L. E.; Gaitan, M. Microfluidic Directed Formation of Liposomes of Controlled Size. *Langmuir* **2007**, *23*, 6289−6293.
(137) Karnik, R.; Gu, F.; Basto, P.; Cannizzaro, C.; Dean, L.; Kyei-Manu, W.; Langer, R.; Farokhzad, O. C. Microfluidic Platform for Controlled Synthesis of Polymeric Nanoparticles. *Nano Lett.* **2008**, *8*, 2906−2912.
(138) Chen, D.; Love, K. T.; Chen, Y.; Eltoukhy, A. A.; Kastrup, C.; Sahay, G.; Jeon, A.; Dong, Y.; Whitehead, K. A.; Anderson, D. G. Rapid

https://doi.org/10.1021/acsnano.4c18274
ACS Nano XXXX, XXX, XXX−XXX

Discovery of Potent siRNA-Containing Lipid Nanoparticles Enabled by Controlled Microfluidic Formulation. *J. Am. Chem. Soc.* **2012**, *134*, 6948−6951.
(139) Stroock, A. D.; Dertinger, S. K. W.; Ajdari, A.; Mezić, I.; Stone, H. A.; Whitesides, G. M. Chaotic Mixer for Microchannels. *Science* **2002**, *295*, 647−651.
(140) Bi, D.; Wilhelmy, C.; Unthan, D.; Keil, I. S.; Zhao, B.; Kolb, B.; Koning, R. I.; Graewert, M. A.; Wouters, B.; Zwier, R.; Bussmann, J.; Hankemeier, T.; Diken, M.; Haas, H.; Langguth, P.; Barz, M.; Zhang, H. On the Influence of Fabrication Methods and Materials for mRNA-LNP Production: From Size and Morphology to Internal Structure and mRNA Delivery Performance In Vitro and In Vivo. *Adv. Healthcare Mater.* **2024**, 2401252.
(141) Johnson, B. K.; Prud'homme, R. K. Chemical processing and micromixing in confined impinging jets. *AIChE J.* **2003**, *49*, 2264−2282.
(142) Markwalter, C. E.; Prud'homme, R. K. Design of a Small-Scale Multi-Inlet Vortex Mixer for Scalable Nanoparticle Production and Application to the Encapsulation of Biologics by Inverse Flash NanoPrecipitation. *J. Pharm. Sci.* **2018**, *107*, 2465−2471.
(143) Liu, Y.; Cheng, C.; Liu, Y.; Prud'homme, R. K.; Fox, R. O. Mixing in a multi-inlet vortex mixer (MIVM) for flash nano-precipitation. *Chem. Eng. Sci.* **2008**, *63*, 2829−2842.
(144) Lim, J.-M.; Swami, A.; Gilson, L. M.; Chopra, S.; Choi, S.; Wu, J.; Langer, R.; Karnik, R.; Farokhzad, O. C. Ultra-High Throughput Synthesis of Nanoparticles with Homogeneous Size Distribution Using a Coaxial Turbulent Jet Mixer. *ACS Nano* **2014**, *8*, 6056−6065.
(145) Baldyga, J.; Bourne, J. Interactions between mixing on various scales in stirred tank reactors. *Chem. Eng. Sci.* **1992**, *47*, 1839−1848.
(146) Kamholz, A. E.; Yager, P. Theoretical Analysis of Molecular Diffusion in Pressure-Driven Laminar Flow in Microfluidic Channels. *Biophys. J.* **2001**, *80*, 155−160.
(147) Boulais, E.; Gervais, T. Two-dimensional convection−diffusion in multipolar flows with applications in microfluidics and groundwater flow. *Phys. Fluids* **2020**, *32*, 122001.
(148) Ottino, J. M. The Kinematics of Mixing: Stretching, Chaos, and Transport. *Cambridge texts in applied mathematics*, 1st ed.; Cambridge University Press: Cambridge, U.K., 1989; Vol. 3.
(149) Bałdyga, J.; Bourne, J. *Turbulent Mixing and Chemical Reactions*; Wiley, 1999.
(150) Maeki, M.; Saito, T.; Sato, Y.; Yasui, T.; Kaji, N.; Ishida, A.; Tani, H.; Baba, Y.; Harashima, H.; Tokeshi, M. A strategy for synthesis of lipid nanoparticles using microfluidic devices with a mixer structure. *RSC Adv.* **2015**, *5*, 46181−46185.
(151) Mishra, K.; Kummer, N.; Bergfreund, J.; Kämpf, F.; Bertsch, P.; Pauer, R.; Nyström, G.; Fischer, P.; Windhab, E. J. Controlling lipid crystallization across multiple length scales by directed shear flow. *J. Colloid Interface Sci.* **2023**, *630*, 731−741.
(152) Meyer, C.; Deglon, D. Particle collision modeling − A review. *Minerals Engineering* **2011**, *24*, 719−730.
(153) Hirst, L. S., Ossowski, A., Fraser, M., Geng, J., Selinger, J. V.; Selinger, R. L. B. Morphology transition in lipid vesicles due to in-plane order and topological defects*Proc. Natl. Acad. Sci. U.S.A.*. Proceedings of the National Academy of Sciences *110*, 3242−3247 (**2013**).
(154) Di Cola, E.; Grillo, I.; Ristori, S. Small Angle X-ray and Neutron Scattering: Powerful Tools for Studying the Structure of Drug-Loaded Liposomes. *Pharmaceutics* **2016**, *8*, 10.
(155) Kamanzi, A.; Gu, Y.; Tahvildari, R.; Friedenberger, Z.; Zhu, X.; Berti, R.; Kurylowicz, M.; Witzigmann, D.; Kulkarni, J. A.; Leung, J.; Andersson, J.; Dahlin, A.; Höök, F.; Sutton, M.; Cullis, P. R.; Leslie, S. Simultaneous, Single-Particle Measurements of Size and Loading Give Insights into the Structure of Drug-Delivery Nanoparticles. *ACS Nano* **2021**, *15*, 19244−19255.
(156) Li, S.; Hu, Y.; Li, A.; Lin, J.; Hsieh, K.; Schneiderman, Z.; Zhang, P.; Zhu, Y.; Qiu, C.; Kokkoli, E.; Wang, T.-H.; Mao, H.-Q. Payload distribution and capacity of mRNA lipid nanoparticles. *Nat. Commun.* **2022**, *13*, 5561.
(157) Saunders, C.; Foote, J. E. J.; Wojciechowski, J. P.; Cammack, A.; Pedersen, S. V.; Doutch, J. J.; Barriga, H. M. G.; Holme, M. N.; Penders, J.; Chami, M.; Najer, A.; Stevens, M. M. Revealing Population Heterogeneity in Vesicle-Based Nanomedicines Using Automated, Single Particle Raman Analysis. *ACS Nano* **2023**, *17*, 11713−11728.
(158) Barriga, H. M. G.; Pence, I. J.; Holme, M. N.; Doutch, J. J.; Penders, J.; Nele, V.; Thomas, M. R.; Carroni, M.; Stevens, M. M. Coupling Lipid Nanoparticle Structure and Automated Single-Particle Composition Analysis to Design Phospholipase-Responsive Nanocarriers. *Adv. Mater.* **2022**, *34*, 2200839.
(159) Mourdikoudis, S.; Pallares, R. M.; Thanh, N. T. K. Characterization techniques for nanoparticles: comparison and complementarity upon studying nanoparticle properties. *Nanoscale* **2018**, *10*, 12871−12934.
(160) Nogueira, S. S.; Samaridou, E.; Simon, J.; Frank, S.; Beck-Broichsitter, M.; Mehta, A. Analytical techniques for the characterization of nanoparticles for mRNA delivery. *Eur. J. Pharm. Biopharm.* **2024**, *198*, 114235.
(161) Chen, C.; Chen, C.; Li, Y.; Gu, R.; Yan, X. Characterization of lipid-based nanomedicines at the single-particle level. *Fundamental Research* **2023**, *3*, 488−504.
(162) Parot, J.; Mehn, D.; Jankevics, H.; Markova, N.; Carboni, M.; Olaisen, C.; Hoel, A. D.; Sigfúsdóttir, M. S.; Meier, F.; Drexel, R.; Vella, G.; McDonagh, B.; Hansen, T.; Bui, H.; Klinkenberg, G.; Visnes, T.; Gioria, S.; Urban-Lopez, P.; Prina-Mello, A.; Borgos, S. E.; Caputo, F.; Calzolai, L. Quality assessment of LNP-RNA therapeutics with orthogonal analytical techniques. *J. Controlled Release* **2024**, *367*, 385−401.
(163) Zhigaltsev, I. V.; Cullis, P. R. Morphological Behavior of Liposomes and Lipid Nanoparticles. *Langmuir* **2023**, *39*, 3185−3193.
(164) Crawford, R.; Dogdas, B.; Keough, E.; Haas, R. M.; Wepukhulu, W.; Krotzer, S.; Burke, P. A.; Sepp-Lorenzino, L.; Bagchi, A.; Howell, B. J. Analysis of lipid nanoparticles by Cryo-EM for characterizing siRNA delivery vehicles. *Int. J. Pharm.* **2011**, *403*, 237−244.
(165) Filippov, S. K.; Khusnutdinov, R.; Murmiliuk, A.; Inam, W.; Zakharova, L. Y.; Zhang, H.; Khutoryanskiy, V. V. Dynamic light scattering and transmission electron microscopy in drug delivery: a roadmap for correct characterization of nanoparticles and interpretation of results. *Materials Horizons* **2023**, *10*, 5354−5370.
(166) Filipe, V.; Hawe, A.; Jiskoot, W. Critical Evaluation of Nanoparticle Tracking Analysis (NTA) by NanoSight for the Measurement of Nanoparticles and Protein Aggregates. *Pharm. Res.* **2010**, *27*, 796−810.
(167) Matthessen, R.; Van Pottelberge, R.; Goffin, B.; De Winter, G. Impact of mixing and shaking on mRNA-LNP drug product quality characteristics. *Sci. Rep.* **2024**, *14*, 19590.
(168) Sheybanifard, M.; Guerzoni, L. P. B.; Omidinia-Anarkoli, A.; De Laporte, L.; Buyel, J.; Besseling, R.; Damen, M.; Gerich, A.; Lammers, T.; Metselaar, J. M. Liposome manufacturing under continuous flow conditions: towards a fully integrated set-up with in-line control of critical quality attributes. *Lab Chip* **2022**, *23*, 182−194.
(169) Thelen, J. L.; Leite, W.; Urban, V. S.; O'Neill, H. M.; Grishaev, A. V.; Curtis, J. E.; Krueger, S.; Castellanos, M. M. Morphological Characterization of Self-Amplifying mRNA Lipid Nanoparticles. *ACS Nano* **2024**, *18*, 1464−1476.
(170) Lin, W.-Z. S.; Bostic, W. K. V.; Malmstadt, N. 3D-printed microfluidic device for high-throughput production of lipid nanoparticles incorporating SARS-CoV-2 spike protein mRNA. *Lab Chip* **2024**, *24*, 162−170.
(171) Vogel, R.; Savage, J.; Muzard, J.; Della Camera, G.; Vella, G.; Law, A.; Marchioni, M.; Mehn, D.; Geiss, O.; Peacock, B.; Aubert, D.; Calzolai, L.; Caputo, F.; Prina-Mello, A. Measuring particle concentration of multimodal synthetic reference materials and extracellular vesicles with orthogonal techniques: Who is up to the challenge? *J. Extracellular Vesicles* **2021**, *10*, No. e12052.
(172) Simon, C.; Borgos, S.; Calzolai, L.; Nelson, B.; Parot, J.; Petersen, E.; Roesslein, M.; Xu, X.; Caputo, F. Orthogonal and complementary measurements of properties of drug products containing nanomaterials. *J. Controlled Release* **2023**, *354*, 120−127.
(173) Comfort, N.; Cai, K.; Bloomquist, T. R.; Strait, M. D.; Ferrante, A. W., Jr.; Baccarelli, A. A. Nanoparticle Tracking Analysis for the

https://doi.org/10.1021/acsnano.4c18274
ACS Nano XXXX, XXX, XXX−XXX

Quantification and Size Determination of Extracellular Vesicles. *J. Visualized Exp.* **2021**, *62447*.
(174) Wang, J.; Zhang, J.; Li, S.; Qian, H.; Liu, D.; Prado, I.; Wang, S.; Bhambhani, A.; Zeng, H. Probing the interaction mechanisms of lipid nanoparticle-encapsulated mRNA with surfaces of diverse functional groups: Implication for mRNA transport. *Chem. Eng. Sci.* **2025**, *301*, 120693.
(175) Jia, X.; Liu, Y.; Wagner, A. M.; Chen, M.; Zhao, Y.; Smith, K. J.; Some, D.; Abend, A. M.; Pennington, J. Enabling online determination of the size-dependent RNA content of lipid nanoparticle-based RNA formulations. *Journal of Chromatography B* **2021**, *1186*, 123015.
(176) Mildner, R.; Hak, S.; Parot, J.; Hyldbakk, A.; Borgos, S.; Some, D.; Johann, C.; Caputo, F. Improved multidetector asymmetrical-flow field-flow fractionation method for particle sizing and concentration measurements of lipid-based nanocarriers for RNA delivery. *Eur. J. Pharm. Biopharm.* **2021**, *163*, 252−265.
(177) Malburet, C.; Leclercq, L.; Cotte, J.-F.; Thiebaud, J.; Bazin, E.; Garinot, M.; Cottet, H. Taylor Dispersion Analysis to support lipid-nanoparticle formulations for mRNA vaccines. *Gene Ther.* **2023**, *30*, 421−428.
(178) Sebastiani, F.; Yanez Arteta, M.; Lerche, M.; Porcar, L.; Lang, C.; Bragg, R. A.; Elmore, C. S.; Krishnamurthy, V. R.; Russell, R. A.; Darwish, T.; Pichler, H.; Waldie, S.; Moulin, M.; Haertlein, M.; Forsyth, V. T.; Lindfors, L.; Cárdenas, M. Apolipoprotein E Binding Drives Structural and Compositional Rearrangement of mRNA-Containing Lipid NanoparticlesCove. *ACS Nano* **2021**, *15*, 6709−6722.
(179) Cho, H.-J.; Hyun, J.-K.; Kim, J.-G.; Jeong, H. S.; Park, H. N.; You, D.-J.; Jung, H. S. Measurement of ice thickness on vitreous ice embedded cryo-EM grids: investigation of optimizing condition for visualizing macromolecules. *J. Anal. Sci. Technol.* **2013**, *4*, 7.
(180) Koning, R. I.; Vader, H.; Van Nugteren, M.; Grocutt, P. A.; Yang, W.; Renault, L. L. R.; Koster, A. J.; Kamp, A. C. F.; Schwertner, M. Automated vitrification of cryo-EM samples with controllable sample thickness using suction and real-time optical inspection. *Nat. Commun.* **2022**, *13*, 2985.
(181) Shepherd, S. J.; Issadore, D.; Mitchell, M. J. Microfluidics for Throughput Scalable Formulation of mRNA Lipid Nanoparticle Technology. Ph.D. Thesis, University of Pennsylvania.
(182) Szebeni, J.; Kiss, B.; Bozó, T.; Turjeman, K.; Levi-Kalisman, Y.; Barenholz, Y.; Kellermayer, M. Insights into the Structure of Comirnaty Covid-19 Vaccine: A Theory on Soft, Partially Bilayer-Covered Nanoparticles with Hydrogen Bond-Stabilized mRNA−Lipid Complexes. *ACS Nano* **2023**, *17*, 13147−13157.
(183) De Chateauneuf-Randon, S.; Bresson, B.; Ripoll, M.; Huille, S.; Barthel, E.; Monteux, C. The mechanical properties of lipid nanoparticles depend on the type of biomacromolecule they are loaded with. *Nanoscale* **2024**, *16*, 10706−10714.
(184) Wang, J.; Zhang, J.; Li, S.; Liu, D.; Bhambhani, A.; Zeng, H. Characterization of structures and molecular interactions of RNA and lipid carriers using atomic force microscopy. *Adv. Colloid Interface Sci.* **2023**, *313*, 102855.
(185) Takechi-Haraya, Y.; Usui, A.; Izutsu, K.-i.; Abe, Y. Atomic Force Microscopic Imaging of mRNA-lipid Nanoparticles in Aqueous Medium. *J. Pharm. Sci.* **2023**, *112*, 648−652.
(186) Safford, H. C.; Shuler, C. F.; Geisler, H. C.; Thatte, A. S.; Swingle, K. L.; Han, E. L.; Murray, A. M.; Hamilton, A. G.; Yamagata, H. M.; Mitchell, M. J. Probing the Role of Lipid Nanoparticle Elasticity on mRNA Delivery to the Placenta. *Nano Lett.* **2025**, *25*, 4800−4808.
(187) Guinier, A.; Fournet, G.; Yudowitch, K. L.; Walker, C. B. *Small-Angle Scattering of X-Rays*, 1st ed.; John Wiley & Sons, Inc.: New York, 1955.
(188) Spinozzi, F.; Moretti, P.; Perinelli, D. R.; Corucci, G.; Piergiovanni, P.; Amenitsch, H.; Sancini, G. A.; Franzese, G.; Blasi, P. Small-angle X-ray scattering unveils the internal structure of lipid nanoparticles. *J. Colloid Interface Sci.* **2024**, *662*, 446−459.
(189) Zheng, L.; Bandara, S. R.; Tan, Z.; Leal, C. Lipid nanoparticle topology regulates endosomal escape and delivery of RNA to the cytoplasm. *Proc. Natl. Acad. Sci. U.S.A.* **2023**, *120*, No. e2301067120.
(190) Caselli, L.; Conti, L.; De Santis, I.; Berti, D. Small-angle X-ray and neutron scattering applied to lipid-based nanoparticles: Recent advancements across different length scales. *Adv. Colloid Interface Sci.* **2024**, *327*, 103156.
(191) Graewert, M. A.; Wilhelmy, C.; Bacic, T.; Schumacher, J.; Blanchet, C.; Meier, F.; Drexel, R.; Welz, R.; Kolb, B.; Bartels, K.; Nawroth, T.; Klein, T.; Svergun, D.; Langguth, P.; Haas, H. Quantitative size-resolved characterization of mRNA nanoparticles by in-line coupling of asymmetrical-flow field-flow fractionation with small angle X-ray scattering. *Sci. Rep.* **2023**, *13*, 15764.
(192) Angelov, B.; Angelova, A.; Filippov, S. K.; Narayanan, T.; Drechsler, M.; Štěpánek, P.; Couvreur, P.; Lesieur, S. DNA/Fusogenic Lipid Nanocarrier Assembly: Millisecond Structural Dynamics. *J. Phys. Chem. Lett.* **2013**, *4*, 1959−1964.
(193) Yu, H.; Angelova, A.; Angelov, B.; Dyett, B.; Matthews, L.; Zhang, Y.; El Mohamad, M.; Cai, X.; Valimehr, S.; Drummond, C. J.; Zhai, J. Real-Time pH-Dependent Self-Assembly of Ionisable Lipids from COVID-19 Vaccines and *In Situ* Nucleic Acid Complexation. *Angew. Chem., Int. Ed.* **2023**, *62*, No. e202304977.
(194) Grant, T. D. Ab initio electron density determination directly from solution scattering data. *Nat. Methods* **2018**, *15*, 191−193.
(195) Dao, H. M.; AboulFotouh, K.; Hussain, A. F.; Marras, A. E.; Johnston, K. P.; Cui, Z.; Williams, R. O. Characterization of mRNA Lipid Nanoparticles by Electron Density Mapping Reconstruction: X-ray Scattering with Density from Solution Scattering (DENSS) Algorithm. *Pharm. Res.* **2024**, *41*, 501−512.
(196) Li, Y.; Ma, C.; Han, Z.; Weng, W.; Yang, S.; He, Z.; Li, Z.; Su, X.; Zuo, T.; Cheng, H. Morphology evolution of lipid nanoparticle discovered by small angle neutron scattering. *Giant* **2024**, *20*, 100329.
(197) Chen, X.; Ye, Y.; Li, M.; Zuo, T.; Xie, Z.; Ke, Y.; Cheng, H.; Hong, L.; Liu, Z. Structural Characterization of mRNA Lipid Nanoparticles in the Presence of Intrinsic Drug-free Lipid Nanoparticles. *bioRxiv* **2024**. DOI: 10.1101/2024.09.27.614859
(198) Castelli, F.; Puglia, C.; Sarpietro, M. G.; Rizza, L.; Bonina, F. Characterization of indomethacin-loaded lipid nanoparticles by differential scanning calorimetry. *Int. J. Pharm.* **2005**, *304*, 231−238.
(199) Bunjes, H.; Unruh, T. Characterization of lipid nanoparticles by differential scanning calorimetry, X-ray and neutron scattering. *Adv. Drug Delivery Rev.* **2007**, *59*, 379−402.
(200) Lewis, R. N.; McElhaney, R. N. Membrane lipid phase transitions and phase organization studied by Fourier transform infrared spectroscopy. *Biochimica et Biophysica Acta (BBA) - Biomembranes* **2013**, *1828*, 2347−2358.
(201) Sych, T.; Schlegel, J.; Barriga, H. M. G.; Ojansivu, M.; Hanke, L.; Weber, F.; Beklem Bostancioglu, R.; Ezzat, K.; Stangl, H.; Plochberger, B.; Laurencikiene, J.; El Andaloussi, S.; Fürth, D.; Stevens, M. M.; Sezgin, E. High-throughput measurement of the content and properties of nano-sized bioparticles with single-particle profiler. *Nat. Biotechnol.* **2024**, *42*, 587−590.
(202) Schultz, D.; Münter, R. D.; Cantín, A. M.; Kempen, P. J.; Jahnke, N.; Andresen, T. L.; Simonsen, J. B.; Urquhart, A. J. Enhancing RNA encapsulation quantification in lipid nanoparticles: Sustainable alternatives to Triton X-100 in the RiboGreen assay. *Eur. J. Pharm. Biopharm.* **2024**, *205*, 114571.
(203) Bizmark, N.; Nayagam, S.; Kim, B.; Amelemah, D. F.; Zhang, D.; Datta, S. S.; Priestley, R. D.; Colace, T.; Wang, J.; Prud'homme, R. K. Ribogreen Fluorescent Assay Kinetics to Measure Ribonucleic Acid Loading into Lipid Nanoparticle Carriers. *Adv. Mater. Interfaces* **2024**, *11*, 2301083.
(204) Liao, S.; Wang, S.; Wadhwa, A.; Birkenshaw, A.; Fox, K.; Cheng, M. H. Y.; Casmil, I. C.; Magana, A. A.; Bathula, N. V.; Ho, C. H.; Cheng, J.-Y.; Foster, L. J.; Harder, K. W.; Ross, C. J. D.; Cullis, P. R.; Blakney, A. K. Transfection Potency of Lipid Nanoparticles Containing mRNA Depends on Relative Loading Levels. *ACS Appl. Mater. Interfaces* **2025**, *17*, 3097−3105.
(205) Henrickson, A.; Kulkarni, J. A.; Zaifman, J.; Gorbet, G. E.; Cullis, P. R.; Demeler, B. Density Matching Multi-wavelength Analytical Ultracentrifugation to Measure Drug Loading of Lipid Nanoparticle Formulations. *ACS Nano* **2021**, *15*, 5068−5076.

(206) Bepperling, A.; Richter, G. Determination of mRNA copy number in degradable lipid nanoparticles via density contrast analytical ultracentrifugation. *Eur. Biophys. J.* **2023**, *52*, 393−400.
(207) Thaller, A.; Schmauder, L.; Frieß, W.; Winter, G.; Menzen, T.; Hawe, A.; Richter, K. SV-AUC as a stability-indicating method for the characterization of mRNA-LNPs. *Eur. J. Pharm. Biopharm.* **2023**, *182*, 152−156.
(208) Zhao, H.; Sousa, A. A.; Schuck, P. Flotation Coefficient Distributions of Lipid Nanoparticles by Sedimentation Velocity Analytical Ultracentrifugation. *ACS Nano* **2024**, *18*, 18663−18672.
(209) Vaidya, A.; Parande, D.; Khadse, N.; Vargas-Montoya, N.; Agarwal, V.; Ortiz, C.; Ellis, G.; Kaushal, N.; Sarode, A.; Karve, S.; DeRosa, F. Analytical Characterization of Heterogeneities in mRNA-Lipid Nanoparticles Using Sucrose Density Gradient Ultracentrifugation. *Anal. Chem.* **2024**, *96*, 5570−5579.
(210) Le Ru, E. C.; Böttger, R.; Andrews, D.; Baumhof, P.; Rakonjac, J. V.; Laufersky, G.; Darby, B. L. Rapid and Accurate Quantification of RNA in Lipid Nanoparticles by Scatter-Free UV/Visible Spectroscopy. *Nano Lett.* **2025**, *25*, 6813.
(211) Li, S.; Hu, Y.; Lin, J.; Schneiderman, Z.; Shao, F.; Wei, L.; Li, A.; Hsieh, K.; Kokkoli, E.; Curk, T.; Mao, H.-Q.; Wang, T.-H. Single-Particle Spectroscopic Chromatography Reveals Heterogeneous RNA Loading and Size Correlations in Lipid Nanoparticles. *ACS Nano* **2024**, *18*, 15729.
(212) Münter, R.; Larsen, J. B.; Andresen, T. L. The vast majority of nucleic acid-loaded lipid nanoparticles contain cargo. *J. Colloid Interface Sci.* **2024**, *674*, 139−144.
(213) De Peña, A. C.; Zimmer, D.; Gutterman-Johns, E.; Chen, N. M.; Tripathi, A.; Bailey-Hytholt, C. M. Electrophoretic Microfluidic Characterization of mRNA- and pDNA-Loaded Lipid Nanoparticles. *ACS Appl. Mater. Interfaces* **2024**, *16*, 26984−26997.
(214) Smith, M. C.; Crist, R. M.; Clogston, J. D.; McNeil, S. E. Zeta potential: a case study of cationic, anionic, and neutral liposomes. *Anal. Bioanal. Chem.* **2017**, *409*, 5779−5787.
(215) Doane, T. L.; Chuang, C.-H.; Hill, R. J.; Burda, C. Nanoparticle Zeta-Potentials. *Acc. Chem. Res.* **2012**, *45*, 317−326.
(216) Sivakumaran, M.; Platt, M. Tunable Resistive Pulse Sensing: Potential Applications in Nanomedicine. *Nanomedicine* **2016**, *11*, 2197−2214.
(217) Ito, T.; Sun, L.; Bevan, M. A.; Crooks, R. M. Comparison of Nanoparticle Size and Electrophoretic Mobility Measurements Using a Carbon-Nanotube-Based Coulter Counter, Dynamic Light Scattering, Transmission Electron Microscopy, and Phase Analysis Light Scattering. *Langmuir* **2004**, *20*, 6940−6945.
(218) Ito, T.; Sun, L.; Crooks, R. M. Simultaneous Determination of the Size and Surface Charge of Individual Nanoparticles Using a Carbon Nanotube-Based Coulter Counter. *Anal. Chem.* **2003**, *75*, 2399−2406.
(219) Cant, D. J. H.; Pei, Y.; Shchukarev, A.; Ramstedt, M.; Marques, S. S.; Segundo, M. A.; Parot, J.; Molska, A.; Borgos, S. E.; Shard, A. G.; Minelli, C. Cryo-XPS for Surface Characterization of Nanomedicines. *J. Phys. Chem. A* **2023**, *127*, 8220−8227.
(220) Penders, J.; Pence, I. J.; Horgan, C. C.; Bergholt, M. S.; Wood, C. S.; Najer, A.; Kauscher, U.; Nagelkerke, A.; Stevens, M. M. Single Particle Automated Raman Trapping Analysis. *Nat. Commun.* **2018**, *9*, 4256.
(221) Franconi, F.; Lemaire, L.; Gimel, J.-C.; Bonnet, S.; Saulnier, P. NMR diffusometry: A new perspective for nanomedicine exploration. *J. Controlled Release* **2021**, *337*, 155−167.
(222) Hallan, S. S.; Sguizzato, M.; Esposito, E.; Cortesi, R. Challenges in the Physical Characterization of Lipid Nanoparticles. *Pharmaceutics* **2021**, *13*, 549.
(223) Ramezanpour, M.; Schmidt, M. L.; Bodnariuc, I.; Kulkarni, J. A.; Leung, S. S. W.; Cullis, P. R.; Thewalt, J. L.; Tieleman, D. P. Ionizable amino lipid interactions with POPC: implications for lipid nanoparticle function. *Nanoscale* **2019**, *11*, 14141−14146.
(224) Wang, M. M.; Wappelhorst, C. N.; Jensen, E. L.; Chi, Y.-C. T.; Rouse, J. C.; Zou, Q. Elucidation of lipid nanoparticle surface structure in mRNA vaccines. *Sci. Rep.* **2023**, *13*, 16744.
(225) Viger-Gravel, J.; Schantz, A.; Pinon, A. C.; Rossini, A. J.; Schantz, S.; Emsley, L. Structure of Lipid Nanoparticles Containing siRNA or mRNA by Dynamic Nuclear Polarization-Enhanced NMR Spectroscopy. *J. Phys. Chem. B* **2018**, *122*, 2073−2081.
(226) Schroder, R.; Dorsey, P. J.; Vanderburgh, J.; Xu, W.; D'Addio, S. M.; Klein, L.; Gindy, M.; Su, Y. Probing Molecular Packing of Lipid Nanoparticles from^{31} P Solution and Solid-State NMR. *Anal. Chem.* **2024**, *96*, 2464−2473.
(227) Chen, T.; He, B.; Tao, J.; He, Y.; Deng, H.; Wang, X.; Zheng, Y. Application of Förster Resonance Energy Transfer (FRET) technique to elucidate intracellular and In Vivo biofate of nanomedicines. *Adv. Drug Delivery Rev.* **2019**, *143*, 177−205.
(228) Gravier, J.; Sancey, L.; Hirsjärvi, S.; Rustique, E.; Passirani, C.; Benoît, J.-P.; Coll, J.-L.; Texier, I. FRET Imaging Approaches for *in Vitro* and *in Vivo* Characterization of Synthetic Lipid Nanoparticles. *Mol. Pharmaceutics* **2014**, *11*, 3133−3144.
(229) Zhao, B.; Kamanzi, A.; Zhang, Y.; Chan, K. Y.; Robertson, M.; Leslie, S.; Cullis, P. R. Determination of the interior pH of lipid nanoparticles using a pH-sensitive fluorescent dye-based DNA probe. *Biosens. Bioelectron.* **2024**, *251*, 116065.
(230) Uebbing, L.; Ziller, A.; Siewert, C.; Schroer, M. A.; Blanchet, C. E.; Svergun, D. I.; Ramishetti, S.; Peer, D.; Sahin, U.; Haas, H.; Langguth, P. Investigation of pH-Responsiveness inside Lipid Nanoparticles for Parenteral mRNA Application Using Small-Angle X-ray Scattering. *Langmuir* **2020**, *36*, 13331−13341.
(231) Israelachvili, J. N.; Marčelja, S.; Horn, R. G. Physical principles of membrane organization. *Q. Rev. Biophys.* **1980**, *13*, 121−200.
(232) Cullis, P. R.; Hope, M. J.; Tilcock, C. P. Lipid polymorphism and the roles of lipids in membranes. *Chem. Phys. Lipids* **1986**, *40*, 127−144.
(233) Hafez, I.; Maurer, N.; Cullis, P. On the mechanism whereby cationic lipids promote intracellular delivery of polynucleic acids. *Gene Ther.* **2001**, *8*, 1188−1196.
(234) Iscaro, J.; Yu, H.; Martinez, N.; Subramaniam, S.; Joyce, P.; Wang, H.; Dyett, B. P.; White, J.; Prestidge, C. A.; Drummond, C. J.; Bozinovski, S.; Zhai, J. Lyotropic Liquid Crystalline Phase Nanostructure and Cholesterol Enhance Lipid Nanoparticle Mediated mRNA Transfection in Macrophages. *Adv. Funct. Mater.* **2024**, *34*, 24765−24774.
(235) Kulkarni, C. V.; Yaghmur, A.; Steinhart, M.; Kriechbaum, M.; Rappolt, M. Effects of High Pressure on Internally Self-Assembled Lipid Nanoparticles: A Synchrotron Small-Angle X-ray Scattering (SAXS) Study. *Langmuir* **2016**, *32*, 11907−11917.
(236) Zhang, J.; Fei, Y.; Sun, L.; Zhang, Q. C. Advances and opportunities in RNA structure experimental determination and computational modeling. *Nat. Methods* **2022**, *19*, 1193−1207.
(237) Ding, J.; Lee, Y.-T.; Bhandari, Y.; Schwieters, C. D.; Fan, L.; Yu, P.; Tarosov, S. G.; Stagno, J. R.; Ma, B.; Nussinov, R.; Rein, A.; Zhang, J.; Wang, Y.-X. Visualizing RNA conformational and architectural heterogeneity in solution. *Nat. Commun.* **2023**, *14*, 714.
(238) Zhao, Q.; Zhao, Z.; Fan, X.; Yuan, Z.; Mao, Q.; Yao, Y. Review of machine learning methods for RNA secondary structure prediction. *PLOS Computational Biology* **2021**, *17*, No. e1009291.
(239) Higgs, P. G. RNA secondary structure: physical and computational aspects. *Q. Rev. Biophys.* **2000**, *33*, 199−253.
(240) Zhao, Y.; Wang, J.; Zeng, C.; Xiao, Y. Evaluation of RNA secondary structure prediction for both base-pairing and topology. *Biophysics Reports* **2018**, *4*, 123−132.
(241) Gutell, R. R.; Lee, J. C.; Cannone, J. J. The accuracy of ribosomal RNA comparative structure models. *Curr. Opin. Struct. Biol.* **2002**, *12*, 301−310.
(242) Bernhart, S. H.; Hofacker, I. L.; Will, S.; Gruber, A. R.; Stadler, P. F. RNAalifold: improved consensus structure prediction for RNA alignments. *BMC Bioinformatics* **2008**, *9*, 474.
(243) Hofacker, I. L.; Fekete, M.; Stadler, P. F. Secondary Structure Prediction for Aligned RNA Sequences. *J. Mol. Biol.* **2002**, *319*, 1059−1066.
(244) Higgins, N. P.; Vologodskii, A. V. Topological Behavior of Plasmid DNA. *Microbiol. Spectr.* **2015**, *3*, 17.

https://doi.org/10.1021/acsnano.4c18274
ACS Nano XXXX, XXX, XXX−XXX

(245) Grzetic, D.; Hamilton, N.; Shelley, J. Coarse-Grained Simulation of mRNA-Loaded Lipid Nanoparticle Self-Assembly. *Mol. Pharmaceutics* **2024**, *21*, 4747−4753.
(246) Bose, R.; Saleem, I.; Mustoe, A. M. Causes, functions, and therapeutic possibilities of RNA secondary structure ensembles and alternative states. *Cell Chemical Biology* **2024**, *31*, 17−35.
(247) Mustoe, A. M.; Corley, M.; Laederach, A.; Weeks, K. M. Messenger RNA Structure Regulates Translation Initiation: A Mechanism Exploited from Bacteria to Humans. *Biochemistry* **2018**, *57*, 3537−3539.
(248) Zhigaltsev, I. V.; Winters, G.; Srinivasulu, M.; Crawford, J.; Wong, M.; Amankwa, L.; Waterhouse, D.; Masin, D.; Webb, M.; Harasym, N. Development of a weak-base docetaxel derivative that can be loaded into lipid nanoparticles. *J. Controlled Release* **2010**, *144*, 332−340.
(249) Garaizar, A.; Díaz-Oviedo, D.; Zablowsky, N.; Rissanen, S.; Köbberling, J.; Sun, J.; Steiger, C.; Steigemann, P.; Mann, F. A.; Meier, K. Toward understanding lipid reorganization in RNA lipid nanoparticles in acidic environments. *Proc. Natl. Acad. Sci. U.S.A.* **2024**, *121*, No. e2404555121.
(250) Unruh, T.; Götz, K.; Vogel, C.; Fröhlich, E.; Scheurer, A.; Porcar, L.; Steiniger, F. Mesoscopic Structure of Lipid Nanoparticle Formulations for mRNA Drug Delivery: Comirnaty and Drug-Free Dispersions. *ACS Nano* **2024**, *18*, 9746−9764.
(251) Ziller, A.; Nogueira, S. S.; Hühn, E.; Funari, S. S.; Brezesinski, G.; Hartmann, H.; Sahin, U.; Haas, H.; Langguth, P. Incorporation of mRNA in Lamellar Lipid Matrices for Parenteral Administration. *Mol. Pharmaceutics* **2018**, *15*, 642−651.
(252) Liu, L.; Kim, J.-H.; Li, Z.; Sun, M.; Northen, T.; Tang, J.; Mcintosh, E.; Karve, S.; DeRosa, F. PEGylated lipid screening, composition optimization, and structure−activity relationship determination for lipid nanoparticle-mediated mRNA delivery. *Nanoscale* **2025**, *17*, 11329.
(253) Trollmann, M. F.; Böckmann, R. A. mRNA lipid nanoparticle phase transition. *Biophys. J.* **2022**, *121*, 3927−3939.
(254) Kulkarni, J. A.; Witzigmann, D.; Leung, J.; Tam, Y. Y. C.; Cullis, P. R. On the role of helper lipids in lipid nanoparticle formulations of siRNA. *Nanoscale* **2019**, *11*, 21733−21739.
(255) Tirosh, O.; Barenholz, Y.; Katzhendler, J.; Priev, A. Hydration of Polyethylene Glycol-Grafted Liposomes. *Biophys. J.* **1998**, *74*, 1371−1379.
(256) Eygeris, Y.; Henderson, M. I.; Curtis, A. G.; Jozić, A.; Stoddard, J.; Reynaga, R.; Chirco, K. R.; Su, G. L.-N.; Neuringer, M.; Lauer, A. K.; Ryals, R. C.; Sahay, G. Preformed Vesicle Approach to LNP Manufacturing Enhances Retinal mRNA Delivery. *Small* **2024**, *20*, 2400815.
(257) Slaughter, K. V.; Donders, E. N.; Jones, M. S.; Sabbah, S. G.; Elliott, M. J.; Shoichet, B. K.; Cescon, D. W.; Shoichet, M. S. Ionizable Drugs Enable Intracellular Delivery of Co-Formulated siRNA. *Adv. Mater.* **2024**, *36*, 2403701.
(258) Kulkarni, J.; Chander, N.; Basha, G.; Ciufolini, M. A., Witzigmann, D.; Cullis, P. U.S. Patent US20240374754A1, 2024.
(259) Henderson, M. I.; Eygeris, Y.; Jozic, A.; Herrera, M.; Sahay, G. Leveraging Biological Buffers for Efficient Messenger RNA Delivery via Lipid Nanoparticles. *Mol. Pharmaceutics* **2022**, *19*, 4275−4285.
(260) Meulewaeter, S.; Nuytten, G.; Cheng, M. H.; De Smedt, S. C.; Cullis, P. R.; De Beer, T.; Lentacker, I.; Verbeke, R. Continuous freeze-drying of messenger RNA lipid nanoparticles enables storage at higher temperatures. *J. Controlled Release* **2023**, *357*, 149−160.
(261) Omo-Lamai, S.; Wang, Y.; Patel, M. N.; Essien, E.-O.; Shen, M.; Majumdar, A.; Espy, C.; Wu, J.; Channer, B.; Tobin, M.; Murali, S.; Papp, T. E.; Maheshwari, R.; Wang, L.; Chase, L. S.; Zamora, M. E.; Arral, M. L.; Marcos-Contreras, O. A.; Myerson, J. W.; Hunter, C. A.; Tsourkas, A.; Muzykantov, V.; Brodsky, I.; Shin, S.; Whitehead, K. A.; Gaskill, P.; Discher, D.; Parhiz, H.; Brenner, J. S. Lipid Nanoparticle-Associated Inflammation is Triggered by Sensing of Endosomal Damage: Engineering Endosomal Escape Without Side Effects. *bioRxiv* **2024**. DOI: 10.1101/2024.04.16.589801
(262) Münter, R.; Christensen, E.; Andresen, T. L.; Larsen, J. B. Studying how administration route and dose regulates antibody generation against LNPs for mRNA delivery with single-particle resolution. *Molecular Therapy - Methods & Clinical Development* **2023**, *29*, 450−459.
(263) Carucci, C.; Philipp, J.; Müller, J. A.; Sudarsan, A.; Kostyurina, E.; Blanchet, C. E.; Schwierz, N.; Parsons, D. F.; Salis, A.; Rädler, J. O. Buffer Specificity of Ionizable Lipid Nanoparticle Transfection Efficiency and Bulk Phase Transition. *ACS Nano* **2025**, *19*, 10829−10840.
(264) Mo, Y.; Keszei, A. F. A.; Kothari, S.; Liu, H.; Pan, A.; Kim, P.; Bu, J.; Kamanzi, A.; Dai, D. L.; Mazhab-Jafari, M. T.; Chen, J.; Leslie, S.; Zheng, G. Lipid-siRNA Organization Modulates the Intracellular Dynamics of Lipid Nanoparticles. *J. Am. Chem. Soc.* **2025**, *147*, 10430.
(265) Muramatsu, H.; Lam, K.; Bajusz, C.; Laczkó, D.; Karikó, K.; Schreiner, P.; Martin, A.; Lutwyche, P.; Heyes, J.; Pardi, N. Lyophilization provides long-term stability for a lipid nanoparticle-formulated, nucleoside-modified mRNA vaccine. *Molecular Therapy* **2022**, *30*, 1941−1951.
(266) AboulFotouh, K.; Southard, B.; Dao, H. M.; Xu, H.; Moon, C.; Williams, R. O., III; Cui, Z. Effect of lipid composition on RNA-Lipid nanoparticle properties and their sensitivity to thin-film freezing and drying. *Int. J. Pharm.* **2024**, *650*, 123688.
(267) Li, Q.; Shi, R.; Xu, H.; AboulFotouh, K.; Sung, M. M.; Oguin, T. H.; Hayes, M.; Moon, C.; Dao, H. M.; Ni, H.; Sahakijpijarn, S.; Cano, C.; Davenport, G. J.; Williams, R. O.; Le Huray, J.; Cui, Z.; Weissman, D. Thin-film freeze-drying of an influenza virus hemagglutinin mRNA vaccine in unilamellar lipid nanoparticles with blebs. *J. Controlled Release* **2024**, *375*, 829−838.
(268) Zimmermann, C. M.; Baldassi, D.; Chan, K.; Adams, N. B.; Neumann, A.; Porras-Gonzalez, D. L.; Wei, X.; Kneidinger, N.; Stoleriu, M. G.; Burgstaller, G.; Witzigmann, D.; Luciani, P.; Merkel, O. M. Spray drying siRNA-lipid nanoparticles for dry powder pulmonary delivery. *J. Controlled Release* **2022**, *351*, 137−150.
(269) Lewis, L. M.; Badkar, A. V.; Cirelli, D.; Combs, R.; Lerch, T. F. The Race to Develop the Pfizer-BioNTech COVID-19 Vaccine: From the Pharmaceutical Scientists' Perspective. *J. Pharm. Sci.* **2023**, *112*, 640−647.
(270) Fan, Y.; Rigas, D.; Kim, L. J.; Chang, F.-P.; Zang, N.; McKee, K.; Kemball, C. C.; Yu, Z.; Winkler, P.; Su, W.-C.; Jessen, P.; Hura, G. L.; Chen, T.; Koenig, S. G.; Nagapudi, K.; Leung, D.; Yen, C.-W. Physicochemical and structural insights into lyophilized mRNA-LNP from lyoprotectant and buffer screenings. *J. Controlled Release* **2024**, *373*, 727−737.
(271) Kudsiova, L.; Lansley, A.; Scutt, G.; Allen, M.; Bowler, L.; Williams, S.; Lippett, S.; Stafford, S.; Tarzi, M.; Cross, M.; Okorie, M. Stability testing of the Pfizer-BioNTech BNT162b2 COVID-19 vaccine: a translational study in UK vaccination centres. *BMJ Open Science* **2021**, *5*. DOI: 10.1136/bmjos-2021-100203
(272) Ruppl, A.; Kiesewetter, D.; Strütt, F.; Köll-Weber, M.; Süss, R.; Allmendinger, A. Don't shake it! Mechanical stress testing of mRNA-lipid nanoparticles. *Eur. J. Pharm. Biopharm.* **2024**, *198*, 114265.
(273) Selmin, F.; Musazzi, U. M.; Franzè, S.; Scarpa, E.; Rizzello, L.; Procacci, P.; Minghetti, P. Pre-Drawn Syringes of Comirnaty for an Efficient COVID-19 Mass Vaccination: Demonstration of Stability. *Pharmaceutics* **2021**, *13*, 1029.
(274) Zhang, H.; Barz, M. Investigating the stability of RNA-lipid nanoparticles in biological fluids: Unveiling its crucial role for understanding LNP performance. *J. Controlled Release* **2025**, *381*, 113559.
(275) Bertrand, N.; Leroux, J.-C. The journey of a drug-carrier in the body: An anatomo-physiological perspective. *J. Controlled Release* **2012**, *161*, 152−163.
(276) Tenzer, S.; Docter, D.; Kuharev, J.; Musyanovych, A.; Fetz, V.; Hecht, R.; Schlenk, F.; Fischer, D.; Kiouptsi, K.; Reinhardt, C.; Landfester, K.; Schild, H.; Maskos, M.; Knauer, S. K.; Stauber, R. H. Rapid formation of plasma protein corona critically affects nanoparticle pathophysiology. *Nat. Nanotechnol.* **2013**, *8*, 772−781.

(277) Mui, B. L.; Tam, Y. K.; Jayaraman, M.; Ansell, S. M.; Du, X.; Tam, Y. Y. C.; Lin, P. J.; Chen, S.; Narayanannair, J. K.; Rajeev, K. G.; Manoharan, M.; Akinc, A.; Maier, M. A.; Cullis, P.; Madden, T. D.; Hope, M. J. Influence of Polyethylene Glycol Lipid Desorption Rates on Pharmacokinetics and Pharmacodynamics of siRNA Lipid Nanoparticles. *Molecular Therapy - Nucleic Acids* **2013**, *2*, No. e139.
(278) Huotari, J.; Helenius, A. Endosome maturation: Endosome maturation. *EMBO Journal* **2011**, *30*, 3481−3500.
(279) Xu, Z.; Seddon, J. M.; Beales, P. A.; Rappolt, M.; Tyler, A. I. I. Breaking Isolation to Form New Networks: pH-Triggered Changes in Connectivity inside Lipid Nanoparticles. *J. Am. Chem. Soc.* **2021**, *143*, 16556−16565.
(280) Bitounis, D.; Jacquinet, E.; Rogers, M. A.; Amiji, M. M. Strategies to reduce the risks of mRNA drug and vaccine toxicity. *Nat. Rev. Drug Discovery* **2024**, *23*, 281−300.
(281) De, A.; Ko, Y. T. Why mRNA-ionizable LNPs formulations are so short-lived: causes and way-out. *Expert Opinion on Drug Delivery* **2023**, *20*, 175−187.
(282) Oude Blenke, E.; Örnskov, E.; Schöneich, C.; Nilsson, G. A.; Volkin, D. B.; Mastrobattista, E.; Almarsson, Ö.; Crommelin, D. J. The storage and in-use stability of mRNA vaccines and therapeutics: Not a cold case. *J. Pharm. Sci.* **2023**, *112*, 386−403.
(283) Müller, J. A.; Schäffler, N.; Kellerer, T.; Schwake, G.; Ligon, T. S.; Rädler, J. O. Kinetics of RNA-LNP delivery and protein expression. *Eur. J. Pharm. Biopharm.* **2024**, *197*, 114222.
(284) Liu, H.; Chen, M. Z.; Payne, T.; Porter, C. J.; Pouton, C. W.; Johnston, A. P. Beyond the Endosomal Bottleneck: Understanding the Efficiency of mRNA/LNP Delivery. *Adv. Funct. Mater.* **2024**, *34*, 2404510.
(285) Arevalo, C. P.; Bolton, M. J.; Le Sage, V.; Ye, N.; Furey, C.; Muramatsu, H.; Alameh, M.-G.; Pardi, N.; Drapeau, E. M.; Parkhouse, K.; Garretson, T.; Morris, J. S.; Moncla, L. H.; Tam, Y. K.; Fan, S. H. Y.; Lakdawala, S. S.; Weissman, D.; Hensley, S. E. A multivalent nucleoside-modified mRNA vaccine against all known influenza virus subtypes. *Science* **2022**, *378*, 899−904.
(286) Zhao, S.; Gao, K.; Han, H.; Stenzel, M.; Yin, B.; Song, H.; Lawanprasert, A.; Nielsen, J. E.; Sharma, R.; Arogundade, O. H.; Pimcharoen, S.; Chen, Y.-J.; Paul, A.; Tuma, J.; Collins, M. G.; Wyle, Y.; Cranick, M. G.; Burgstone, B. W.; Perez, B. S.; Barron, A. E.; Smith, A. M.; Lee, H. Y.; Wang, A.; Murthy, N. Acid-degradable lipid nanoparticles enhance the delivery of mRNA. *Nat. Nanotechnol.* **2024**, *19*, 1702−1711.
(287) Han, X.; Alameh, M.-G.; Butowska, K.; Knox, J. J.; Lundgreen, K.; Ghattas, M.; Gong, N.; Xue, L.; Xu, Y.; Lavertu, M.; Bates, P.; Xu, J.; Nie, G.; Zhong, Y.; Weissman, D.; Mitchell, M. J. Adjuvant lipidoid-substituted lipid nanoparticles augment the immunogenicity of SARS-CoV-2 mRNA vaccines. *Nat. Nanotechnol.* **2023**, *18*, 1105−1114.
(288) Xue, L.; Gong, N.; Shepherd, S. J.; Xiong, X.; Liao, X.; Han, X.; Zhao, G.; Song, C.; Huang, X.; Zhang, H.; Padilla, M. S.; Qin, J.; Shi, Y.; Alameh, M.-G.; Pochan, D. J.; Wang, K.; Long, F.; Weissman, D.; Mitchell, M. J. Rational Design of Bisphosphonate Lipid-like Materials for mRNA Delivery to the Bone Microenvironment. *J. Am. Chem. Soc.* **2022**, *144*, 9926−9937.
(289) Kim, H.-K.; Davaa, E.; Myung, C.-S.; Park, J.-S. Enhanced siRNA delivery using cationic liposomes with new polyarginine-conjugated PEG-lipid. *Int. J. Pharm.* **2010**, *392*, 141−147.
(290) He, X.; Payne, T. J.; Takanashi, A.; Fang, Y.; Kerai, S. D.; Morrow, J. P.; Al-Wassiti, H.; Pouton, C. W.; Kempe, K. Tailored monoacyl poly(2-oxazoline)- and poly(2-oxazine)-lipids as PEG-lipid alternatives for stabilization and delivery of mRNA-lipid nanoparticles. *Biomacromolecules* **2024**, *25*, 4591−4603.
(291) Liu, S.; Cheng, Q.; Wei, T.; Yu, X.; Johnson, L. T.; Farbiak, L.; Siegwart, D. J. Membrane-destabilizing ionizable phospholipids for organ-selective mRNA delivery and CRISPR−Cas gene editing. *Nat. Mater.* **2021**, *20*, 701−710.
(292) Cheng, Q.; Wei, T.; Farbiak, L.; Johnson, L. T.; Dilliard, S. A.; Siegwart, D. J. Selective organ targeting (SORT) nanoparticles for tissue-specific mRNA delivery and CRISPR−Cas gene editing. *Nat. Nanotechnol.* **2020**, *15*, 313−320.
(293) Vaidya, A.; Moore, S.; Chatterjee, S.; Guerrero, E.; Kim, M.; Farbiak, L.; Dilliard, S. A.; Siegwart, D. J. Expanding RNAi to kidneys, lungs, and spleen via selective organ targeting (SORT) siRNA lipid nanoparticles. *Adv. Mater.* **2024**, *36*, 2313791.
(294) Wang, X.; Liu, S.; Sun, Y.; Yu, X.; Lee, S. M.; Cheng, Q.; Wei, T.; Gong, J.; Robinson, J.; Zhang, D.; Lian, X.; Basak, P.; Siegwart, D. J. Preparation of selective organ-targeting (SORT) lipid nanoparticles (LNPs) using multiple technical methods for tissue-specific mRNA delivery. *Nat. Protoc.* **2023**, *18*, 265−291.
(295) Wei, T.; Sun, Y.; Cheng, Q.; Chatterjee, S.; Traylor, Z.; Johnson, L. T.; Coquelin, M. L.; Wang, J.; Torres, M. J.; Lian, X.; Wang, X.; Xiao, Y.; Hodges, C. A.; Siegwart, D. J. Lung SORT LNPs enable precise homology-directed repair mediated CRISPR/Cas genome correction in cystic fibrosis models. *Nat. Commun.* **2023**, *14*, 7322.
(296) Dilliard, S. A.; Cheng, Q.; Siegwart, D. J. On the mechanism of tissue-specific mRNA delivery by selective organ targeting nanoparticles. *Proc. Natl. Acad. Sci. U.S.A.* **2021**, *118*, No. e2109256118.
(297) Su, K.; Shi, L.; Sheng, T.; Yan, X.; Lin, L.; Meng, C.; Wu, S.; Chen, Y.; Zhang, Y.; Wang, C.; Wang, Z.; Qiu, J.; Zhao, J.; Xu, T.; Ping, Y.; Gu, Z.; Liu, S. Reformulating lipid nanoparticles for organ-targeted mRNA accumulation and translation. *Nat. Commun.* **2024**, *15*, 5659.
(298) Kim, M.; Jeong, M.; Hur, S.; Cho, Y.; Park, J.; Jung, H.; Seo, Y.; Woo, H. A.; Nam, K. T.; Lee, K.; Lee, H. Engineered ionizable lipid nanoparticles for targeted delivery of RNA therapeutics into different types of cells in the liver. *Sci. Adv.* **2021**, *7*, No. eabf4398.
(299) Parhiz, H.; Shuvaev, V. V.; Pardi, N.; Khoshnejad, M.; Kiseleva, R. Y.; Brenner, J. S.; Uhler, T.; Tuyishime, S.; Mui, B. L.; Tam, Y. K.; Madden, T. D.; Hope, M. J.; Weissman, D.; Muzykantov, V. R. PECAM-1 directed re-targeting of exogenous mRNA providing two orders of magnitude enhancement of vascular delivery and expression in lungs independent of apolipoprotein E-mediated uptake. *J. Controlled Release* **2018**, *291*, 106−115.
(300) Breda, L.; Papp, T. E.; Triebwasser, M. P.; Yadegari, A.; Fedorky, M. T.; Tanaka, N.; Abdulmalik, O.; Pavani, G.; Wang, Y.; Grupp, S. A.; Chou, S. T.; Ni, H.; Mui, B. L.; Tam, Y. K.; Weissman, D.; Rivella, S.; Parhiz, H. In vivo hematopoietic stem cell modification by mRNA delivery. *Science* **2023**, *381*, 436−443.
(301) Rurik, J. G.; Tombacz, I.; Yadegari, A.; Mendez Fernandez, P. O.; Shewale, S. V.; Li, L.; Kimura, T.; Soliman, O. Y.; Papp, T. E.; Tam, Y. K.; Mui, B. L.; Albelda, S. M.; Pure, E.; June, C. H.; Aghajanian, H.; Weissman, D.; Parhiz, H.; Epstein, J. A. CAR T cells produced in vivo to treat cardiac injury. *Science* **2022**, *375*, 91−96.
(302) Nong, J.; Gong, X.; Dang, Q. M.; Tiwari, S.; Patel, M.; Wu, J.; Hanna, A.; Park, W.-J.; Atochina-Vasserman, E. N., Huang, H.-T.; Marcos-Contreras, O. A.; Morris-Blanco, K. C.; Miner, J. J.; Weissman, D.; Muzykantov, V. R.; Gupta, K.; Issadore, D.; Myerson, J. W.; Wang, Z.; Brenner, J. S. Multi-stage-mixing to control the supramolecular structure of lipid nanoparticles, thereby creating a core-then-shell arrangement that improves performance by orders of magnitude*bioRxiv* **2024**. DOI: 10.1101/2024.11.12.623321
(303) Zhou, H.; Chen, D. S.; Hu, C. J.; Hong, X.; Shi, J.; Xiao, Y. Stimuli-Responsive Nanotechnology for RNA Delivery. *Adv. Sci.* **2023**, *10*, 2303597.
(304) Lu, Z.-R.; Laney, V. E. A.; Hall, R.; Ayat, N. Environment-Responsive Lipid/siRNA Nanoparticles for Cancer Therapy. *Adv. Healthcare Mater.* **2021**, *10*, 2001294.
(305) Cheng, L.; Zhu, Y.; Ma, J.; Aggarwal, A.; Toh, W. H.; Shin, C.; Sangpachatanaruk, W.; Weng, G.; Kumar, R.; Mao, H.-Q. Machine learning elucidates design features of plasmid deoxyribonucleic acid lipid nanoparticles for cell type-preferential transfection. *ACS Nano* **2024**, *18*, 28735−28747.
(306) Wang, W.; Feng, S.; Ye, Z.; Gao, H.; Lin, J.; Ouyang, D. Prediction of lipid nanoparticles for mRNA vaccines by the machine learning algorithm. *Acta Pharmaceutica Sinica B* **2022**, *12*, 2950−2962.
(307) Maharjan, R.; Hada, S.; Lee, J. E.; Han, H.-K.; Kim, K. H.; Seo, H. J.; Foged, C.; Jeong, S. H. Comparative study of lipid nanoparticle-based mRNA vaccine bioprocess with machine learning and combinatorial artificial neural network-design of experiment approach. *Int. J. Pharm.* **2023**, *640*, 123012.

(308) Sato, S.; Sano, S.; Muto, H.; Kubara, K.; Kondo, K.; Miyazaki, T.; Suzuki, Y.; Uemoto, Y.; Ukai, K. Understanding the manufacturing process of lipid nanoparticles for mRNA delivery using machine learning. *Chem. Pharm. Bull.* **2024**, *72*, 529−539.
(309) Maharjan, R.; Kim, K. H.; Lee, K.; Han, H.-K.; Jeong, S. H. Machine learning-driven optimization of mRNA-lipid nanoparticle vaccine quality with XGBoost/Bayesian method and ensemble model approaches. *Journal of Pharmaceutical Analysis* **2024**, *14*, 100996.
(310) Bae, S.-H.; Choi, H.; Lee, J.; Kang, M.-H.; Ahn, S.-H.; Lee, Y.-S.; Choi, H.; Jo, S.; Lee, Y.; Park, H.-J.; Lee, S.; Yoon, S.; Roh, G.; Cho, S.; Cho, Y.; Ha, D.; Lee, S.-Y.; Choi, E.-J.; Oh, A.; Kim, J.; Lee, S.; Hong, J.; Lee, N.; Lee, M.; Park, J.; Jeong, D.-H.; Lee, K.; Nam, J.-H. Rational Design of Lipid Nanoparticles for Enhanced mRNA Vaccine Delivery via Machine Learning. *Small* **2025**, *21*, 2405618.
(311) Abostait, A.; Abdelkarim, M.; Bao, Z.; Miyake, Y.; Tse, W. H.; Di Ciano-Oliveir, C.; Buerki-Thurnherr, T.; Allen, C.; Keijzer, R.; Labouta, H. I. Optimizing lipid nanoparticles for fetal gene delivery in vitro, ex vivo, and aided with machine learning. *J. Controlled Release* **2024**, *376*, 678−700.
(312) Dorsey, P. J.; Lau, C. L.; Chang, T.-c.; Doerschuk, P. C.; D'Addio, S. M. Review of machine learning for lipid nanoparticle formulation and process development. *J. Pharm. Sci.* **2024**, *113*, 3413−3433.
(313) Siegwart, D. J.; Whitehead, K. A.; Nuhn, L.; Sahay, G.; Cheng, H.; Jiang, S.; Ma, M.; Lytton-Jean, A.; Vegas, A.; Fenton, P.; Levins, C. G.; Love, K. T.; Lee, H.; Cortez, C.; Collins, S. P.; Li, Y. F.; Jang, J.; Querbes, W.; Zurenko, C.; Novobrantseva, T.; Langer, R.; Anderson, D. G. Combinatorial synthesis of chemically diverse core-shell nanoparticles for intracellular delivery. *Proc. Natl. Acad. Sci. U.S.A.* **2011**, *108*, 12996−13001.
(314) Hao, J.; Kos, P.; Zhou, K.; Miller, J. B.; Xue, L.; Yan, Y.; Xiong, H.; Elkassih, S.; Siegwart, D. J. Rapid Synthesis of a Lipocationic Polyester Library via Ring-Opening Polymerization of Functional Valerolactones for Efficacious siRNA Delivery. *J. Am. Chem. Soc.* **2015**, *137*, 9206−9209.
(315) Sago, C. D.; Lokugamage, M. P.; Paunovska, K.; Vanover, D. A.; Monaco, C. M.; Shah, N. N.; Gamboa Castro, M.; Anderson, S. E.; Rudoltz, T. G.; Lando, G. N.; Munnilal Tiwari, P.; Kirschman, J. L.; Willett, N.; Jang, Y. C.; Santangelo, P. J.; Bryksin, A. V.; Dahlman, J. E. High-throughput in vivo screen of functional mRNA delivery identifies nanoparticles for endothelial cell gene editing. *Proc. Natl. Acad. Sci. U.S.A.* **2018**, *115*. DOI: 10.1073/pnas.1811276115
(316) Pan, I.; Mason, L. R.; Matar, O. K. Data-centric engineering: integrating simulation, machine learning and statistics. Challenges and opportunities. *Chem. Eng. Sci.* **2022**, *249*, 117271.
(317) Destro, F.; Inguva, P. K.; Srisuma, P.; Braatz, R. D. Advanced methodologies for model-based optimization and control of pharmaceutical processes. *Current Opinion in Chemical Engineering* **2024**, *45*, 101035.
(318) Inguva, P. K.; Mukherjee, S.; Walker, P. J.; Kanso, M. A.; Wang, J.; Wu, Y.; Tenberg, V.; Santra, S.; Singh, S.; Kim, S. H.; Trout, B. L.; Bazant, M. Z.; Myerson, A. S.; Braatz, R. D. Mechanistic Modeling of Lipid Nanoparticle Formation for the Delivery of Nucleic Acid Therapeutics. *arXiv* **2024**. DOI: 10.48550/arXiv.2408.08577
(319) Jing, H.; Wang, Y.; Desai, P. R.; Ramamurthi, K. S.; Das, S. Formation and Properties of a Self-Assembled Nanoparticle-Supported Lipid Bilayer Probed through Molecular Dynamics Simulations. *Langmuir* **2020**, *36*, 5524−5533.
(320) Paloncýová, M.; Čechová, P.; Šrejber, M.; Kührová, P.; Otyepka, M. Role of Ionizable Lipids in SARS-CoV-2 Vaccines As Revealed by Molecular Dynamics Simulations: From Membrane Structure to Interaction with mRNA Fragments. *J. Phys. Chem. Lett.* **2021**, *12*, 11199−11205.
(321) Maeki, M.; Kimura, N.; Okada, Y.; Shimizu, K.; Shibata, K.; Miyazaki, Y.; Ishida, A.; Yonezawa, K.; Shimizu, N.; Shinoda, W.; Tokeshi, M. Understanding the effects of ethanol on the liposome bilayer structure using microfluidic-based time-resolved small-angle X-ray scattering and molecular dynamics simulations. *Nanoscale Advances* **2024**, *6*, 2166−2176.
(322) Paloncýová, M.; Valério, M.; Dos Santos, R. N.; Kührová, P.; Šrejber, M.; Čechová, P.; Dobchev, D. A.; Balsubramani, A.; Banáš, P.; Agarwal, V.; Souza, P. C. T.; Otyepka, M. Computational Methods for Modeling Lipid-Mediated Active Pharmaceutical Ingredient Delivery. *Mol. Pharm.* **2025**, *22*, 1110.
(323) Kimura, N.; Maeki, M.; Sato, Y.; Note, Y.; Ishida, A.; Tani, H.; Harashima, H.; Tokeshi, M. Development of the iLiNP device: Fine tuning the lipid nanoparticle size within 10 nm for drug delivery. *ACS Omega* **2018**, *3*, 5044−5051.
(324) Na, G.-S.; Joo, J.-U.; Lee, J. Y.; Yun, Y.; Kaang, B. K.; Yang, J.-S.; Kim, K.; Kim, D.-P. Full-cycle study on developing a novel structured micromixer and evaluating the nanoparticle products as mRNA delivery carriers. *J. Controlled Release* **2024**, *373*, 161−171.
(325) Yang, Y.; Corona, A.; Henson, M. A. Experimental investigation and population balance equation modeling of solid lipid nanoparticle aggregation dynamics. *J. Colloid Interface Sci.* **2012**, *374*, 297−307.
(326) Mendes, B. B.; Conniot, J.; Avital, A.; Yao, D.; Jiang, X.; Zhou, X.; Sharf-Pauker, N.; Xiao, Y.; Adir, O.; Liang, H.; Shi, J.; Schroeder, A.; Conde, J. Nanodelivery of nucleic acids. *Nat. Rev. Methods Primers* **2022**, *2*, 24.
(327) Luther, D. C.; Huang, R.; Jeon, T.; Zhang, X.; Lee, Y.-W.; Nagaraj, H.; Rotello, V. M. Delivery of drugs, proteins, and nucleic acids using inorganic nanoparticles. *Adv. Drug Delivery Rev.* **2020**, *156*, 188−213.
(328) Moazzam, M.; Zhang, M.; Hussain, A.; Yu, X.; Huang, J.; Huang, Y. The landscape of nanoparticle-based siRNA delivery and therapeutic development. *Molecular Therapy* **2024**, *32*, 284−312.
(329) Eweje, F.; Walsh, M. L.; Ahmad, K.; Ibrahim, V.; Alrefai, A.; Chen, J.; Chaikof, E. L. Protein-based nanoparticles for therapeutic nucleic acid delivery. *Biomaterials* **2024**, *305*, 122464.
(330) Boisguérin, P.; Konate, K.; Josse, E.; Vivès, E.; Deshayes, S. Peptide-Based Nanoparticles for Therapeutic Nucleic Acid Delivery. *Biomedicines* **2021**, *9*, 583.
(331) Amaya, L.; Grigoryan, L.; Li, Z.; Lee, A.; Wender, P. A.; Pulendran, B.; Chang, H. Y. Circular RNA vaccine induces potent T cell responses. *Proc. Natl. Acad. Sci. U.S.A.* **2023**, *120*, No. e2302191120.
(332) Yang, W.; Mixich, L.; Boonstra, E.; Cabral, H. Polymer-Based mRNA Delivery Strategies for Advanced Therapies. *Adv. Healthcare Mater.* **2023**, *12*, 2202688.
(333) Kumar, P.; Wu, H.; McBride, J. L.; Jung, K.-E.; Hee Kim, M.; Davidson, B. L.; Kyung Lee, S.; Shankar, P.; Manjunath, N. Transvascular delivery of small interfering RNA to the central nervous system. *Nature* **2007**, *448*, 39−43.
(334) Tai, W.; Gao, X. Functional peptides for siRNA delivery. *Adv. Drug Delivery Rev.* **2017**, *110*−*111*, 157−168.
(335) Hoyer, J.; Neundorf, I. Peptide Vectors for the Nonviral Delivery of Nucleic Acids. *Acc. Chem. Res.* **2012**, *45*, 1048−1056.
(336) Mohanty, A.; Uthaman, S.; Park, I.-K. Utilization of Polymer-Lipid Hybrid Nanoparticles for Targeted Anti-Cancer Therapy. *Molecules* **2020**, *25*, 4377.
(337) Bangera, P. D.; Kara, D. D.; Tanvi, K.; Tippavajhala, V. K.; Rathnanand, M. Highlights on Cell-Penetrating Peptides and Polymer-Lipid Hybrid Nanoparticle: Overview and Therapeutic Applications for Targeted Anticancer Therapy. *AAPS PharmSciTech* **2023**, *24*, 124.

https://doi.org/10.1021/acsnano.4c18274
ACS Nano XXXX, XXX, XXX−XXX